NASA Contractor Report 182111

Development of Sensors for Ceramic Components in Advanced Propulsion Systems

Final Report: Survey and Evaluation of Measurement Techniques for Temperature, Strain, and Heat Flux for Ceramic Components in Advanced Propulsion Systems

W.H. Atkinson, M.A. Cyr, and R.R. Strange
United Technologies Corporation
Pratt & Whitney
Commercial Engineering
East Hartford, Connecticut

June 1988

Prepared for
Lewis Research Center
Under Contract NAS3-25141

NASA
National Aeronautics and
Space Administration

UNITED TECHNOLOGIES
PRATT&WHITNEY

In reply please refer to:
WHA:da;MS 116-01
Ref. No. NASA CR-182111 (PWA-6113-12)

August 19, 1988

To: National Aeronautics and Space Administration
Lewis Research Center
21000 Brookpark Road
Cleveland, Ohio 44135

Attention: Mr. Ray Holanda, Project Manager
Mail Stop 77-1

Subject: Final Report (Tasks 1 and 2) for the Development of Sensors for Ceramic Components in Advanced Propulsion Systems

Reference: Contract NAS3-25141

Enclosure: Fifty copies of Subject Report, NASA CR-182111 (PWA-6113-12)

Gentlemen:

We are pleased to submit the Final Report (Tasks 1 and 2) in accordance with the Statement of Work of the referenced contract.

Sincerely yours,

UNITED TECHNOLOGIES CORPORATION
Pratt & Whitney
Commercial Engineering

William H. Atkinson
Program Manager

William H. Atkinson

cc: Administrative Contracting Officer
Air Force Plant Representative Office
UTC/Pratt & Whitney Group
East Hartford, CT 06108

NASA National Aeronautics and Space Administration

Report Documentation Page

1. Report No.	2. Government Accession No.	3. Recipient's Catalog No.
NASA CR-182111		

4. Title and Subtitle
Final Report: Survey and Evaluation of Measurement Techniques for Temperature, Strain, and Heat Flux for Ceramic Components in Advanced Propulsion Systems

5. Report Date
June 1988

6. Performing Organization Code

7. Author(s)
W. H. Atkinson, M. A. Cyr, and R. R. Strange

8. Performing Organization Report No.
PWA-6113-12

10. Work Unit No.

9. Performing Organization Name and Address
UNITED TECHNOLOGIES CORPORATION
Pratt & Whitney
Commercial Engineering
East Hartford, Connecticut 06108

11. Contract or Grant No.
NAS3-25141

13. Type of Report and Period Covered
Contractor Report Final

12. Sponsoring Agency Name and Address
NATIONAL AERONAUTICS AND SPACE ADMINISTRATION
Lewis Research Center
21000 Brookpark Road
Cleveland, Ohio 44135

14. Sponsoring Agency Code

15. Supplementary Notes
Project Manager, Mr. Ray Holanda, MS 77-1
NASA-Lewis Research Center; Cleveland, Ohio 44135

16. Abstract

This report presents the final results of Tasks 1 and 2, "Development of Sensors for Ceramic Components in Advanced Propulsion Systems" program (NAS3-25141). During Task 1, an extensive survey was conducted of sensor concepts which have the potential for measuring surface temperature, strain, and heat flux on ceramic components for advanced propulsion systems. Each sensor concept was analyzed and evaluated under Task 2; sensor concepts were then recommended for further development. For temperature measurement, both pyrometry and thermographic phosphors are recommended for measurements up to and beyond the melting point of ceramic materials. For lower temperature test programs, the thin-film techniques offer advantages in the installation of temperature sensors. Optical strain measurement techniques are recommended because they offer the possibility of being useful at very high temperature levels. Techniques for the measurement of heat flux are recommended for development based on both a surface mounted sensor and the measurement of the temperature differential across a portion of a ceramic component or metallic substrate.

17. Key Words (Suggested by Author(s))	18. Distribution Statement
Ceramic; Temperature; Strain; Heat Flux	

19. Security Classif. (of this report)	20. Security Classif. (of this page)	21. No. of pages	22. Price
UNCLASSIFIED	UNCLASSIFIED	119	

NASA FORM 1626 OCT 86

TABLE OF CONTENTS

TABLE OF CONTENTS (continued)

LIST OF ILLUSTRATIONS

LIST OF ILLUSTRATIONS (continued)

LIST OF ILLUSTRATIONS (continued)

LIST OF TABLES

1.0 INTRODUCTION

The objective of Phase I of this program is to survey, analyze, evaluate, and recommend sensor concepts for the measurement of surface temperature, strain, and heat flux on ceramic components for advanced propulsion systems. Such sensor systems require unique properties and exceptional durability due to both the need for compatibility with the nonmetallic materials expected to be used in advanced propulsion systems and the need to operate in an extremely hostile environment with regard to temperature, pressure, and cycling. Considerable development work has been performed on sensor systems for metallic components for both low- and high-temperature applications. However, none of these applications combines the requirements for materials compatibility, miniaturization, and survival in the hostile environment that will be required to obtain accurate measurements on nonmetallic materials in advanced propulsion system applications.

One of the most demanding areas of advanced propulsion systems is that of hypersonic propulsion. Recently, interest in hypersonic aircraft has increased dramatically. The possible applications are numerous, including: fast response, high speed aircraft to protect the Naval surface fleet; transatmospheric vehicles to significantly reduce long distance airline travel time; and an advanced hypersonic transatmospheric spaceplane with operation scenarios more similar to a current aircraft than a spacecraft. This renewed interest in hypersonic technology has been enhanced by significant increases in progress in the areas of propulsion, materials, and computational fluid dynamics.

The requirement still exists, however, for further progress in many areas including the propulsion system. No current propulsion system is optimum for the full range of Mach numbers that will be required for a hypersonic vehicle. Various combined systems, such as a turbo/ramjet for the Mach 0 to Mach 6 range combined with a hydrogen-fueled supersonic combustion ramjet (SCRAMJET) for the Mach 6+ range, are being considered. While the exact nature of the propulsion systems that will be used in hypersonic vehicles is still not clear, certain requirements are obvious. Durable materials will be required that are strong and yet significantly lighter than the materials currently in use. At the same time, those new materials must have extended temperature range capabilities relative to currently used materials.

Ceramics and other nonmetallics will, therefore, find wide use in hypersonic vehicles both in the airframe and the propulsion system. These nonmetallic materials will have a wide range of characteristics. Some will be coatings (such as thermal barriers) on metal parts; some will be present in a monolithic condition; and some will be composites.

Accurate measurement of parameters (e.g., temperature, strain, and heat flux) is required to verify and improve the design models used for the refinement of advanced propulsion systems. These same types of measurements will be required to support the safe and cost-effective testing of experimental advanced propulsion systems.

Development of the required sensor systems for nonmetallic components in advanced applications presents some unique problems. The temperatures that the sensors must endure are much higher (to 2200K) than those encountered in the development of sensors for metal components. In addition, wide differences in the ceramic materials properties relative to metallic components must be considered. For sensors in contact with the ceramics, these material differences will dictate changes in materials choice and construction techniques. For optical sensors, the problem of optical access must be considered, as well as the ceramic optical properties. In some instances, the presence of a hot combusting gas stream also must be considered.

2.0 EVALUATION AND SELECTION OF SENSOR CONCEPTS

When this contract was initiated, a survey of measurement techniques was conducted. The measurement techniques that were identified in that survey, as well as those identified in-house, were evaluated for their applicability to ceramic materials and for compatibility with the advanced propulsion system environments. In addition, the techniques were reviewed in terms of the amount of development that would be required to reduce them to practice and the degree of risk associated with those development programs. The ten factors addressed in the analysis of the instrumentation concepts are reviewed below, and a brief discussion of each factor is presented.

Usable Temperature Range

The feasibility of attaining the target temperature goal of 2200K must be considered. However, since it is unlikely that any one technique will yield valid data for all materials at all temperatures, concepts should not be rejected simply because they cannot cover the entire temperature range or achieve the maximum desired temperature.

Accuracy

The target accuracy goals are:

- o ±2% of Absolute Temperature
- o ±10% Full-Scale Static Strain
- o ±5% of Full-Scale Dynamic Strain
- o ±5% of Full-Scale Heat Flux.

The minimum acceptable accuracies are:

- o ±5% of Absolute Temperature
- o ±15% of Full-Scale Static Strain
- o ±10% of Full-Scale Dynamic Strain
- o ±10% of Full-Scale Heat Flux.

The capabilities of the sensor systems to meet these accuracy goals or minimum acceptable error limits must be considered. Sensor installation effects must be carefully examined. The sensor must not unacceptably perturb the parameter of interest by interactions with the component or the flow over the component being measured. In addition, sensor calibration methods must be developed that take into account installation effects and yield accurate calibration results for the installed sensor.

Compatibility with Propulsion System Environment

For optical measurements, the possible presence of a combusting environment must be considered. For direct contact strain measurements, vibration frequency range of the dynamic strain measurement and fatigue life of both dynamic and static strain sensors must be compatible with the system component operation limits. In addition, sensor design must consider that the environment may include hot turbulent flow of particle-laden gases, and a high centripetal acceleration field on rotating components (20,000 to 100,000 G).

Compatibility of Materials in Contact (i.e., Sensor/Substrate Compatibility)

If a sensor is mounted directly on or within the component, then matching of temperature coefficients of thermal expansion, adherence to the ceramic material, and electrical insulation from the material may be important factors. Mechanical and chemical stability of the materials in contact (including oxidation and other chemical reactions, formation of eutectics or amalgams or other material phases) must be taken into consideration.

Life Expectancy

The sensor life must be sufficient to obtain the information required. The sensor lifetime goal of 50% survival after 50 hours in the test environment will be considered. In some extreme cases, short lifetime (even expendable) sensors may be required to obtain the desired data.

Size

The size of the sensing area must be considered. For example, ceramics in general have lower thermal conductivity than metals and, therefore, often have larger thermal gradients. This must be considered in the design of thermal measurement systems. Good strain spatial resolution is desirable on the order of 3 mm x 3 mm on surfaces and 3 mm x 3 mm x 1 mm at interior locations near fillets, holes, notches, edges, corners, and laminations. Strain mapping over large areas (several centimeters) may also be desirable. The possibility of non-one-dimensional heat flow must be considered in the choice of size for heat flux instrumentation.

Cost

The cost of obtaining the measurements must be considered. This includes not only the sensor cost, but also the cost of installing the sensors into the propulsion system. The development costs which cannot be neglected are considered separately and are not reflected as a component of the sensor cost.

Data Acquisition and Reduction Requirements

The cost and complexity of acquiring data under realistic test environments must be considered. The data reduction requirement to process raw data into meaningful engineering units must also be considered.

Fabricability

Means must be considered for obtaining measurements on both complex specimen shapes (vanes, blades, disks, burner liner segments, case segments, thrust reverser segments, etc.) as well as on simple specimens such as flat plates or cylinders. The requirement for measurements at line-of-sight surface locations, non-line-of-sight surface locations, and material interior locations, on moving and stationary components must be considered.

Special Application Techniques

The feasibility of special or new application techniques must be considered and critical issues affecting the success of these techniques defined. Examples of new techniques are sputtering of cermet materials and ion implantation.

3.0 MATERIALS

The ceramic structural materials (Table I) to be used for propulsion components at operating temperatures above 1300K have electrical, optical, chemical, and mechanical characteristics which are generally quite different from the characteristics of the superalloy structural materials presently used at temperatures below 1300K. An understanding of the material properties is required in order to evaluate concepts for measurement of temperature, strain, and heat flux on the surfaces or in the interior of components fabricated from these ceramic materials.

3.1 THERMAL BARRIER COATINGS

Thermal barrier coatings are used to protect metallic components from high temperature environments. They act as an insulating layer on cooled components and, therefore, reduce the base metal operating temperatures. They also act to reduce the effects of thermal transients. The use of these coatings can reduce component cooling needs and allow operation to higher temperatures which can result in increases to engine efficiency (ref. 1).

The most common thermal barrier materials currently used are:

- Yttria stabilized zirconia
- Zirconia stabilized magnesia.

The properties of different ceramic materials can vary significantly. The thermal barrier coatings for nickel-base superalloys provide a mechanically hard, electrically somewhat conductive and chemically inert surface, with a thermal expansion coefficient matched to the nickel-base superalloys by means of an interface layer. The optical properties of these materials are also highly variable. Both the total and spectral emissivity of 7% yttria stabilized zirconia, for example, have been found to vary with different methods of preparation.

The maximum amount of yttria used to stabilize the zirconia appears to be approximately 8%. The 8% yttria stabilized zirconia seems to be more durable than compositions containing more yttria. This seems to be due to an oxidation reaction with the bond coat. The ZrO_2 - 8% Y_2O_3 thermal barrier coating has also proved to be superior in high heat flux situations (ref. 1).

TABLE I. CERAMIC MATERIALS CHARACTERISTICS FOR THE "SENSORS FOR CERAMIC COMPONENTS IN ADVANCED PROPULSION SYSTEMS" PROGRAM

(The numbers 1 through 9 beside each entry are the reference source and correspond to those listed in the box on the right-hand side of the table.)

Material	ZrO_2/Y_2O_3	Si_3N_4	SiC	SiC/LAS (0/90 SiC) CompglasTM	SiC/Si_3N_4 (Unidir. SiC)	Carbon/ Carbon T-300 Fiber Quasi-Isotrop. CVD Dens.	Al_2O_3	MgO	ZrO_2	SiO_2	Mullite $Al_2O_3+SiO_2$	Fosterite $MgO+SiO_2$	Zircon ZrO_2+SiO_2
Directional?	Isotropic	Isotropic	Isotropic	Direct'nl	Direct'nl	Direct'nl	Isotropic	Isotropic	Isotropic	Isotropic	Isotropic	Isotropic	Isotropic
Melting Temp.	1950K 2	2170K 1	3000K 1	2170K 8	3000K 8	3700K 4	2300K 1	3070K 4	2500K 1	1980K 1	1800K 6	1800K 6	1950K 6
Operating Temp. in Present Program	1650K (2500F)	1900K (3000F)	1900K (3000F)	1900K (3000F)	1900K (3000F)	2200K (3500F)							
Maximum Temp. in Present Program	2150K (3400F)	2400K (3900F)	2400K (3900F)	2400K (3900F)	2400K (3900F)	2700K (4400F)							
Density, gm/cm^3	5 8	3.2 1	3.3 1	3.2 8	3.3 8	3.2 4	4.0 1	3.6 4	5.8 1	2.2 1			
Resistivity 300K	10^4 8	10^{10} 9	10 9	10^{10} 8	10^{10} 8	.001 9	10^{14} 4	10^{14} 4	10^4 6	10^{14} 6	10^{14} 4	10^{14} 4	10^{14} 4
1650K	5 3						10^5 6	10^5 6	10 6	10^5 6			
1900K							10^4 6	10^4 6	2 6	---- 6			
2200K							10^3 6	10^3 6	1 6	---- 6			
Thermal Expan., $K^{-1} \times 10^{-6}$ α 300K	10 8	3.1 1	5.0 1	3 8	5 8	1.0 5	6.9 1	13 6	10 1	0.5 1			
1650K													
1900K													
2200K													
Young's Mod. GPa E 300K	210 8	290 1	430 1	75 7	240 7	70 7	360 1	200 9	210 1	75 1			
1650K				100 7									
1900K													
2200K						60 7							
Bend Strength MPa Su 300K	600 8	800 1	750 1	350 7	550 7	240 7	450 1	160 7	600 1	90 1			
1650K		0 1	100 1	200 7									
1900K													
2200K						300 7							
Strain Failure cm/cm x 10^{-6} 300K	2900 8	2800 2	1700 2	4600 2	2300 2	3400 2	1200 2	1000 2	2900 2	1200 2			
1650K				2000 2									
1900K													
$\mu = Su/E$ 2200K						5000 2							
Thermal Conductivity W/aK	2 8	30 1	100 1	50 8	50 8	125 9	20 1	25 6	2 1	2 1			
Thermal Shock Index K (Su/[(α)(E)])	300 2	900 2	300 2	1500 2	500 2	3400 2	200 2	100 2	300 2	2200 2			
				700 2		5000 2							
Thermal Mismatch Index Relative to MAR M200 K (Su/[(14-α)(E)])	700 2	250 2	200 2	400 2	250 2	260 2	200 2	1000 2	700 2	100 2			
				200 2		400 2							

References:

1. Parker, Proc Inst ME, v 199 A3
2. Calculated from numbers in this table
3. Adv. in Cer., v 3, Am. Cer. Soc.
4. Handbook of Chemistry and Physics, CRC
5. Hitec
6. Seaco
7. UTRC
8. Estimated
9. Marks 8th ed., p. 6-176

This Page Intentionally Left Blank

3.2 MONOLITHIC CERAMICS

Monolithic ceramics can be used in the manufacture of structural components. Examples of applications of these components include turbine rotors and vanes in the Automotive Gas Turbines (refs. 2 and 3). These ceramics have the greatest potential for use in environments where high temperature resistance, strength, stability, and resistance to thermal shock are necessary.

The materials considered include:

- o SiC
- o Si_3N_4
- o Al_2O_3
- o SiO_2.

SiC and Si_3N_4 are both used for their high strength at elevated temperatures, resistance to thermal shock, and high resistance to corrosion and erosion. Different fabrication methods produce different thermal and mechanical properties for these materials. Al_2O_3 and SiO_2 are too brittle to be used for structural components, but are used extensively as coatings.

The Si_3N_4 and SiC monolithic materials are all similar to each other in that they depend upon the formation of a glassy silica coating to prevent excessive oxidation. The silica (SiO_2) is produced by reactions of the type $Si_3N_4+O_x \rightarrow SiO_2+NO_x$ and $SiC+O_2 \rightarrow SiO_2+CO_x$ which become important at temperatures above 1300K. This glassy layer, in addition to being a poor electrical insulator, becomes very soft at extremely high temperatures. Its "softness" and ductility permit it to deform in step with the substrate and transfer substrate strain to the exterior surface. If, however, the glassy layer becomes so thick and has such a low viscosity that it provides a mechanism for shear flow to occur within the glass, then measurement of strain at the exterior surface could cause a serious underestimation of strain in the substrate. Reaction of this silica glass to form a more refractory bond with surface mounted sensor materials is desirable.

Monolithic ceramics can be very hard, making machining difficult and expensive. These same materials are also brittle. Therefore, the reliability of monolithic ceramic components has been suspect (refs. 3 and 4).

3.3 CERAMIC COMPOSITES

Ceramic composite materials are used to fabricate structural components, offering higher temperature capability, high strength, and reduced weight in comparison with metallic components.

The most common composite materials include:

- o SiC/Si_3N_4
- o SiC/SiC
- o Whisker reinforced Si_3N_4.

Ceramic composites consist of a matrix material, for example a monolithic ceramic, reinforced with ceramic fibers. These fibers act to diffuse fractures and thereby increase the toughness of the matrix material. Ceramic composites are stronger and harder than superalloys currently in use, have low thermal expansion, and are resistant to erosion. They do, however, lose their strength at elevated temperatures (ref. 3).

3.4 CARBON/CARBON COMPOSITES

Carbon/carbon composites are being investigated for various uses including components suitable for use in cruise missile engines and other applications exposed to extreme environments. The basic high temperature material is carbon plus a coating for oxidation protection.

Components manufactured from carbon/carbon composites must be coated to provide oxidation resistance. The characteristics of the coating, as well as the substrate, must be considered during instrument development. For example, optical pyrometer measurements would depend on the optical properties of the coating.

The development of carbon/carbon composites suitable for use in cruise missile engines is the subject of a major U. S. Air Force program currently being managed by the Material Laboratory at United Technologies Research Center (UTRC), ref. 5. The major program goal is 10 hours of useful life in air at 2200K. The life-limiting problem at high temperatures in air is the rapid reaction of carbon with metal to form carbides and with oxygen to form volatile oxides such as CO_2. Thus far, UTRC has developed two types of coatings which successfully resist oxidation. The first type consists of a proprietary layer on the carbon/carbon and a top coating of Si_3N_4. At high temperatures, the silicon nitride oxidizes to form a protective coating of SiO_2. This coating system works well at 2100K but not at 2150K, where bubbles (carbon and nitrogen oxides) begin to form in the glass. The rate of recession of the coating with time at high temperatures in a high speed gas stream due to the evaporation of the silica is also a serious problem with this system.

The second type of multilayer coating for carbon/carbon is useful up to 2200K. It consists of an inner layer of a carbide which bonds well to the carbon. Next is a layer of iridium (an oxygen diffusion barrier), and then a layer of iridium aluminate. The aluminate reacts with air to form a final outer surface layer of alumina. A variant of this coating replaces the aluminate with an electron beam-physical vapor deposition (EB-PVD) coating of stabilized zirconia. Both the alumina and the zirconia coatings have columnar microstructures and, for all practical purposes, are 100% dense.

4.0 SENSORS FOR SURFACE TEMPERATURE MEASUREMENT

4.1 THIN FILMS

4.1.1 Thermocouples

Thin-film thermocouples have been developed for use on MCrAlY-coated superalloy materials in jet engine applications (refs. 39, 41-42, 60-63, and 66). This thin-film form of thermocouple is fabricated by sputtering suitable layers of metals, and insulating materials if necessary, directly on the material surface. In the typical form, the two legs of the thermocouple circuit are formed of sputtered metal stripes of dissimilar metals overlapped at one point to form a temperature measurement junction. The two stripes extend as lead films to a point convenient for the attachment of lead wires by resistance welding.

Figure 1 shows the 14 thin-film thermocouples installed on turbine vanes and then operated to 1250K by NASA in combustor exit flow during the High Pressure Facility test program in 1985 (ref. 39). The metal films and lead wires are Pt and Pt-10%Rh. The sputtered insulation layer under the thermocouples is Al_2O_3. The vanes are nickel-base superalloy which have been NiCoCrAlY-coated by vapor deposition. The NiCoCrAlY layer was oxidized to form a starting layer of thermally grown Al_2O_3 before sputtering, to attain adherence of the sputtered Al_2O_3, which otherwise would spall and delaminate at turbine vane temperatures. Figure 2 shows a schematic of a cross section through the films (refs. 41, 42, and 63).

Three considerations determine the upper temperature limit of these sensors. The first consideration is the melting points of the precious metals employed (e.g., Pt 2043K, Pt-10%Rh 2103K, and Rh 2293K). Beyond these temperatures, the development of new thermocouple materials would be required, perhaps of ceramic or mixed ceramic-metal (cermet) compositions. For example, Searcy and Meschi (ref. 40) identify the internal thermodynamic mechanisms affecting the high-temperature electronic semiconductor properties of ceramics in contact with other materials. Advancement would require a major research and development program based on using such considerations to design atomic structural modifications, and appears to be well beyond the scope of the present program. The thin-film thermocouple based on the noble metal elements remains feasible for consideration up to about 1900K. The second consideration is the upper limit of reliable thermocouple behavior, including the effects of erosion, corrosion, insulation shunting, and contamination. The third consideration is the upper limit for mechanical adherence and durability.

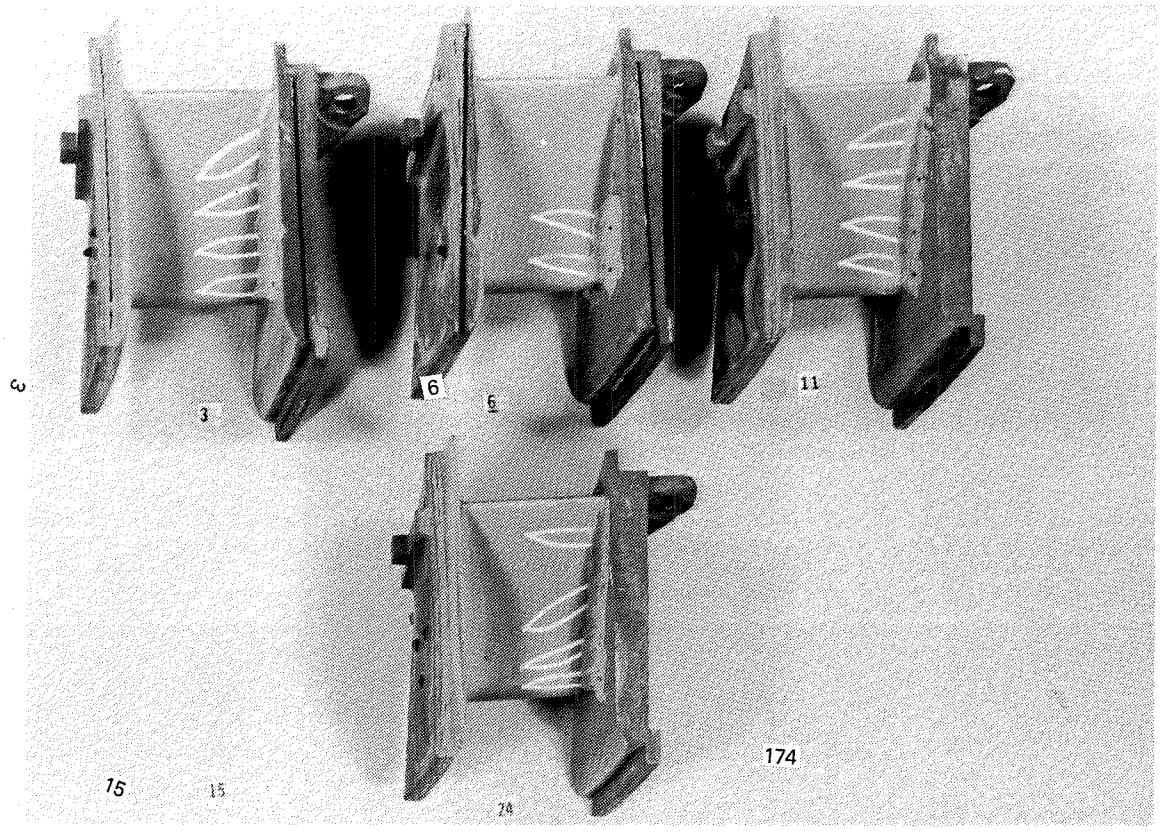

PRATT & WHITNEY THIN-FILM THERMOCOUPLES ON FOUR NASA-LEWIS RESEARCH CENTER VANES: PRESSURE SURFACE

Figure 1 Thin-Film Thermocouples

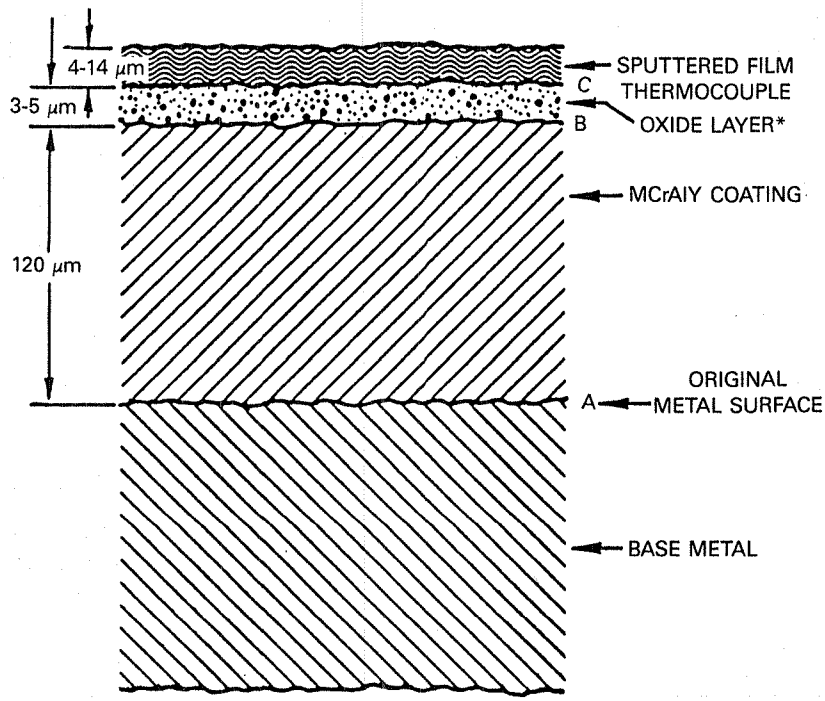

*THE STABLE ADHERENT Al_2O_3 INSULATING LAYER IS OBTAINED BY AT LEAST 50 HOURS OXIDATION (AT 1300K) OF THE COATING, FOLLOWED BY Al_2O_3 SPUTTERING

Figure 2 Schematic Cross Section through the Films

The initial accuracy of Pt versus Pt-10%Rh thin-film sputtered thermocouples on superalloy blades and vanes in combustor flow is found to be within the limits of ANSI standard for Pt versus Pt-10%Rh thermocouple wire over the range tested to date: +1.1C or +0.75% of Celsius temperature, for 300K to 1250K (refs. 41 and 42). This accuracy is not measurably altered by 50 hours exposure to high temperature combustor flow, except for an oxidation effect in a particular part of the thermocouple system somewhere between the hot junction and the cold junction (ice temperature or room temperature) where the thermocouple leads pass through the temperature range in which rhodium oxidizes readily: 600K to 950K. For long-term stability, this part of the system must be fabricated of thick wire or films (ref. 42 concludes that 14μm Pt-10%Rh films produce satisfactory results) or protected from oxidation by sheaths or coatings. The shift in calibration ΔT (Kelvin) due to this oxidation of Rh in the PtRh leg is found empirically to be a function of three parameters: PtRh film thickness a (μm) in the critical region, oxygen partial pressure p (atmospheres), and time t (hours) as follows:

$$\Delta T = (40)\ (p^{0.6})\ (t^{0.33})\ /\ (a) \qquad (1)$$

The oxidation problem can be avoided by using a pure Pt versus pure Rh system, but the extension wire of pure Rh is difficult to install reliably due to its low strength.

Two other potential sources of major error are contamination and shunting effects.

Contamination effects are difficult to estimate. No calibration data above 1250K have been found for thin-film thermocouples. It is known that the increased chemical activity of many atomic species above 1250K may result in contamination of thin films of noble metals resulting in changes in thermoelectric voltage with time at temperature. For example, a 10% shift in calibration would occur if the Pt leg became contaminated with about 1% concentration of Rh (or possibly other species such as Si).

The effect of electrical shunting due to insulation leakage is estimated as follows. It is first observed that, to keep the effects within reason, the insulation resistance should be at least 10 times the sensor resistance. The geometry of thin-film stripes on insulation layers results in the following constraint on insulation resistivity, r_1:

$$r_1/r = 10\ (L/a)^2\ (a/a_1) \qquad (2)$$

where r is sensor resistivity, L is sensor length, a is sensor thickness, and a_1 is insulation thickness. The ratio L/a for thin-film thermocouples is typically greater than 100, for reasonable isolation between point of measurement and point of lead wire attachment. Then, even if the insulation thickness is 10 times the sensor thickness, the insulation resistivity must be about 10^4 times higher than the sensor resistivity. The data in Table I suggest that this may be attainable up to about 1900K, but probably not to 2200K, based on Al_2O_3 as insulators.

The thin-film gages are found to be essentially unaffected by the vibrations, strains, erosion, and acceleration loadings (to 100,000 G) experienced in engine hot section testing. Loss of several percent of the thin film thickness due to erosion has no effect on thermocouple accuracy, for example, except when insulation resistance is marginal. Environmental problems center on the problem of materials in contact.

There are four major concerns about the materials in contact with the sensor. First, does electrical insulation resistance decrease without limit as temperature (T) increases, short-circuiting the thin-film thermocouples? Second, does contamination of metal thermocouple elements occur at high T, resulting in unacceptable calibration drift with time at temperature? Third, is delamination a more serious problem due to any of three causes: increased effects of temperature coefficient of expansion mismatch, increased thermal shock due to impact of hotter particulate matter, or softening of the ceramic surface? Finally, if thicker insulation or overcoat layers are required to protect against erosion, corrosion, contamination or shunting, will these heavy layers result in increased problems of delamination?

In tests at Pratt & Whitney, Pt versus Pt-10%Rh thin-film thermocouples on samples of lithium alumino-silicate (LAS) glass/SiC fiber composite ceramic survived furnace cycles to 1400K in air. At UCLA, Pt-10%Rh/Pt thin-film thermocouples on Si_3N_4 substrates were tested successfully to 1300K in air (ref. 43). Tests of this kind must be carried out on several candidate ceramic materials and must be extended to the upper limit of the thermocouple materials (1900K). Accuracy must be determined quantitatively over this entire range by comparison with heavy wire thermocouples (in isothermal furnace testing) and pyrometers (where surface emittance has been established).

Failure is defined for an individual sensor as increase in the uncertainty of the measurement beyond acceptable limits, due either to catastrophic failure or gradual deterioration. Failure of less than 50% of thin-film thermocouples installed has been achieved for 50 to 150 hours in engine tests and combustor rig tests, in which surface peak temperatures were 1250K and average on the order of 1100K. Gradual failure modes include: calibration shifts due to contamination; increase in leakage to ground (secondary junctions); and the special oxidation effects described earlier. Catastrophic failure modes include: delamination (failure of adherence) of the sensors or the lead wires; or open circuit due to 100% erosion; or open or intermittent circuit due to failure of lead wires or connections.

The total thickness of a cross-section through the film installation of figure 2 above the MCrAlY surface is about 10 μm, at the point of temperature measurement. This thickness does not include the 120 μm NiCoCrAlY undercoating which is required on the superalloy components but will probably not be needed on ceramic components. This is an order of magnitude less than the buildup (or groove depth) required for reliable wire thermocouple installation. The result is negligible aerodynamic disturbance, negligible mechanical damping, local stress concentration or stiffening, and negligible temperature redistribution in the component. It is expected that surface grooving will not be permitted

on ceramic components because of the risk of local crack initiation. The thin-film thermocouple applied externally meets the desired noninterference requirements. The size of the thermocouple junction (overlapped leg area) can be as small as 0.1 mm x 0.1 mm, but 1.5 mm x 1.5 mm is recommended to allow for possible loss of material through erosion or impact. At the point where lead wires are attached to the films, thickness buildup is typically 150 μm above the surface including lead wire and a protective overcoat of cement. A location well away from the point of measurement should be selected.

Standard commercial thermocouple data acquisition equipment and data reduction procedures are used with the thin-film thermocouples. The equipment can be recalibrated at any time during a test by substituting reference input voltages for thermocouple voltages. The sensors and lead wires cannot be readily recalibrated. To do so requires imposing a known temperature gradient on each portion of the thermocouple leadwork (and not simply a known temperature at the measuring point). This is not usually possible in tests of aircraft engines or hypersonic vehicle structures, and is a fundamental difficulty in using either conventional wire thermocouples or thin-film thermocouples. The thermocouple sensors and lead wires must, therefore, be conservatively designed for high stability, incorporating oversized conductors and protection from the chemical contaminations that might result in calibration drifts. The thin-film thermocouples are readily used in rotating systems through slip rings or radio telemetry.

Fabrication of thin-film thermocouples is complicated. Minimum involvement requires masking of the part and sputtering of patterns of two dissimilar thermocouple materials overlapping at selected locations to form junctions. Attachment of lead wires of thermocouple materials to the films is then necessary. Finally, the lead wires must be bonded to the components to be tested and routed to a data acquisition system.

The sputtering processes are carried out in a vacuum chamber in which atomic cleanliness must be preserved. Adherence and proper composition of films is not achieved if a few atomic layers of moisture, organics, or other contaminants remain on the surface. The ceramic components on which thin-film thermocouples are to be fabricated must therefore be cleanable and then stable when baked to 673K in hard vacuum (10^{-7} torr). The components must fit in available vacuum sputtering chambers (dimensions less than 30 cm are typical). The specialized nature of sputtering equipment makes difficult the transfer of the thin-film technology from one facility to another.

The critical concerns in extending the thin-film sputtered thermocouple technique to ceramic components at higher temperatures center on the problems discussed previously. These concerns may result in a necessity for development of improved protective layers under or over the thin-film sensors to provide barriers to contamination or improve local mechanical stability of the ceramic surface.

4.1.2 Resistance Thermometers

A thin-film resistance temperature sensor can be fabricated by sputtering a suitable layer of a material whose electrical resistance is highly sensitive to temperature (such as any pure metal), and insulating materials if necessary, directly on the ceramic component surface. The sensing element can consist of a single line or grid of platinum or conductive ceramic or cermet. A pattern such as that shown schematically in figure 3 would provide a small sensor and wide low-resistance lead films extending to a point convenient for the attachment of lead wires by resistance welding.

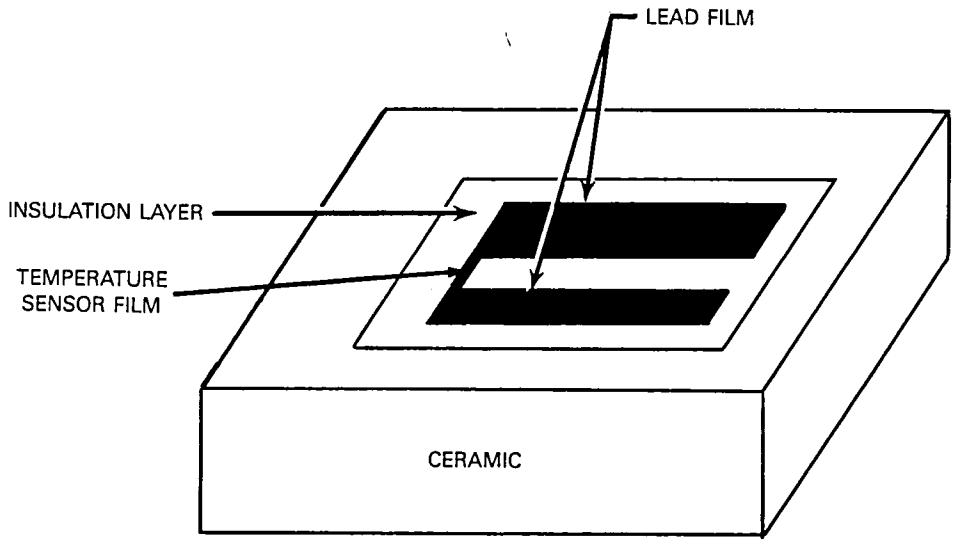

Figure 3 Thin-Film Resistance Thermometer

The fabrication technology employed is basically the same as that employed in fabricating thin-film thermocouples, discussed previously.

Three considerations affect the estimate of upper temperature limit:

1. The melting point of the sensor element material (e.g., platinum at 2043K)

2. The upper limit of reliable resistance behavior, including the electrical effects of erosion, corrosion, insulation shunting and sensor contamination

3. The upper limit for mechanical adherence and deterioration as the temperature is raised.

The second and third problems are more severe for the resistance thermometer than for the thin-film thermocouple discussed earlier because of the direct dependence of sensor electrical resistance on oxidation, erosion, shunting,

and contamination. This will require more effective barrier layers to be added over, and perhaps under, the sensor. If these barrier layers are thicker and heavier than in the thin-film thermocouple case, then the layers will promote larger thermally-induced mechanical stresses if the thermal expansion mismatches are not changed.

The platinum resistance thermometer is considered equal to, or superior to, the best reference grade thermocouples in accuracy of temperature measurement for temperatures up to 1100K (better than 1%). At higher temperatures, it may be possible to provide enough protection against erosion, corrosion, shunting, and contamination to attain useful accuracy. A major development program would be required.

In estimating the effect of contamination, for example, it can be noted that the influence coefficient relating percent change in resistance to change in metal alloy composition is typically on the order of 10 (10% resistance change for 1% contamination).

The effect of shunting due to insulation leakage is estimated as follows. It is first observed that the insulation resistance should be at least 10 times the sensor resistance. The equation defining the constraint on insulation resistivity as a function of sensor film dimensions, sensor film resistivity, and film thicknesses was discussed previously. The sensor length-to-thickness ratio L/a must be typically greater than 100 for reasonable resistance in the sensor. As stated in Section 4.1.1, even if the insulation thickness is 10 times the sensor thickness, the insulation resistivity must be about 10^4 times higher than the sensor resistivity. The data in Table I suggest that this requirement may be attainable up to about 1900K, but probably not to 2200K, based on Al_2O_3 as insulators.

In the previous discussion, it was noted that thin-film thermocouple gages have been found essentially unaffected by the vibrations, strains, erosion, and acceleration loadings (to 100,000 G) experienced in engine hot section testing. For thin-film resistance thermometers, the environment is a greater concern. More effective protective layers will be required to prevent erosion, corrosion, shunting, and contamination. If these layers are heavy, then the likelihood of delamination is increased when subjected to temperature shock, mechanical shock, vibration, and acceleration loadings.

The concerns about materials in contact with the sensor, which were identified for the thin-film thermocouple systems, are even more serious potential problems for thin-film resistance thermometers. In particular, the materials in contact will play a decisive role in erosion and contamination, discussed above. The resistance thermometer sensor must be protected by coatings over and under the sensor which provide good insulation and barriers to diffusion of atomic species which could alter the composition and electrical resistivity of the sensor by reaction, amalgamation, or alloying, or formation of new material phases.

The useful life of thin-film resistance thermometers is likely to be shorter than the useful life of thin-film thermocouples, for the reasons outlined in the two preceding sections. Attainment of 50 hours average time before failure may be achievable. Attainment of this goal will hinge on development of coatings to provide protection against erosion, shunting, and contamination.

The total thickness of a cross-section through the thin-film resistance thermometer installation is expected to be on the order of 50 μm, including undercoat, sensor, and overcoat. This is thicker than the thin-film thermocouple installations described earlier, because of the additional protective coatings required over and under the sensor.

The thin-film resistance thermometer applied externally, therefore, meets the desired noninterference requirements. The size of the temperature sensing region can be as small as 0.1 mm x 0.1 mm, but 3 mm x 3 mm is recommended to allow for use of a grid of thicker films to reduce surface-to-volume ratio and, thereby, reduce susceptibility to contamination and erosion. At the point where lead wires are attached to the films, thickness buildup will be typically 150 μm above the surface. A location well away from the point of measurement should be selected.

Standard commercial resistance Wheatstone bridge data acquisition equipment and data reduction procedures are used with the thin-film resistance thermometers. The equipment can be recalibrated at any time during a test by applying shunt resistors or test voltages. The sensors and lead wires cannot be readily recalibrated. To do so requires returning to a precisely known previous operating condition of the test engine or vehicle. This is not usually possible in tests of aircraft engines or hypersonic vehicle structures, and is a fundamental difficulty in using conventional or thin-film thermocouples, or conventional or thin-film resistance thermometers. The sensors and lead wires must therefore be conservatively designed for high stability, incorporating oversized conductors and protection from the chemical contaminations that might result in calibration drifts. The thin-film resistance thermometers are readily used in rotating systems, through slip rings or radio telemetry.

Fabrication of thin-film resistance thermometers is complicated, involving as a minimum the masking and sputtering of patterns of conductive material to form sensors, and then attachment of lead wires to the films. Finally, the lead wires must be bonded to the components to be tested and routed to a data acquisition system.

Thin-film deposition processes, with higher energy of arrival at the surface than the sputtering process, could be employed (such as ion implantation or ion milling), but each would require a major development program. Low-energy methods, such as evaporation or firing of painted suspensions, do not provide the required durability at high temperatures.

As discussed in Section 4.1.1, the sputtering processes are carried out in a vacuum chamber in which atomic cleanliness must be preserved. The critical concerns in extending the thin-film sputtered resistance thermometer technique

to ceramic components at higher temperatures center on the problems discussed in the previous sections. These concerns may result in a necessity for development of improved protective layers under or over the thin-film sensors to provide barriers to contamination or improve local mechanical stability of the ceramic surface.

4.1.3 Insulating Layer or Substrate Resistance

A common problem with thin film sensors for both temperature and strain is the change in the resistance of the insulation layer with temperature. There have been attempts to compensate for these changes, such as recommendations to use strain gages of lower resistance to minimize these effects. It may be possible to select an insulating layer that exhibits large shifts in resistance with temperature and to use that change as the basis for a temperature measurement technique. Electrical connections would be attached to both sides of the insulating layer, and the electrical resistance of the layer would be measured as shown in figure 4. This resistance could be calibrated as a function of the temperature of the layer. In the case of electrically conductive substrates, the substrate would be used as one electrical connection and the other connection would be formed by sputtering a lead onto the insulating layer. In the case of an electrically insulating substrate, a lead would be sputtered on the substrate, the insulating layer applied and the other lead sputtered onto the insulating layer.

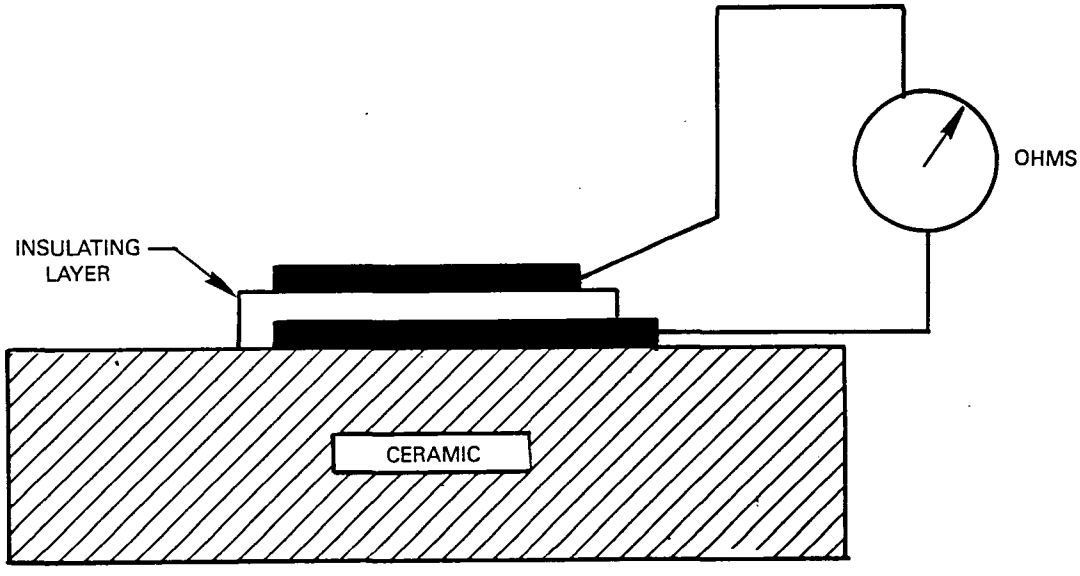

Figure 4 Resistance of Insulating Layer

A variation of this concept is shown in figure 5. In this sensor, two thin-film leads are sputtered directly onto the ceramic. The ceramic itself then serves as the sensing element with the resistance between the two leads being monitored. In principle, by varying lead spacing and by using high-frequency AC excitation, the user would have some control over the depth of the temperature measurement. Close lead spacing and high sensing frequency would yield a surface temperature measurement. Wider lead spacing or lower sensing frequency would increase the depth into the ceramic over which the temperature is averaged. The accuracy of this method is probably limited by the variability in the high-temperature electrical properties of the ceramic materials. For example, the resistivity of alumina at elevated temperatures is readily degraded by small impurity levels. The values reported in the literature vary by a factor of ten. The values are affected by the structure, porosity, method of preparation, surrounding metals, surrounding atmosphere, and insulator purity (ref. 162). This consideration, along with the uncertainty in the precision of dimensional control in the lead spacing, may permit use of this technique only in the unusual case where in-situ temperature calibration of the sensor is possible after installation.

The thin-film techniques appear to be adaptable to ceramic materials. The current practices of resistance welding thermocouples to the surface and embedding lead wires in the surface will not transfer directly to the ceramic materials. Sputtering offers a method of bonding the sensors to the surface. Many of the nonmetallic materials are not electrically conductive, and the thermoelements and leads can be sputtered directly onto the surface.

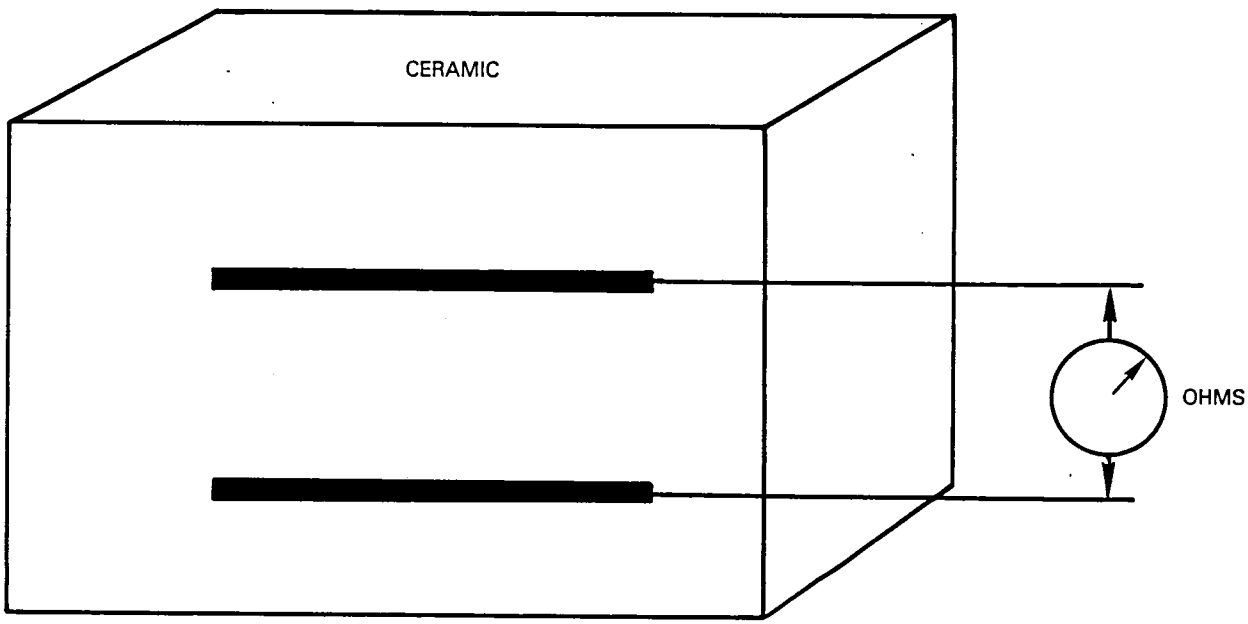

Figure 5 Substrate Resistance

The sputtered sensors are temperature limited both by the bond failures resulting from thermal expansion mismatches and the melting points of the metallic elements. However, the thin-film sensors will be useful for low-temperature testing. The sputtering technique may also prove useful in providing lead wires for other sensor installations.

4.2 ACOUSTIC WAVE TEMPERATURE SENSOR

One possible noncontact temperature measurement technique is a laser ultrasonic thermometer that has been investigated by Rockwell for the NASA Marshall Space Flight Center (ref. 44). This technique is shown schematically in figure 6. In this technique, a pulsed laser would be used to generate an ultrasonic pulse in the ceramic. The phase variation induced in a separate probe laser beam by the acoustic wave would be used to detect the pulse as well as reflections of the initial pulse. Since the speed of sound in the ceramic will vary with temperature, the average ceramic temperature could be determined by the delay in the reflected pulse from the opposite surface of the ceramic. If the speed of the surface acoustic wave across the ceramic was measured, the ceramic surface temperature could be determined. This sensor type was not chosen for development under this contract for several reasons. This sensor exists only as a conceptual design. Since it has not been demonstrated, it has a very high risk. The need to introduce two lasers with high spatial definition as well as detection optics into the propulsion system environment poses formidable challenges. Since these systems have not been built, the feasibility of their use in the harsh acoustic and vibrational environment of advanced propulsion systems cannot be determined.

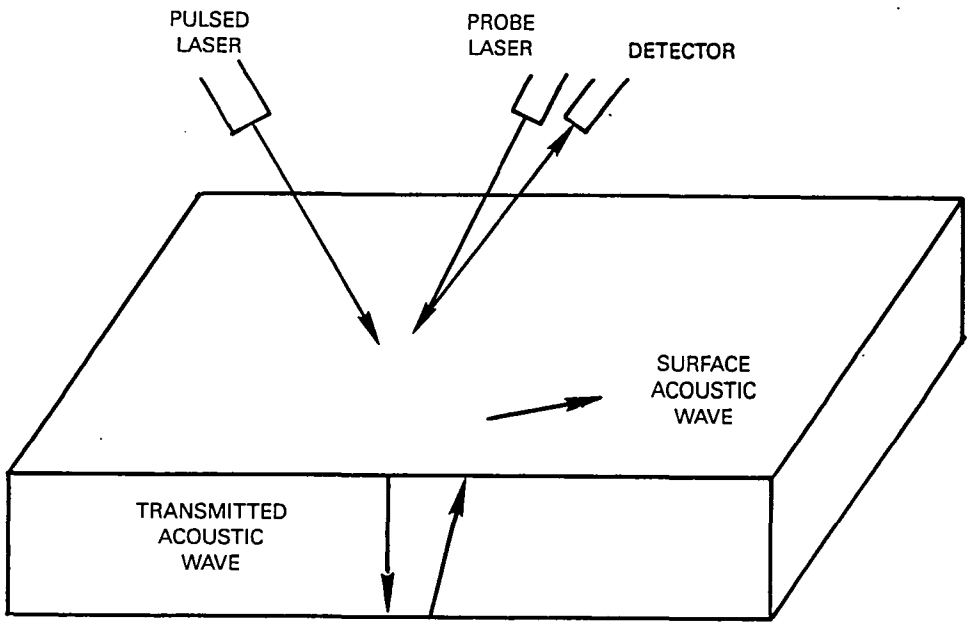

Figure 6 Acoustic Wave Sensor

4.3 PEAK TEMPERATURE MEASUREMENT TECHNIQUES

An additional family of temperature measurement techniques does not measure temperature in real time but does allow post test determination of the maximum temperature reached by the part. One such technique is the use of temperature indicating paints which change color when certain temperatures are attained. Paints are available that span the temperature range of 310K to 1625K. Some paints have several color changes occurring at different temperatures, so relatively detailed thermal profiles can be obtained. The main advantage of this technique is that a large amount of semi-quantitative data can be obtained at very low cost without need for lead wires, optical access, etc. Limited testing has shown the paints to be compatible with the ceramic materials of interest to this contract.

A slight variation on the color-change paints is the use of materials with calibrated known melting points. Such materials are available in several forms, including lacquers and crayons. When these materials are applied to a surface, they have a dull opaque appearance. If the melting point of the paint is exceeded, it will liquify. When the surface is cooled, the paint will resolidify. The appearance of the resolidified material is distinctly different from the original paint. It is glossy, fused looking, and may be transparent. These phase change materials are available covering the temperature range of 310K to 1650K.

While both types of paints will, undoubtedly, continue to find wide use on ceramics in the development of advanced propulsion systems, they are not recommended for further development under this contract. The paints do not give real time information, which can be a major drawback. The paints only indicate the maximum temperature reached by each portion of the part. They do not give information related to when the temperature was reached nor what the gradients in the part were during transients.

Another method that has been used to obtain the profiles of maximum temperatures reached on metallic components is the use of radioactive gases such as Kr-85 (ref. 45). Krypton has been the noble gas used for most studies. Kr-85 has a 10.6 year half-life, is a beta emitter, and is chemically inert. In this technique, the krypton gas is forcibly diffused into the component of interest at elevated temperatures and pressures. The krypton atoms become captive in the lattice structure of the base material and will not be liberated unless the lattice cells are spatially changed such as by heating. The kryponated parts are then installed in the propulsion system and the test program of interest performed. Following the test program, the kryptonated parts are returned to the laboratory and examined to determine the maximum temperature reached by the part. This is usually done by a scheme called the residual counting method, the results of which are shown schematically in figure 7.

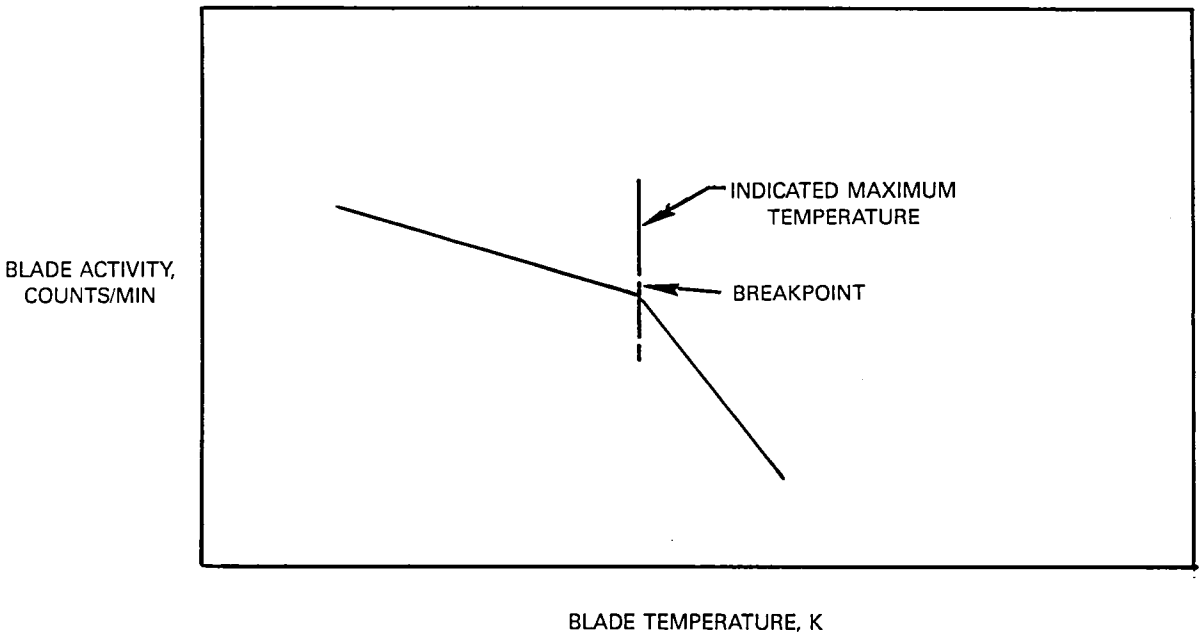

Figure 7 Kr-85 Residual Counting Method

If a kryptonated part is heated in an inert atmosphere to temperatures that are lower than the maximum temperature seen by the part during test, there will be little activity loss. If the part is heated to temperatures higher than it had previously seen, significant activity loss would occur as previously untapped krypton atoms with higher binding energy are liberated. To determine the maximum temperature reached, a kryptonated test piece is heated progressively in steps from a temperature substantially below its previous maximum to a level above that maximum temperature. The residual activity is measured after each heating. A plot of residual activity versus heating temperature will yield a curve with two distinct slopes. The breakpoint in that curve will be the previous maximum temperature to which the part was heated. If several locations on the part were monitored, maximum temperature profiles could be obtained. Spatial resolution on the order of 0.3 cm should be possible.

This technique is not recommended for further development under this contract. It has the same disadvantages as the paints in that no real time data is obtained, and only the maximum temperature seen can be retrieved after the test. Also, the requirement for stepwise heating makes the data reduction process time-consuming and costly.

4.4 EDDY CURRENT PROBES

Since the electrical conductivity of ceramics varies as a function of their temperature, eddy current probes could be used as temperature measuring devices. This technique is shown schematically in figure 8. The use of eddy current probes is based on the fact that the energy transfer between a probe generating an electric field and an adjacent material depends on the electrical conductivity of the material. By measuring the energy transfer, the electrical conductivity of the material and, therefore, the temperature of the material could be determined. In principle, by adjusting the frequency of the electric field, the depth of the field penetration into the ceramic and, therefore, the depth of the averaged temperature measurement could be altered.

This sensor type is not recommended for additional development under this contract. Unless the eddy current probe was relatively close to the object being measured, the temperature would be averaged over a relatively large surface area. If the probe was moved close to the object, it would introduce perturbations in the convection and radiation boundary conditions of the object being measured. There also are several other factors that could alter the energy coupling in addition to temperature effects. Probe to surface spacing, surface microcracks, etc., could all adversely affect the accuracy of this technique.

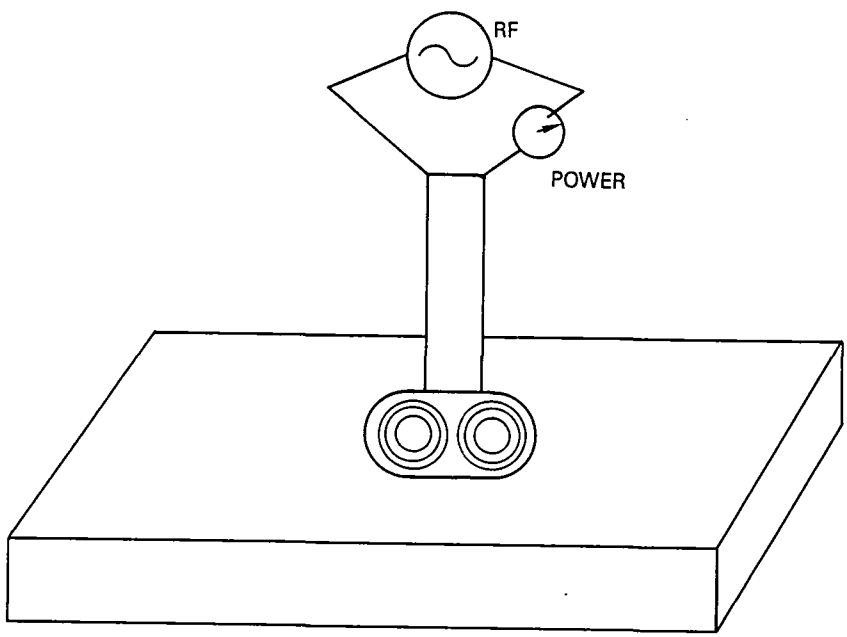

Figure 8 Eddy Current Probe

4.5 NEUTRON DIFFRACTION

Diffraction of a monochromatic beam of neutrons could be used to measure crystalline plane spacing, as shown in figure 9. When an incident neutron beam strikes a specimen, it is diffracted at an angle that depends on the distance between the planes of atoms in the crystal lattice. That angle could be measured with a neutron spectrometer, and the plane spacing could be calculated. Since this spacing will vary as the ceramic expands with increasing temperature, this could be used for temperature determination. Using a calibrated neutron source and precise targeting of the beam, the volume of the specimen could be probed. Plane spacing resolution of a fraction of an angstrom is, in principle, possible.

There are several disadvantages to this technique, such as the variation in plane spacing due to factors other than temperature (e.g., strain). The main factor, however, that eliminates this technique from serious consideration is the need for an intense monochromatic neutron source (such as a nuclear reactor) in very close proximity to the component being tested.

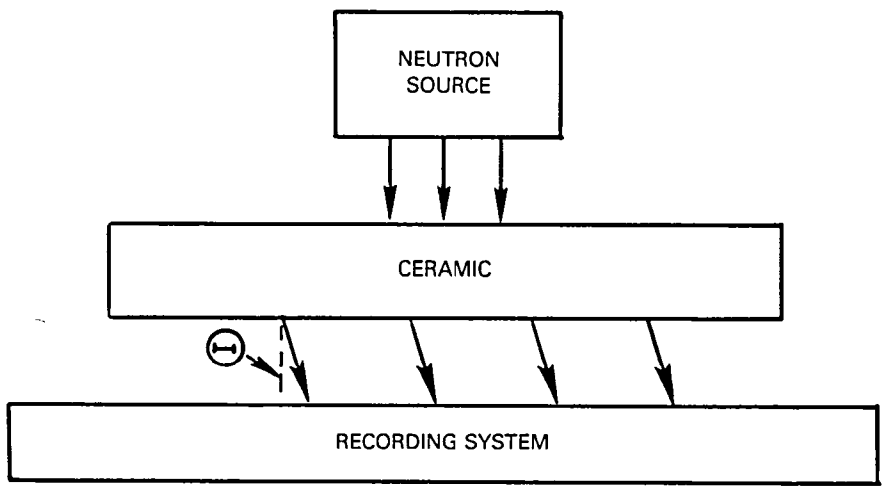

LATTICE SPACING CHANGES WITH TEMPERATURE
WHICH CHANGES DIFFRACTION ANGLE θ

Figure 9 Neutron Diffraction

4.6 PYROMETRY

Radiation pyrometry provides a means for surface temperature measurement without perturbing either surface or surrounding medium. Selection of a particular pyrometer measurement system is based on the radiative properties of the surface, the medium in the optical path, required frequency response, and calibration to achieve the desired measurement accuracy.

All substances at a temperature above absolute zero emit radiant energy as shown in figure 10. Substances undergoing radiative energy interchange have the ability to emit, absorb, and transmit energy at various levels. The relationship between the radiant properties of transmission, absorption, and emission at given conditions is characteristic to each substance. The radiant properties are referenced to an ideal surface called a "black body." This surface is opaque and absorbs all incident energy. The expression for the emissive radiant flux from a black body was determined from first principles by Max Planck (ref. 46) and is given by:

$$P(\lambda,T) = \frac{C_1}{\lambda^5 \left[e^{\left(\frac{C_2}{\lambda T}\right)} - 1 \right]} \tag{3}$$

where: $P(\lambda,T)$ = monochromatic black body intensity of emission ($W/m^2\mu$)

λ = wavelength (microns)

C_1 = constant 3.743×10^8 W micron$^4/m^2$

C_2 = constant 1.439×10^4 micron K

T = temperature of surface (Kelvin).

Planck's equation indicates that the radiant flux increases with increase in temperature at all wavelengths. A pyrometer works on this principle. Real surfaces, however, emit only a portion of the energy radiated by a black body at the same temperature. For a real surface, the amount of energy radiated is given by:

$$E(\lambda,T) = \epsilon(\lambda,T)\, P(\lambda,T) \tag{4}$$

where: $E(\lambda,T)$ = actual intensity of emission ($W/m^2\mu$)

$\epsilon(\lambda,T)$ = surface emittance $0 \leqslant \epsilon(\lambda,T) \leqslant 1$

$P(\lambda,T)$ = Planck's function defined above.

In an optical pyrometer, the thermal radiation from a defined surface area is collected by an optical system and transferred to a detector. The detector produces an electrical signal proportional to the radiant power over a wavelength interval determined by the detector and associated optics.

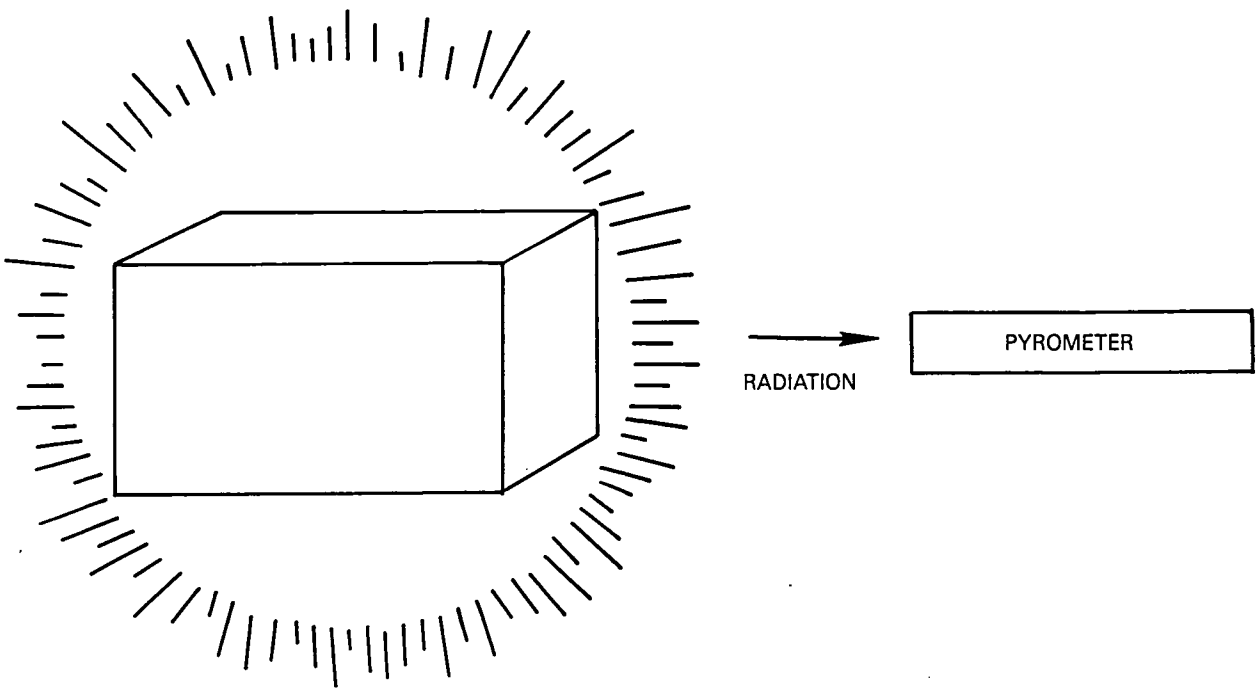

Figure 10 Radiant Energy Emission

4.6.1 Single-Color Pyrometry

If the emittance of a surface can be measured with reasonable accuracy, single-color pyrometry can often be used to obtain relatively accurate temperature data. In this technique, the amount of energy emitted by the surface in some spectral band is measured. The measurement is then corrected in the signal processor for the known emittance of the sample. The corrected energy can then be compared to the known black body energy curve to determine sample temperature.

Commercial units are available to measure temperatures to above 3000K. Pyrometry is a noncontact method and there is no upper temperature limit. The higher the temperature, the more energy there is to measure. If necessary, due to detector saturation, the energy can be reduced by the use of suitable filters.

The accuracy of single-color pyrometry is strongly dependent on the environmental conditions of the test. In the laboratory, the accuracy is generally within 2K. Under realistic engine test conditions, this would be greater than 50K due to reflected energy considerations.

Single-color pyrometers are not particularly well suited for all propulsion system applications. The environment found in propulsion systems contains large amounts of reflected energy. Single-color instruments cannot discriminate between energy originating in the combustor fireball and reflected from the target from energy emitted from the object of interest. For the single-color method to work with acceptable accuracy, the amount of reflected energy may have to be reduced. As with any optical technique, optical access into the area of interest would be required.

This is a noncontact method and the measurements are done optically. Hence, there is no problem with compatibility with the ceramic materials.

The life expectancy of this system is that of the pyrometer itself. These are commercial instruments that have good reliability. Periodic cleaning of the optics may be required to maintain acceptable accuracy.

The probes presently in use at Pratt & Whitney consist of a 1.6 cm diameter water-cooled jacket protruding into a vane cluster. Work is being done to reduce the size of the probe. Target spot sizes can be as small as 0.1 cm, depending on detector and lens systems and the required lower temperature limit and speed requirements of the pyrometer.

Pyrometer units typically come with a direct temperature readout. If further data analysis is required, computers and storage devices can be connected to these units.

Single-color pyrometers are available commercially. The design and fabrication of parts necessary to mount the detectors on engines and an optical access to view the components of interest would be necessary.

4.6.2 Emittance Measurements

4.6.2.1 Emittance Compensating Pyrometer

In conventional single-color pyrometer systems, the temperature is estimated directly from the measured energy. This requires that the surface emittance must be measured or estimated. One method used to determine emittance of surfaces to be measured in some commercial pyrometry systems is shown in figure 11 (refs. 37 and 38). As in conventional single-color pyrometry, the amount of energy emitted by the target in some spectral range is measured. In these emittance compensating units, a light source with known output in the spectral range of the pyrometer is also reflected off the target. The amount of reflected energy is then measured by the pyrometer. Since for opaque materials, the emittance and absorptance at each wavelength are the same, an estimate of surface emittance can be determined. The emitted energy measurement is then corrected for this estimated emittance. If the surface is perfectly diffuse (a Lambertian surface), this technique works well for relatively cool surfaces. For surfaces where the emittance varies with angle, such as many ceramics, or surfaces so hot that the light source reflected component is small compared to the amount of surface emitted energy, this technique can lead to significant errors.

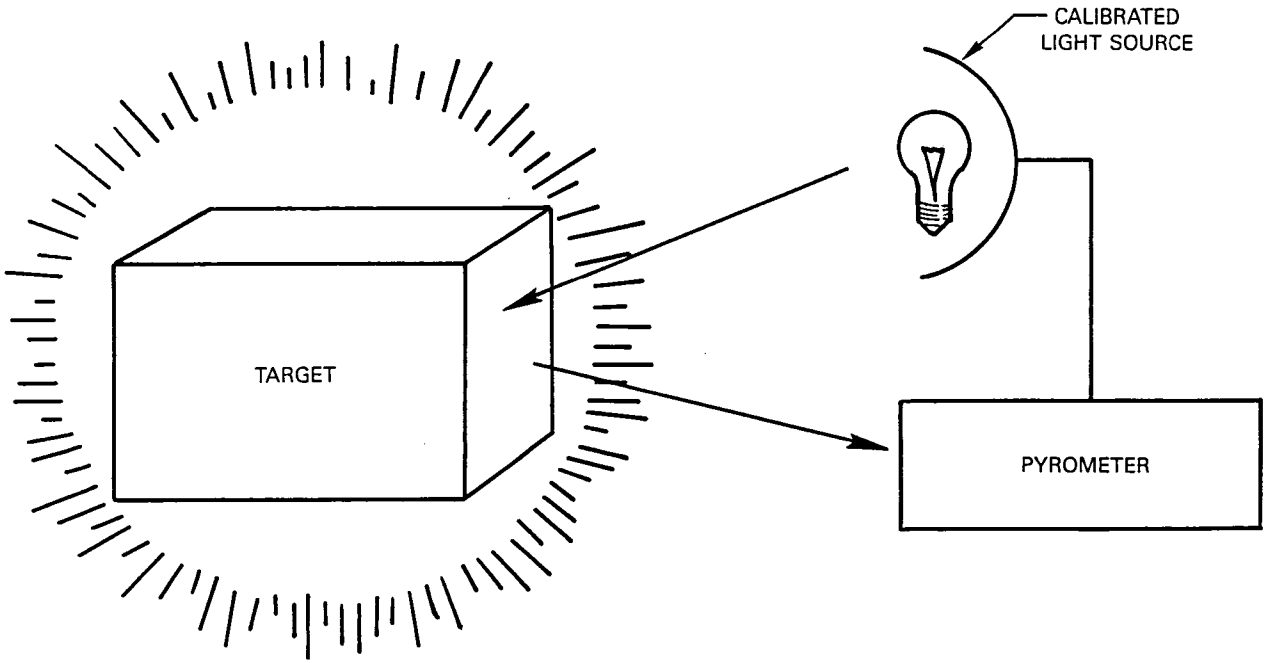

Figure 11 Emittance Compensating Pyrometer

4.6.2.2 Direct Emittance Measurements

At Pratt & Whitney, emittance measurements of various surfaces at high temperature have been made using a Thermogage Emissometer. Figure 12 shows a schematic of that device, while the device itself is shown in figure 13. The test specimen is mounted on the end of a graphite rod. The rod is then pulled into a black body cavity and heated. Depending on the purpose of the test, a broad spectrum or narrow spectral range radiometer is used to make emissivity measurements. The radiometer is connected to a digital storage oscilloscope so that the resulting trace can be captured. While the test specimen is at equilibrium in the black body, the radiometer is positioned to look into the cavity at the specimen. A trace is triggered. The radiometer is then shuttered for a second (to obtain a zero energy baseline). The radiometer is unshuttered and the black body energy is measured; then the specimen is propelled out to the end of the black body tube and the energy from the specimen is measured. The movement is fast enough that the change in specimen temperature is negligible. This produces a trace similar to figure 14. The emissivity of the specimen equals the ratio of the energy emitted by the specimen at the end of the tube to the energy emitted by the specimen inside the black body.

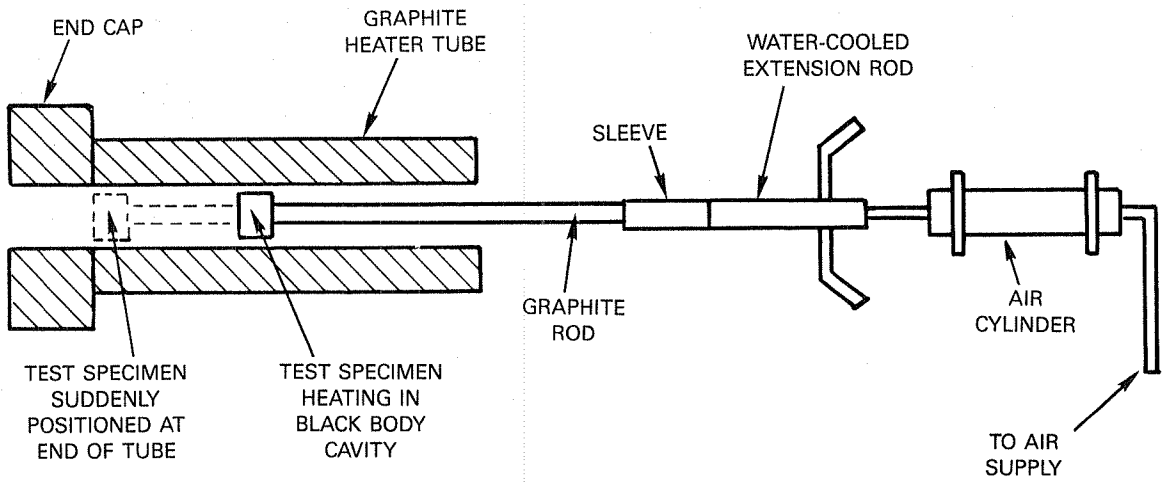

Figure 12 Thermogage Emissometer Schematic

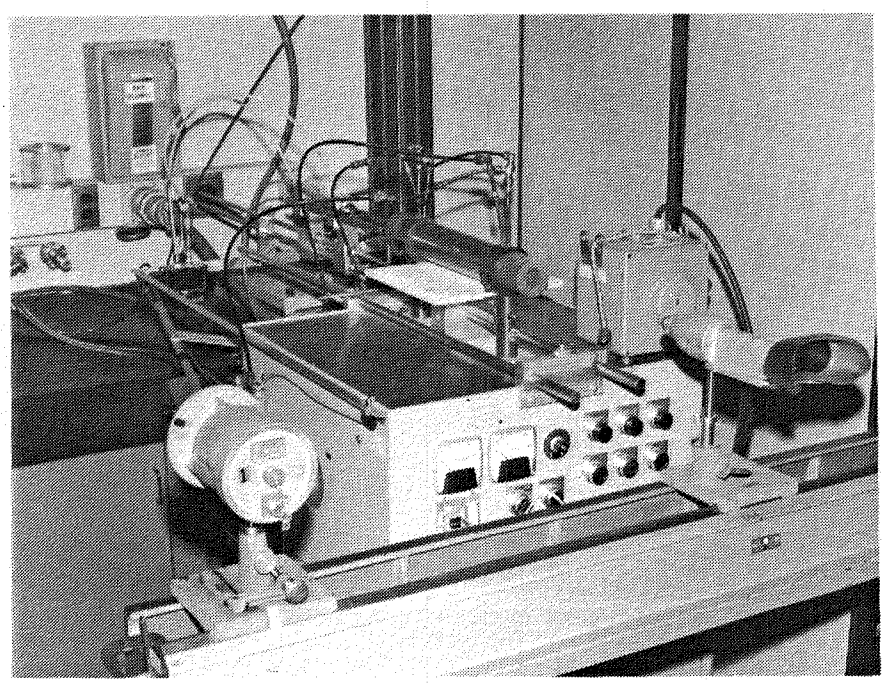

Figure 13 Thermogage Emissometer

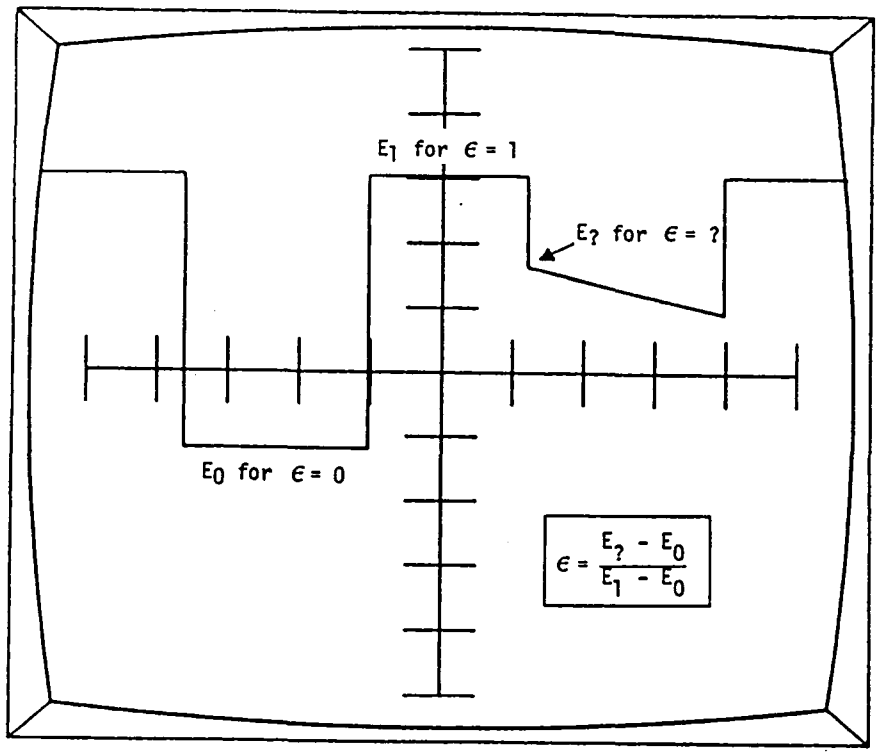

Figure 14 Emissometer Scope Trace

Emissivity measurements have been made on several ceramics. Results show that ZrO_2/Y_2O_3 ceramics have emissivities that vary widely depending on manufacturing processes, application methods, and material content. SiC and Si_3N_4 exhibit high emittances across the spectrum. Compglas® composites have also been tested, and results show high emittances in the 5 to 14 micron range. Figures 15 through 17 show emittance data obtained for Si_3N_4, SiC, and ZrO_2/Y_2O_3 respectively.

It can be seen that for all these materials the emittance is quite high and stable at long wavelengths (approximately 10 microns). This is typical of most ceramics of interest. A single-color pyrometer with spectral sensitivity at this long wavelength would appear to be a good candidate for obtaining accurate temperature measurements on ceramics.

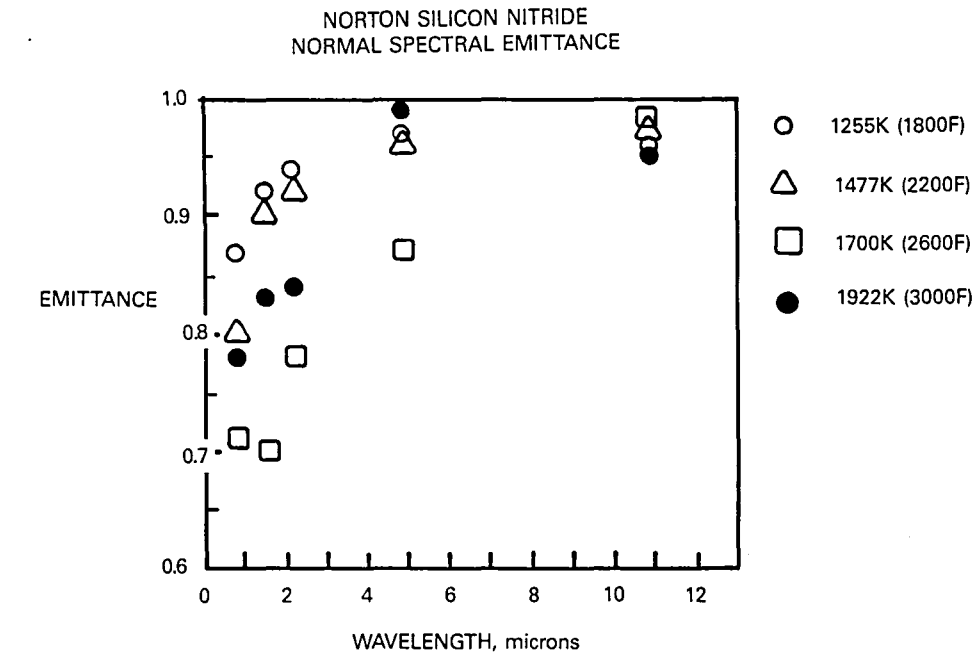

Figure 15 Emittance of Si_3N_4 Versus Wavelength

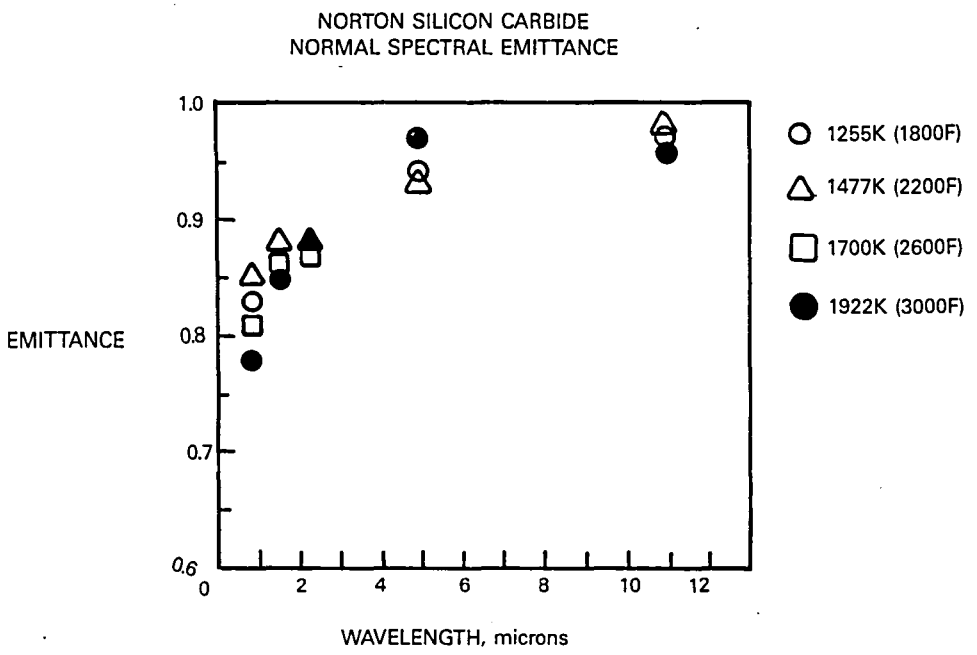

Figure 16 Emittance of SiC Versus Wavelength

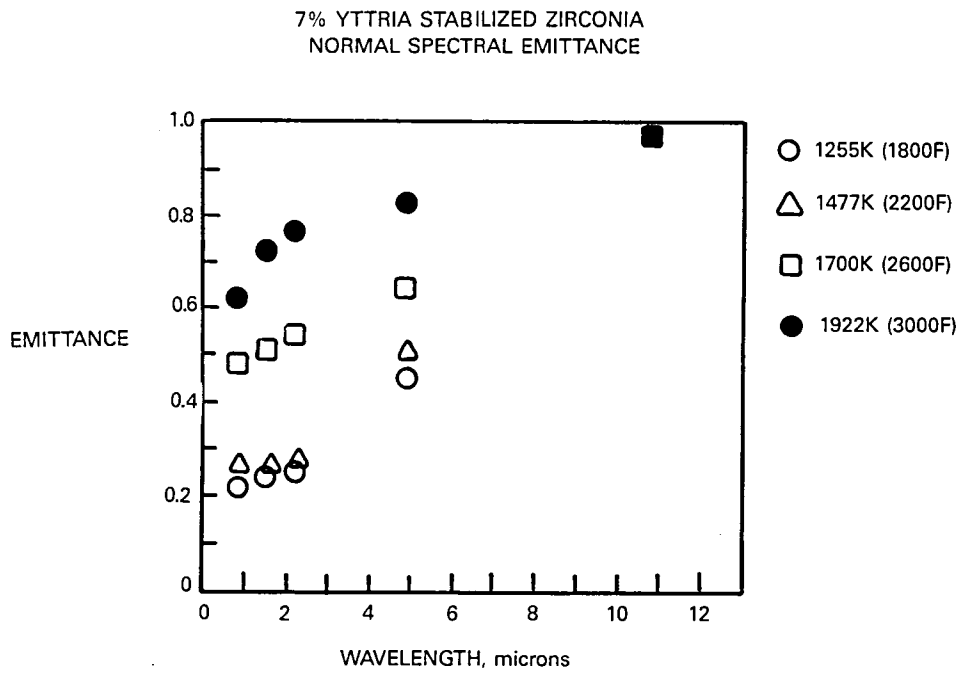

Figure 17 Emittance of ZrO_2/Y_2O_3 Versus Wavelength

4.6.3 Ratio Pyrometers

In some pyrometers, such as shown in figure 18, a ratio technique is used in an attempt to eliminate the error caused by emittance uncertainty. For a ratio pyrometer, data are taken in two different spectral bands, and the ratio of the energy in the two bands is calculated. If the emittance of the surface is the same in both wavelength bands (referred to as a grey body), the ratio is a function only of temperature independent of emittance. This technique works quite well on oxidized metals. Testing at Pratt & Whitney has shown that the emittance of most ceramics varies considerably with wavelength. In those cases, attempts to use ratio pyrometry can lead to large errors.

4.6.4 Dual Spectral Area Pyrometry

Conventional pyrometer measurement systems may have limited application in the critical hot section of gas turbine engines due to the presence of reflected energy from the combustor fireball. Unlike the spectral line radiation from CO_2 and H_2O, this is broadband black body radiation present at all wavelengths. It, therefore, cannot be avoided by choice of detector spectral band. For some hypersonic applications (such as the hydrogen-fueled SCRAMJET) that do not use hydrocarbon fuels, this problem may not exist.

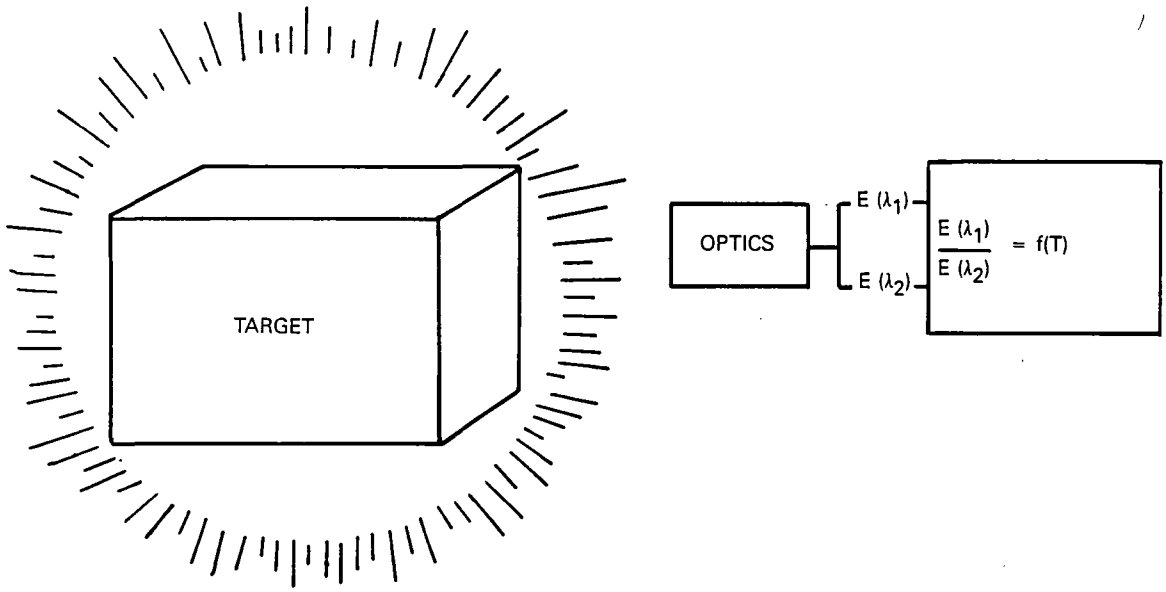

Figure 18 Ratio Pyrometer

For those applications where hydrocarbon fuels are used, the capability of correcting for reflected combustor radiation must be considered in order to obtain pyrometry temperature measurement with acceptable accuracy. Spectral radiation measurements on test engines at Pratt & Whitney indicate that, for oxidized metallic first turbine airfoils, as much as 60% of the radiant energy collected by the pyrometer between 0.35 and 1.15 microns originates in the combustor and reflects from the turbine blade. At this level of reflected energy for a surface at 1250K, the error in the indicated pyrometer temperature is approximately 100K.

The Dual Spectral Area Pyrometry (DSAP) technique (refs. 47-49) was developed at Pratt & Whitney specifically for aircraft engine diagnostics. The implementation of that technique has matured to the point where it has become routine instrumentation on all development engines. An advanced version of this system measures reflection-corrected temperature with 200 KHz frequency response providing instantaneous temperature as a function of position on rotating turbine blades. Engine control pyrometers under test for the PW5000 advanced fighter engine employ the DSAP technique with an advanced algorithm which significantly reduces complexity, size, and weight of pyrometer hardware.

The DSAP reflection compensation is based on the fact that two pyrometers sensitive to different wavelengths will not be equally affected by reflected energy from an external high-temperature radiation source. The spectral ranges of the two pyrometers are selected such that the measured temperature difference between them is indicative of the existence of a reflected component. If the two measurements agree, there is reasonable certainty that

there is no significant reflection error present. If the indicated temperatures do not agree and certain assumptions are made concerning the radiative characteristics of the external source and of the reflecting properties of the surface being measured, then the difference between the two signals can be used to estimate the magnitude of the reflected component. True surface temperature can, thereby, be determined.

In the Dual Spectral Area Pyrometer, two simultaneous equations are solved assuming a known or measured temperature of the reflection source. Below 50% reflected energy, the corrected surface temperature is relatively insensitive to an error in the reflection source temperature. A change of +275K in the reflection source temperature results in only approximately a $\pm$12K change in the calculated surface temperature. As the reflected energy component increases above approximately 50% of the pyrometer signal, errors resulting from uncertainty in the reflection source temperature increase rapidly as was shown by various trade studies conducted on the DSAP (ref. 49).

4.6.5 Advanced Dual Spectral Area Pyrometry

Pratt & Whitney has been investigating a number of approaches for extending the capability of the Dual Spectral Area Pyrometry system to handle larger amounts of reflected energy. Improvements over the current system appear feasible, but the practical use of advanced techniques will have to be demonstrated. The Advanced Dual Spectral Area Pyrometer (ADSAP) system will be capable of working with approximately 70% to 75% reflected energy by making provisions to input the temperature of the reflection source. If acceptable accuracy is to be obtained, however, it will be required that a method be developed to accurately measure the reflection source temperature. It also will be necessary to demonstrate that the reflection source temperature is constant at a steady-state engine operating point.

As with most noncontact optical pyrometer systems, there is no inherent upper temperature range to the ADSAP unit. As surfaces become hotter, the signal-to-noise ratio actually improves and accuracy improves.

The ADSAP should be able to produce a typical accuracy of approximately $\pm$12K as long as an adequate method is developed to account for the temperature of large reflected energy sources.

Optical access to view the area of interest is necessary for any pyrometer system. This may include probes protruding into the gas path as in the case of systems for scanning the first turbine blades. In those cases, fiber optics are often used. The spectral transmission characteristics of available filters must be considered in determining possible wavelengths for pyrometer operation. In other cases, nonintrusive probes with line of sight to the target from outside the high speed gas stream may be used.

Since this is a noncontact method with the measurements done optically, there is little problem with material compatibility. Also since this is a passive noncontact technique, the life expectancy of the instrument is long and indefinite, governed only by accumulation of dirt on the system optics which is dependent on the details of each specific installation.

The optical resolution (spot size) of these pyrometry systems is governed only by the system signal-to-noise ratio. Sufficient photons must be collected to compensate for thermal noise in the detector. The spot size is, therefore, limited only by pyrometer lens size, lens to surface spacing, and required system speed. For the reasonably high temperatures of interest for application of these systems to ceramic, spot sizes on the order of 0.15 cm should be possible.

These pyrometer units contain a direct temperature readout. In cases where data need to be recorded for further processing, the pyrometer can be connected to computers or recording equipment.

4.6.6 Active Pyrometry

A temperature measurement technique known as Active Pyrometry is being developed at the United Technologies Research Laboratory. In this technique, the component surface temperature is modulated at a known frequency with an external energy source such as a laser. Synchronous detection at the modulating frequency is used to measure the energy fluctuations at the surface in two or more spectral bands. The ratio of the energy fluctuations in different spectral bands is a function only of the temperature and optical characteristics of the surface. The reflected radiation component acts as a steady-state bias and does not affect the ratio of the energy fluctuations. Hence, it is possible this method could make direct temperature measurements of engine components in the presence of a large reflected radiation component. The basic scheme is illustrated in figure 19.

Using Wein's approximation to Planck's law, the spectral radiant intensity per unit area collected from a hot body at wavelength λ and temperature T is given by:

$$E(\lambda,T) = G\epsilon(\lambda)\ 2\pi \frac{C^2 h}{\lambda^5}\ \mathrm{Exp}\left(\frac{-hC}{K\lambda T}\right) \qquad (5)$$

where:
- λ = wavelength
- C = speed of light
- K = Boltzmann constant
- h = Planck's constant
- $\epsilon(\lambda)$ = surface emittance at wavelength λ
- G = geometric factor related to collection efficiencies.

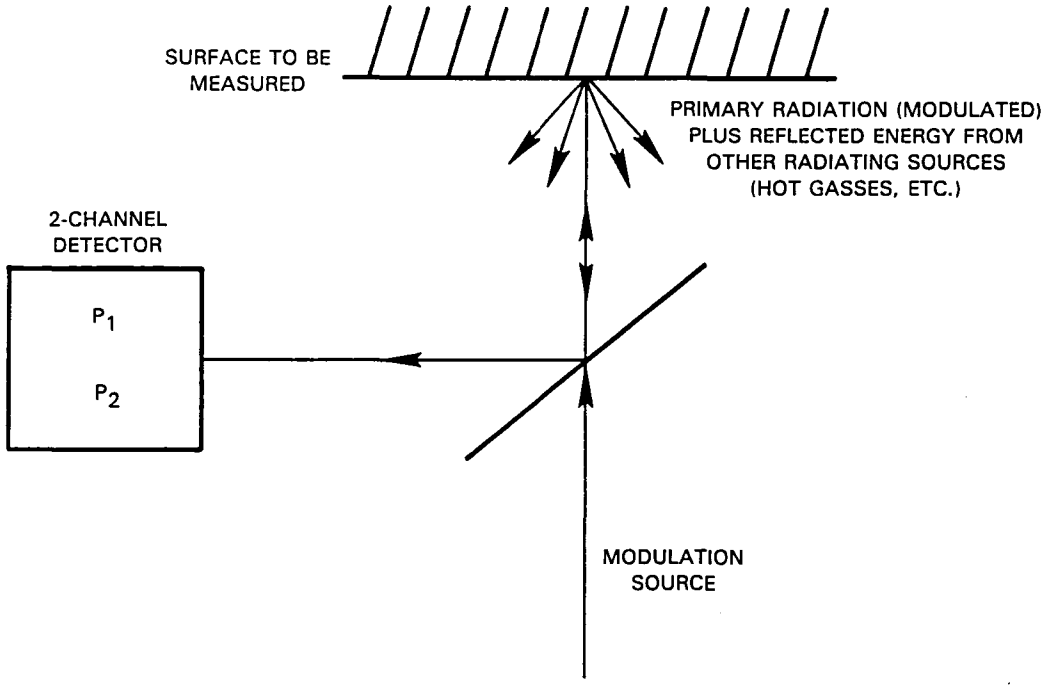

Figure 19 Active Pyrometry Concept

If power is measured in a narrow wavelength band $\Delta\lambda$ and the temperature is changed by some small amount ΔT, the change in energy radiated from the surface will be given by:

$$\Delta P = \frac{d\,E(\lambda,T)}{dT}\ \Delta T\,\Delta\lambda$$

$$\Delta P = G\,\epsilon(\lambda)\,\frac{2\pi C^3 h^2}{\lambda^6 T^2}\,e^{\left(\frac{-hC}{K\lambda T}\right)}\ \Delta T\,\Delta\lambda \qquad (6)$$

If data is obtained in two different spectral ranges, the ratio of the power in the two spectral ranges is given by:

$$\frac{\Delta P_1}{\Delta P_2} = \frac{G\,\epsilon(\lambda_1)\ \frac{2\pi C^3 h^2}{\lambda_1^6\ T^2}\ e^{\left(\frac{-hC}{K\lambda_1 T}\right)}\ \Delta T\,\Delta\lambda_1}{G\,\epsilon(\lambda_2)\ \frac{2\pi C^3 h^2}{\lambda_2^6\ T^2}\ e^{\left(\frac{-hC}{K\lambda_2 T}\right)}\ \Delta T\,\Delta\lambda_2} \qquad (7)$$

and simplifying

$$\frac{\Delta P_1}{\Delta P_2} = \frac{\epsilon(\lambda_1)}{\epsilon(\lambda_2)} \left(\frac{\lambda_2}{\lambda_1}\right)^6 \frac{\Delta\lambda_1}{\Delta\lambda_2} \quad e^{-\frac{hC}{KT}\left(\frac{1}{\lambda_1} - \frac{1}{\lambda_2}\right)} \tag{8}$$

The important point to note here is that the power ratio is independent of both the magnitude of the temperature modulation and the geometric factor G.

After choosing λ_1, λ_2, $\Delta\lambda_1$, $\Delta\lambda_2$ and determining the emissivity ratio $[\epsilon(\lambda_1) / \epsilon(\lambda_2)]$, the temperature can be calculated from the ratio of the power variations as:

$$T = \frac{hC\left(\frac{1}{\lambda_2} - \frac{1}{\lambda_1}\right)}{K\ell n\left[\frac{\Delta P_1}{\Delta P_2} \frac{\epsilon(\lambda_2)}{\epsilon(\lambda_1)} \left(\frac{\lambda_1}{\lambda_2}\right)^6 \frac{\Delta\lambda_2}{\Delta\lambda_1}\right]} \tag{9}$$

In order to verify the active pyrometry concept, a very simple experiment was undertaken at the United Technologies Research Center. Two sample types were used. One was a section of a superalloy turbine vane, and the other was an Al_2O_3 ceramic. These were heated to about 1300K by an electrical heater. The temperature of the surface was modulated slightly at a low frequency by means of a chopped CO_2 laser. The radiation from the surface was collected in two spectral regions. One region was the entire response curve of a silicon detector. The measurement in the second region used the same detector, but wavelengths longer than about 1 micron were blocked by a dielectric reflector. The signals from the detector were synchronously detected, and the ratio of the powers in the two regions was calculated. The results obtained are shown in figures 20 and 21. This experiment demonstrated that the thermal emission of a hot object can be modulated by an external radiation source and that the ratio of the modulated emission in two different spectral regions provides a monotonic indication of the temperature. No attempt was made to optimize the spectral regions used in the measurement.

Active pyrometry appears to be a viable technique for temperature measurements on ceramics in the presence of background radiation. If the intensity of the background radiation is constant, extremely good discrimination should be achievable. In a realistic situation, the background radiation will fluctuate and power density of these fluctuations in the electrical bandwidth of the detection system will lead to an error. The severity of this problem can be minimized by using a narrow bandwidth system (i.e., a long integration time on the synchronous detectors) and by choosing the modulation frequency in a region where the fluctuations of the background are small. In the experiment described above, no attempt was made to simulate a fluctuating background since the spectrum of the fluctuations would be very specific to the particular application of the technique. Since active pyrometry makes use of a narrowband electrical detection system, it is most suited for steady-state temperature measurements. In the case of transient measurements, the background discrimination would be severely degraded.

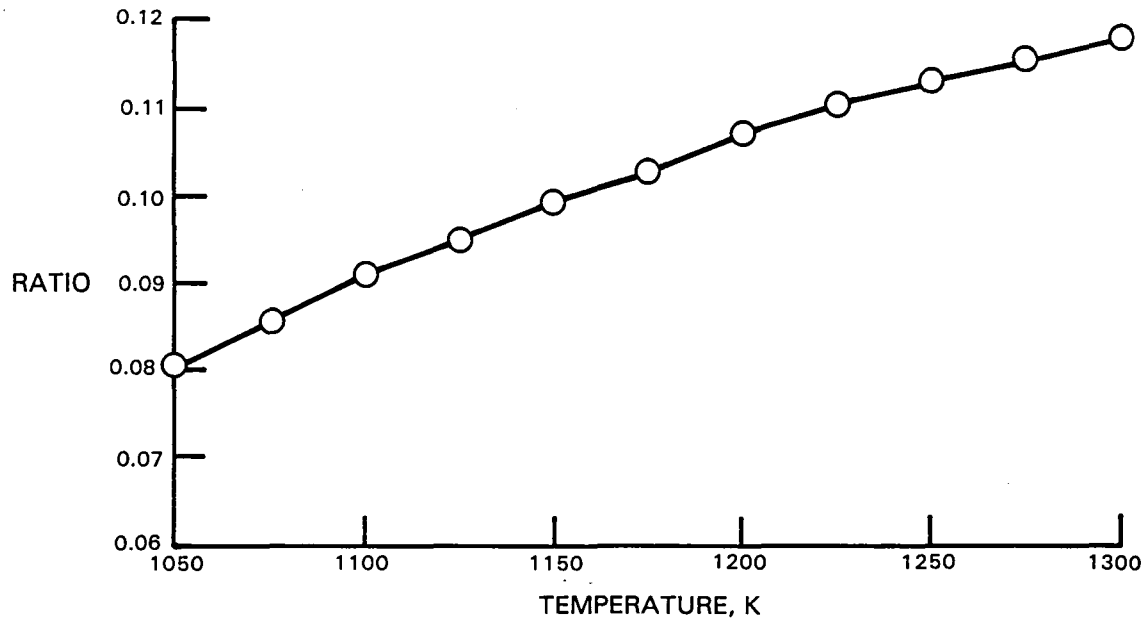

Figure 20 Active Pyrometry Results from a Turbine Vane

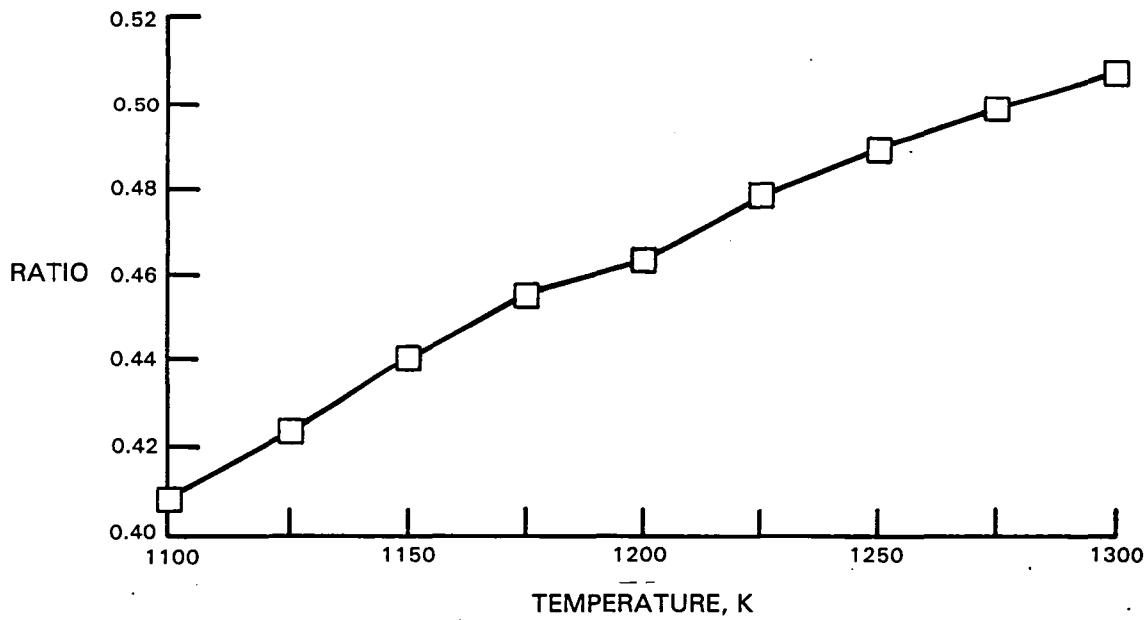

Figure 21 Active Pyrometry Results from Al_2O_3

A more advanced form of active optical pyrometry has also been proposed. In this version, the dependence on the emissivity ratio is eliminated. This version requires the availability of radiation sources at two different optical wavelengths that are capable of modulating the surface temperature. The first source is used to modulate the temperature of the component, and the modulated thermal emission is detected at the wavelength of the second source. The process is then reversed; the second source is used to modulate the temperature, and the modulated thermal radiation is detected at the wavelength of the first source. It may be shown that the ratio of the two detected powers is independent of the emissivity of the surface. It is also independent of any wavelength dependent transmission of the medium lying between the object to be sensed and the source and detector combination. The feasibility and practicality of this approach remains to be demonstrated.

This is a noncontact technique and should be usable to the melting point of the material. Since it is noncontact, materials compatibility is also no problem.

The accuracy is estimated to be ±25K under realistic test conditions. Better accuracy is attainable in the laboratory.

Active pyrometry is compatible with propulsion system environments. In its basic version, active optical pyrometry requires a means to modulate the temperature of the component and a means to collect and analyze the radiation coming from the surface. A laser is convenient to use but not the only way to modulate the temperature. The power required is of the order of a few watts (dependent on the thermal properties of the component). Potential laser sources include CO_2, Nd:YAG, argon ion, copper or other metal vapor, and excimer lasers. The laser radiation can be transported to the sensing probe by optical fibers. The collection and analysis of the radiation is fairly straightforward. United Technologies Corporation has built numerous imaging and nonimaging optical probes for NASA, EPRI and for internal use. These have been operated successfully on a variety of combustors and full-scale engines, and would be appropriate for an active pyrometer.

The life expectancy is that of the laser and the detection system and should be hundreds of hours. Spot sizes as small as 0.15 cm can be achieved.

A detector system is required to collect the radiation from the surface of interest. Data processing equipment could include storage devices and a computer for data reduction.

Probes and hardware to mount the optical system to view the areas of interest will be necessary. Optical access to the target is required. The energy to modulate the surface temperature must be transmitted through a fiber optic. There may be problems in getting enough energy through the fiber.

4.6.7 Synchronous Detection Pyrometry

In some cases, it may be possible to use the active pyrometry technique without the complexity of the active modulating source. This would be possible if there were already present periodic variations in the ceramic surface temperature (e.g., those resulting from such sources as a periodic variation in the convective heat transfer coefficient or other engine related causes). As long as the frequency band of those variations did not include significant amounts of variation in the reflected radiant heat load on the ceramic, the active pyrometry technique should be capable of utilizing those naturally occurring variations. Except for the elimination of the need for the laser source, all other characteristics of these systems would be the same as the active pyrometer discussed previously.

4.7 THERMOGRAPHIC PHOSPHORS

This temperature measurement technique involves the application of a fluorescent coating to the surface to be measured and then exciting the phosphor with a laser (fig. 22). The intensity, spectral content, and decay time of the resulting fluorescence are temperature dependent (fig. 23). Two different detection methods have been demonstrated to make temperature measurements. The first method requires that the spectral variation of the fluorescence be analyzed. The thermographic phosphors show unique variations in emission line intensities as a function of temperature (refs. 50 and 51). The second method requires that the decay rate of one emission line be measured after the phosphors have been excited (refs. 52-56). These decay rates are a function of temperature.

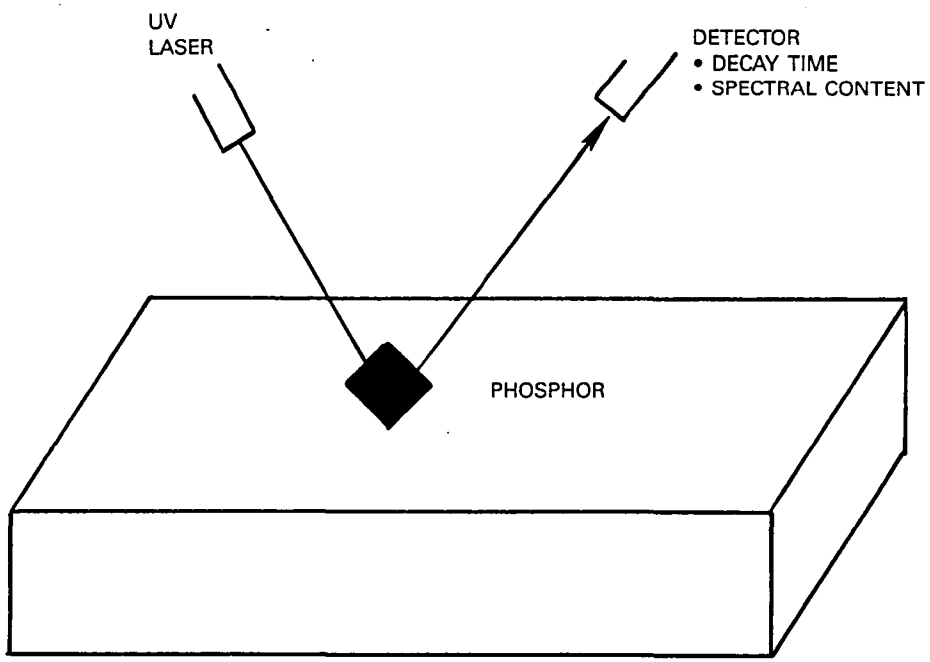

Figure 22 Thermographic Phosphors Concept

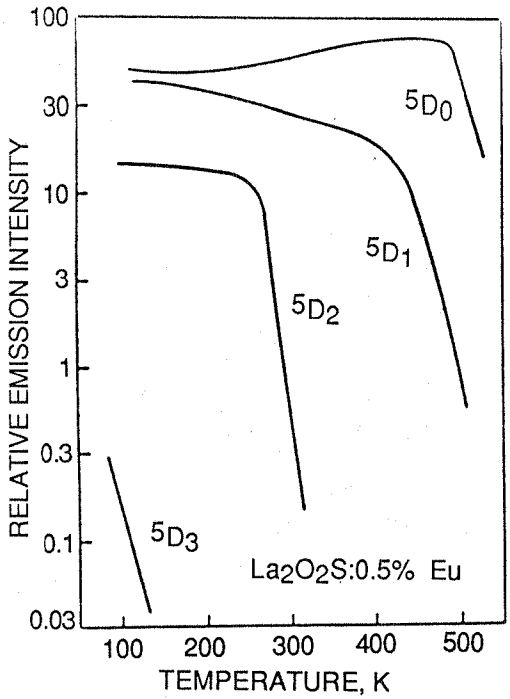

(a) TEMPERATURE DEPENDENCE FOR D EMISSION LINES OF La_2O_2S:Eu

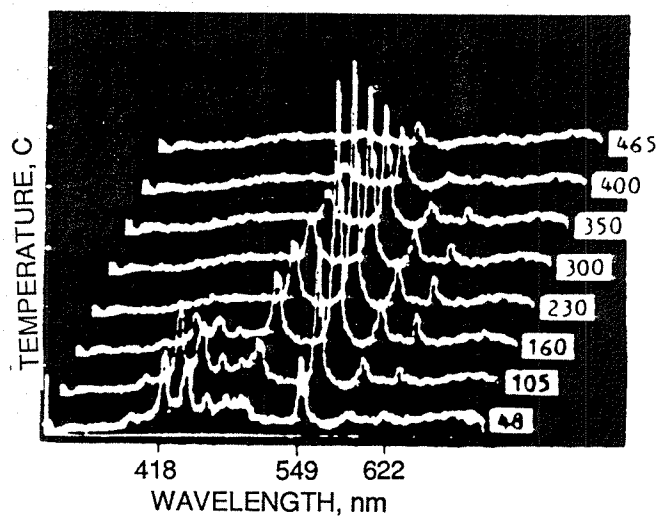

(b) VARIATION WITH TEMPERATURE OF A PORTION OF THE EMISSION SPECTRUM OF Y_2O_3:Gd

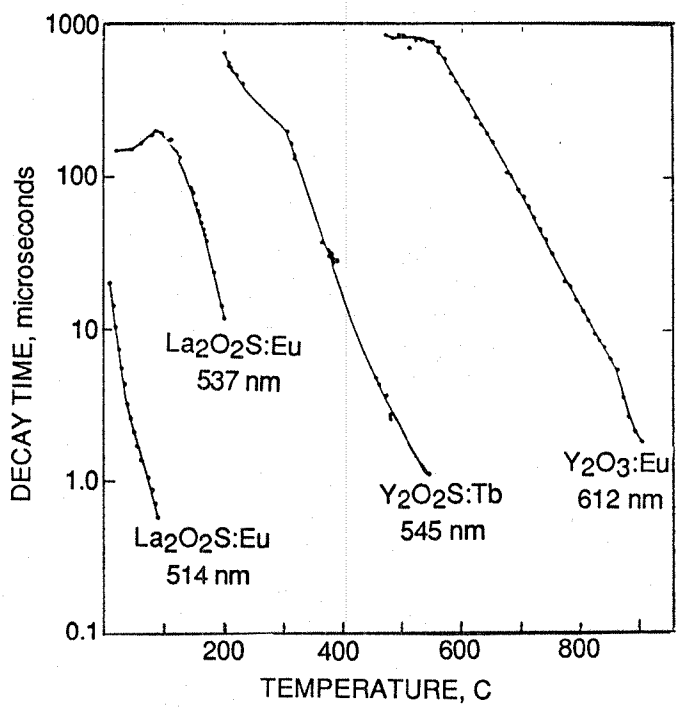

(c) CHARACTERISTIC DECAY TIMES VS. TEMPERATURE

Figure 23 Temperature Dependence of Phosphors

A test series was recently conducted in a Pratt & Whitney burner rig facility in cooperation with the Department of Energy (figs. 24 and 25). The decay rate method of temperature measurement was used. Pieces of turbine blades and vanes were coated with a NiCoCrAlY coating and then had thermographic phosphors applied by plasma spraying. The test pieces were mounted in front of an atmospheric burner rig and rotated. This test was conducted to demonstrate the possibility of temperature measurement in an environment similar to gas turbine engines. The two phosphors chosen, Y_2O_3:Eu and YVO_4:Eu, had previously been tested in the same facility to determine adherence and erosion characteristics in a hot combustion gas stream. Both had survived test conditions of 1600K gas temperatures at 0.3 Mach. Data were taken up to temperatures of 1200K. At higher temperatures, problems were encountered because the large amounts of flame present produced an unacceptable signal-to-noise ratio. This was the result of the low power excitation laser used. The problem could have been overcome had a larger laser been available. Measurements were also taken with an optical pyrometer to verify the results obtained with the phosphors. Preliminary results showed good agreement between the two measurement techniques.

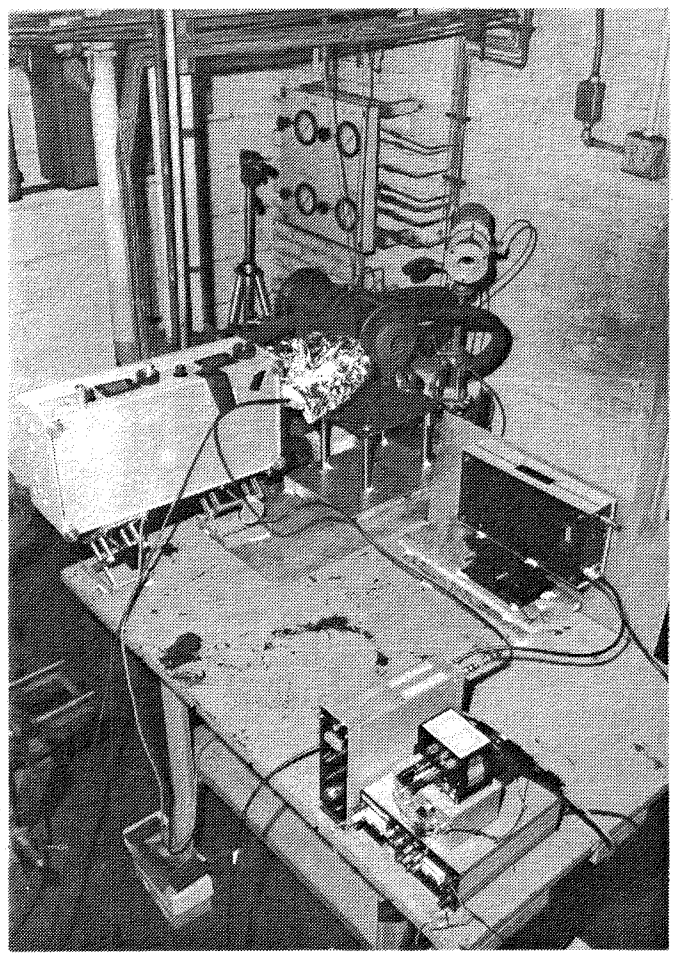

Figure 24 Burner Rig Test - Equipment Setup

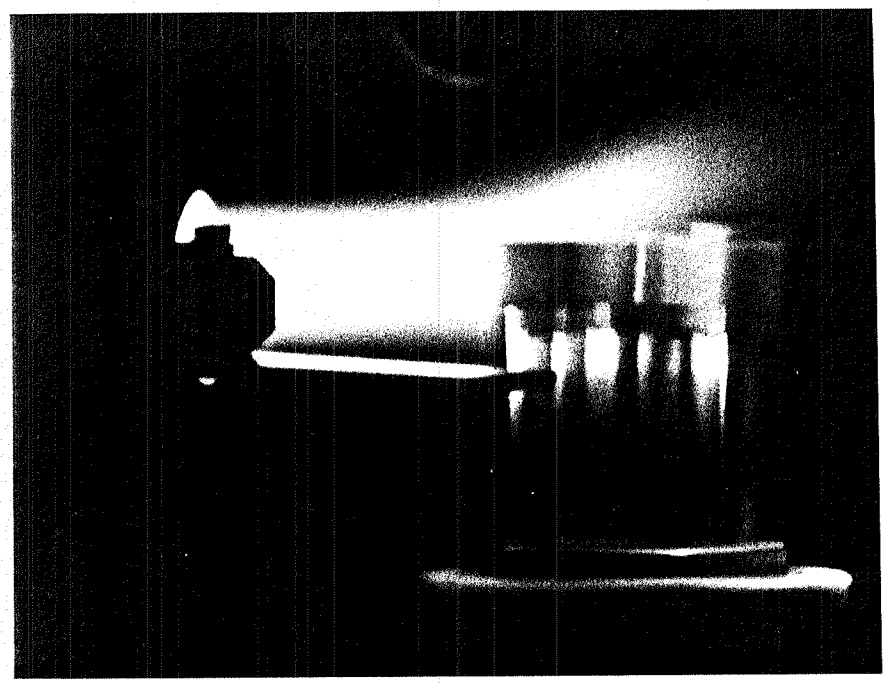

Figure 25 Burner Rig Test - Specimen in Flame

Lab tests have been conducted using thermographic phosphors, primarily Y_2O_3:Eu, up to 1500K. It is known that Y_2O_3:Eu fluoresces to 2700K, its melting point. Other phosphors are being developed for higher temperature work. The use of a sufficiently powerful laser will overcome the problem of incandescence from the surface of the target drowning out the fluorescence from the phosphors. With the proper selection of phosphors, the technique should be good to the melting point of the materials. The technique is potentially quite accurate. Laboratory testing has demonstrated an accuracy of 1% of reading at elevated temperatures. Similar accuracy should be obtainable in the engine environment.

Thermographic phosphors are compatible with propulsion system environments. Optical access to excite the phosphor and receive fluorescence is the biggest obstacle to be overcome. The optical system must have a clear line of sight to the target phosphor area. In some applications, fiber optics may be necessary to carry the laser pulse to the phosphor and the fluorescence to the detector. If the target area rotates, a speed pickup would be required so that laser and detector triggering could be accomplished. Burner rig trials on phosphor coatings show that they stand up well to the combustion environment. However, there may be erosion of the coatings in extreme environments.

The phosphors include rare-earth doped refractory oxides and oxysulfides including Y_2O_3:Eu. These materials should be compatible with ceramic surfaces and existing thermal barrier coatings.

Life expectancies of the thermographic phosphors will depend mostly on erosion of the phosphor or overcoating with carbon. Lab testing conducted in burner rigs with a gas temperature of 1700K at a Mach number of 0.3 indicate good fluorescence after 8 hours.

The target size required is a function of the luminescence of the environment as well as how much laser power is available and how strong the fluorescence is. Spot sizes as small as 0.15 cm have been used in experiments.

The most expensive item needed for this procedure is a fairly powerful nitrogen laser. This would cost approximately $20,000. Total cost for implementing a thermographic phosphor measurement system would be approximately $40,000 to $50,000 including optics, monochrometer and photo multiplier tube, recording system, digitizer and analysis system. The cost of the phosphors and the application of coatings to hardware should be negligible. It may be possible to integrate the phosphor into the thermal barrier coatings, eliminating the need for a separate coating operation.

Data are acquired through the use of a detector system that is input to some kind of storage/recorder system. This may include a transient recorder, digitizer, strip chart (for spectral measurements), or a high-speed storage oscilloscope. An analysis system is also needed. This could be included in the recording system. A Tektronix 7854 programmable oscilloscope or a separate external computer could be used. Data reduction is accomplished using pre-test calibration data.

Special techniques are required for successful applications of the phosphors to the surfaces. At this point, successful bondings of the phosphors to metals and thermal barrier coatings have been achieved. Further development may be required to apply the phosphors to some ceramics.

4.8 TWIN CORE FIBER OPTIC SENSOR

The twin core fiber temperature sensor (refs. 57-59) is a technique developed by the United Technologies Research Center. This technique is shown schematically in figure 26. In this sensor, light is conducted in a single fiber with coupled, single-mode twin cores. The optical characteristics of the fiber are configured to limit propagation to two fundamental modes: a symmetric twin-core mode and an asymmetric counterpart. The propagation constants for the two modes are slightly different leading to periodic interference along the device length. This results in complete switching of optical power, alternately, from one core to the other and back again: crosstalk. The length of the crosstalk period is the beat length. External disturbances can result in changes in both the sensor length and the crosstalk beat length. This will yield a net phase shift between the two modes at the output of the sensor. By appropriate choice of thermo-optic properties of the fiber, this principle can be used to produce a temperature sensor.

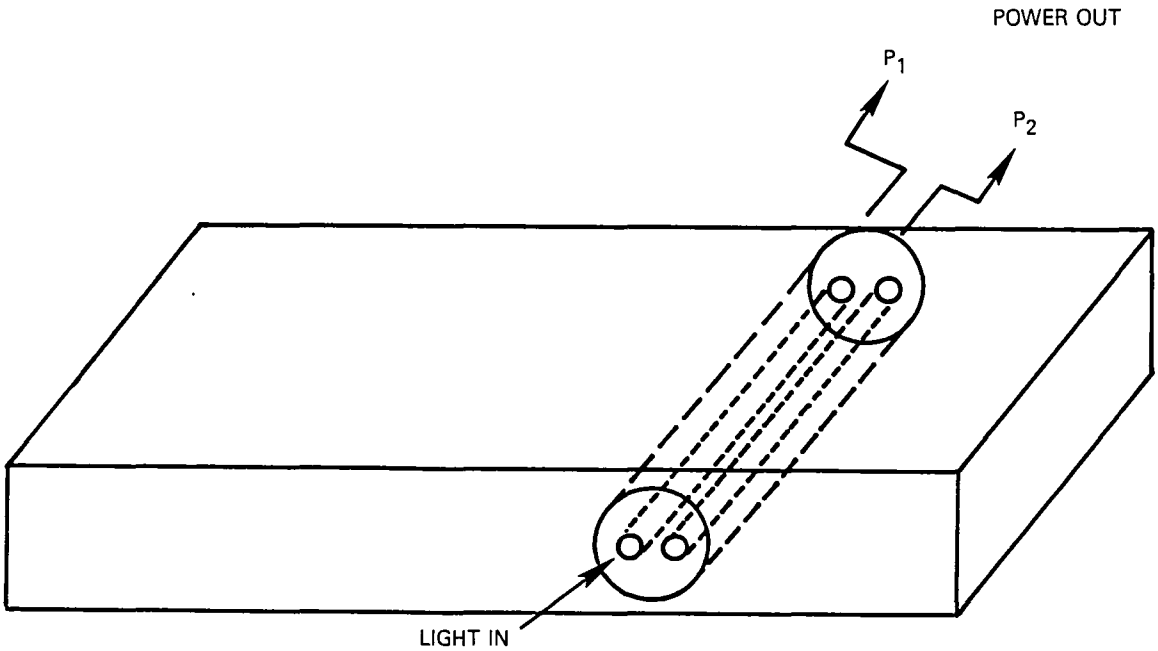

Figure 26 Twin Core Fiber Optic Sensor

A more detailed description of this sensor type is provided in Section 5.3. For reasons discussed in that section, it was felt that this sensor was more appropriate for development for strain measurement. That was partially because this technique has been demonstrated to only approximately 1000K, while other techniques for temperature measurement on ceramics have been demonstrated to significantly higher temperatures.

4.9 RECOMMENDATIONS FOR TEMPERATURE SENSORS

The three temperature measurement techniques recommended for further development are thin films, pyrometry and thermographic phosphors.

The thin film temperature sensors recommended are thin film noble metal thermocouples of Pt versus Pt-10%Rh (ANSI Type S) sputtered directly on the surface of ceramic components. This approach is limited to use on nonconductive ceramic materials, and to use at temperatures up to 2040K (melting point of platinum).

In arriving at this selection, the following alternative thin film temperature sensor approaches that were discussed above have been ruled out as being less promising on ceramics at high temperatures for the reasons reviewed here.

Thin film resistance thermometers (RT) of sputtered pure metals or dilute alloys are expected to be less accurate than thin film thermocouples (TC) because of greater sensitivity to impurities arising from diffusion or chemical reaction with materials in contact at high temperature. For example, 1% rhodium added to pure platinum increases the resistivity by 15%, but 1%

rhodium added to both legs of a Type S thermocouple changes thermocouple emf by less than 4%. Similar relationships would be expected for absorption of Si, Mg, or other atomic species present at the ceramic surfaces. The thin film RT has another drawback relative to a thin film TC, in that any resistance drift or temperature sensitivity of resistance in lead films or lead wires introduces a further uncertainty in the RT measurement.

If the thin film RT is fabricated of a concentrated alloy, then the increase in resistivity that results (order of ten times higher) suppresses lead wire problems. Accuracy is still expected to be poor because this high resistivity now produces great sensitivity to electrical shunting in insulation layers at the ceramic surface.

A thin film RT based on the changes with temperature of properties of the ceramic material itself is expected to be least accurate of all, particularly in the region near the surface of the ceramic component where the ceramic material is subject to erosion and chemical reactions with the environment. Deep within a ceramic component, the approach offers interesting possibilities, but exploitation would require fabrication of sensor leads or films as an integral part of the interior of the ceramic component. This possibility is judged to be beyond the scope of the present program because it would require study of the effect of sensor leads on the ceramic forming process, the interior integrity, and the directional properties of the component.

A thin film TC based on conductive ceramics or cermets sputtered or deposited on the nonconductive surface of ceramic components is another approach judged to be beyond the scope of the present program. No promising candidate ceramic thermocouple materials were found in the literature search. A fundamental materials development program would be required.

The thin film temperature sensor recommended is, therefore, the thin-film Pt versus Pt-10%Rh TC, sputtered directly on the surface of the ceramic components. Pt is selected because it is the least reactive of all metals even though it is known to form silicides at high temperatures. Rh is selected because it is the most stable alloy with Pt, forming a continuous solid solution at all concentrations and temperatures. This thin film TC system has been used successfully to 1250K on superalloy metal components in engines, limited by the melting point of the engine components. Qualitative tests to 1350K on LAS-glass ceramic components show that adhesion and integrity of the thin film system remains good.

The intent of the proposed program is to determine to what upper limit of temperature this existing technique can be extended. The practical upper limit is expected to lie somewhere between 1250K and 2043K. This upper limit must be determined by methodical trial and error with deposition of sputtered films on selected ceramics and exposure to incrementally increased temperatures in an experimental arrangement permitting quantitative measurement of repeatability.

The pyrometry area includes the investigation of single wavelength pyrometry, dual spectral area pyrometry, and active pyrometry. Spectral emittance determinations have shown that pyrometers in the 8 to 14 micron range are appropriate for the ceramic materials because of the high and stable emittance of the ceramics in that spectral range. Due to the high temperatures anticipated in advanced propulsion systems, it is anticipated that there may be large amounts of reflected radiation present, either from the combustion heat source or from other hot surfaces. If the reflected energy is less than 75% of the signal, it may be possible to use a variation of the dual spectral area pyrometry technique. Higher levels of reflected energy may be made tractable with an implementation of the active pyrometry techniques.

The thermographic phosphors (Laser Induced Fluorescence) technique appears to be well suited for application on ceramic materials. The phosphors themselves are ceramics and there should be minimal compatibility problems. The phosphors exhibit fluorescence up to their melting point and, hence, the technique, in principle, is not temperature limited. In addition, the technique appears usable even when there are large amounts of reflected radiation and background radiation present. The technique has been demonstrated capable of producing temperature measurements in realistic engine environments. The development work required centers around selecting the optimum phosphor, bonding the phosphors to the surface, and simplifying data acquisition procedures.

5.0 SENSORS FOR STRAIN MEASUREMENT

5.1 SURFACE MOUNTED GAGES

5.1.1 Conventional Wire Form Strain Gage

Small resistive wire strain gages are used routinely (ref. 90) in aircraft engine testing and airframe testing, for measurement of dynamic strain (isothermal short-duration strain variations) reliably up to 1250K, and static strain (nonisothermal strain variations) up to about 700K. Figure 27 shows a typical design. The sensing system consists of:

- Component surface
- Insulating layer
- Strain sensing element and temperature compensating element
- Connection to leads
- Lead installation on component surface
- Overcoats and bonding coats
- Data acquisition system.

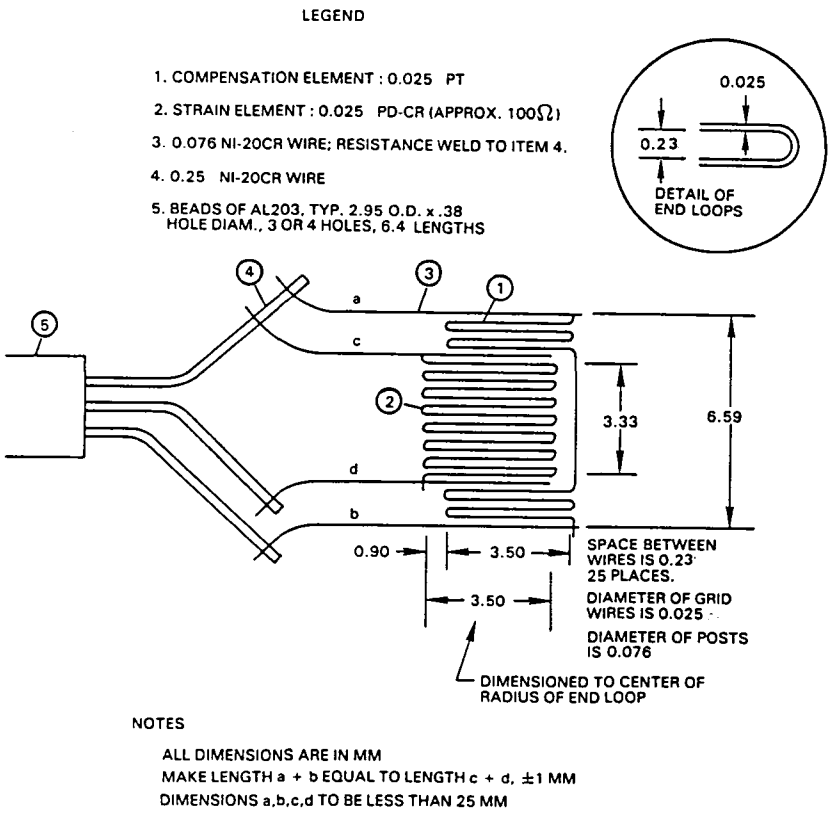

Figure 27 High-Temperature Resistance Wire Strain Gage

The difference in useable temperature range for dynamic and static strain applications stems from the different requirements on stability of the metal alloys used in the gages, discussed more fully below, after some comments on the other properties needed in the gage alloy.

The gage alloy must have fairly low tcr (temperature coefficient of resistance), ruling out any pure metals including refractory noble metals such as platinum. Yet, the alloy must have a high melting point and high stability in an oxidizing atmosphere. The only suitable alloys that have been found are the NiCr, FeCrAl, and PdCr families. These alloys form self-protecting surface oxides, and have tcr values low enough to be useful. The melting points are in the 1700K to 1800K range. These alloys cannot be expected to have useful stability much above 1250K.

To extend the use of strain gages to ceramic surfaces at higher temperatures will require developing radically new types of resistance materials, not presently available commercially in wire or foil form. Examples of such materials are the conductive-ceramic strain gage materials being studied under NASA grant at Northwestern University (ref. 91). It is not reasonable to expect that resistance gages can be developed which will meet all goals on all materials at all temperatures of the present program. There is reason to expect that resistance gages can be developed for application on the surface of each of the ceramic material types of Table I, at temperatures up to a maximum between 1600K and 1900K. Beyond 1900K, new constraints appear because of the decreasing electrical insulation resistance achievable with presently known insulation materials (Table I).

High accuracy is difficult to achieve at high temperatures in the resistance strain gage system. The measure of strain is the fractional change in gage resistance, $\Delta R/R$, due to the mechanical strain, $\Delta L/L$, in the electrical resistance of a fine-wire grid element attached to the engine component. The measurement system has been analyzed in many references, such as Perry and Lissner (ref. 92).

For accuracy in this method, there are three requirements: good strain transfer from the component surface to the strain gage element; good stability and repeatability of gage resistance, R; and an accurate knowledge of the gage factor, G.

The gage factor is related to the other properties of the gage material:

$$G = (\Delta R/R) \; / \; (e) = 1 + 2\mu + (\Delta\rho/\rho) \; / \; (e) \qquad (10)$$

In this equation, ρ is resistivity, μ is Poisson's ratio, and e is $\Delta L/L$ (strain). G is found to be about 2 for typical strain gage alloys.

Accuracy can be severely degraded by oxidation, contamination, or insulation leakage to ground, because the strains to be measured are small, typically 0.2%. The measurement is accomplished by inserting the strain gage in a conventional Wheatstone bridge circuit. The bridge is balanced initially. Changes in the output voltage from the bridge due to resistance change in the gage are then recorded.

If only rapid vibrational dynamic strains are of interest, during a period in which temperature is relatively constant ("dynamic strain"), the bridge output can be AC coupled to a fast recorder and the DC level ignored. In this case, gradual drift in the gage resistance of several percent is acceptable, since the only effect is a slight alteration in bridge sensitivity. Dynamic strain accuracy of 10% to 15% has been obtained up to 1250K in this way.

If the entire strain history is required, including gradual changes in the strain during periods in which temperature may vary widely ("static strain"), then the direct bridge output must be recorded and any gradual drift in the strain gage resistance not due to strain must be kept very small, typically 0.02%. It is for this reason that static strain measurements have not been successful so far at temperatures above about 700K with small wire strain gages. The resistance stability of the NiCr and FeCrAl alloys in fine-wire form deteriorates rapidly at about this temperature due to reversible metallurgical phase changes characterized by temperature-dependent relaxation times. The PdCr alloys are metallurgically stable but, due to a much higher tcr, require self temperature compensation to cope with the large local temperature gradients that become significant at the higher temperatures. Demonstration of temperature compensation techniques is in progress (ref. 94), but is not yet available.

The effects of contamination (change in the sensor resistivity due to alloying or chemical reaction) and oxidation (change in resistance due to loss of material) are serious for both the wire strain gages and for the thin-film sensors discussed previously, because of the large surface-to-volume ratio of films and fine wires. For example, the surface-to-volume ratio S/V for wire of diameter D, and for thin films of thickness T and width W are given by the following equations:

Wire - : $S/V = 4/D$
Film - (a) all surfaces : $S/V = 2/T + 2/W$
Film - (b) top and edges only: $S/V = 1/T + 2/W$

A few examples are tabulated below.

Wire D	μm	25	20			
Film T	μm			25	10	5
Film W	μm			25	250	250
Wire S/V	μm^{-1}	0.16	0.20			
Film S/V (a)	μm^{-1}			0.16	0.208	0.408
Film S/V (b)	μm^{-1}			0.12	0.108	0.208

Note that a 20 μm wire has S/V comparable to a 5 μm x 250 μm film.

The effect of decrease in insulation resistance at higher temperatures (shunting the gage) is more serious for strain gages than for thermocouples or resistance temperature sensors. This happens because the strain gages must be fabricated of low-tcr alloys, which are all intrinsically high-resistivity alloys. It has been shown above (in the discussion on surface-mounted temperature sensors) that insulation resistivity on the order of 10^4 times the resistivity of the sensor is required. The strain gage alloys have typically ten times higher resistivity than the thermocouple or temperature sensor alloys. This constraint alone probably limits the use of resistance strain gages to temperatures below 1900K.

The strain transfer to a strain gage may be affected by the softening of surface layers at high temperatures on ceramics. The error will be greatest for thick gage installations and stiff gage elements.

The conventional wire-form resistance strain gages are susceptible to several failure modes when exposed to the vibrations, strains, erosion, and acceleration loadings (to 100,000 G) experienced in engine hot section testing.

To provide a combination of reliable bonding to the surface and good electrical insulation, the only attachment technique successful to 1250K on superalloy blades, vanes, and structures uses a powder flame-sprayed precoat of a NiCrAl alloy (Metco 443) followed by a flame-sprayed insulation layer of aluminum oxide (Rokide H) under the gage and lead wires, and flame-sprayed layers of aluminum oxide over the installation. The overcoat also provides protection from oxidation and erosion.

To avoid delamination in service, the installation must be performed with meticulous care by highly trained technicians, with particular attention to keeping all flame-sprayed layers uniform and thin. If the total buildup exceeds about 0.4 mm, then delamination in service is likely.

Lead wire attachment is generally by tweezer welding. The leads are oriented along low-stress directions where possible (at 45 or 90 degrees to the strain gage) for best fatigue life. In rotating systems, the lead wire path is made convoluted or wavy to increase frictional retention, and leads are routed along inside surfaces rather than outside wherever possible. Unsupported jumps across radial openings are avoided.

To extend this technology to ceramic surfaces at temperatures far above 1250K, major alterations in design will be required. The ceramic surfaces are characterized by relatively soft, multiphase, and reactive oxides, nitrides, and carbides (as described in Section 3.2) rather than the single-phase hard inert alumina found on superalloy surfaces at 1250K. Development of attachment methods will require experimentation with high-temperature glassy ceramics which are compatible with this surface to achieve bonding, insulation, and protection from attack by oxidation, chemical reactions, alloying, amalgamation, and erosion.

The useful life of conventional wire-form strain gages at the elevated temperatures contemplated in this program is likely to be shorter than the life in present engine testing to 1250K, for the reasons outlined in the two preceding sections. Attainment of 50 hours average time before failure at 1900K may be possible. Failure is defined as an increase in the uncertainty of the measurement beyond acceptable limits, due either to a catastrophic event or gradual deterioration. Attainment of this goal will hinge on development of new gage element resistive materials and new coatings to provide protection against erosion, shunting, and contamination. Each of these required advances is a major challenge that is likely to require large-scale development effort by specialist teams over several years.

The total thickness of a cross-section through conventional wire-form strain gages is on the order of 0.4 mm, including undercoats, sensor, and overcoats. This is only marginally acceptable on small thin-walled structural components, and may result in significant perturbation of the strain to be measured. In addition, the thickness implies significant stiffness which may result in poor strain transfer on soft surfaces. These consequences of size would require investigation in a development program.

The size of the strain sensing region can be as small as 3 mm x 3 mm, marginally meeting the area goals of the program. Development of significantly smaller wire-form strain gages is not likely, since the smaller wire diameter required would result in poorer durability and reliability.

For data acquisition and data reduction, standard strain gage translator equipment is commercially available. The equipment utilizes resistance Wheatstone bridge circuits and closely regulated power supplies. The equipment can be recalibrated at any time during a test by applying shunt resistors or test voltages.

The sensors and lead wires cannot be readily recalibrated. To do so requires returning to a precisely-known previous operating condition of the test engine or vehicle. This is not usually possible in tests of aircraft engines or advanced vehicle structures, and is a fundamental difficulty in using conventional or thin-film resistance strain gages. The strain gage sensors and lead wires must, therefore, be conservatively designed for high stability, incorporating oversized conductors and protection from the chemical contaminations (see Sections 4.1.1 and 4.1.2) that might result in calibration drifts.

Fabrication and installation of high-temperature surface-mounted resistance strain gages is complicated, involving elaborate surface preparation, meticulous care in forming gages without over-stressing, and attachment to the surface by a series of operations to provide adherence, insulation, and protection. Finally, the lead wires must be attached to the strain gage, bonded to the components to be tested and routed to a data acquisition system. The resistance strain gages are readily used in rotating systems, through slip rings or radio telemetry.

At present, the gage alloys and insulation materials required for the high-temperature applications on ceramic components do not exist. Entirely new materials and installation processes will be required.

The critical concerns in extending the conventional wire-form resistance strain gage technique to ceramic components at higher temperatures center on the materials problems. This includes the requirement for a stable resistance element material for use at temperatures above 1250K and the need for new high-temperature insulative bonding and protective layer materials under and over the gages.

5.1.2 Thin-Film Strain Gage

A thin-film resistance strain gage can be fabricated by sputtering suitable layers of a strain gage alloy and insulating and protective materials directly on the ceramic component surface. The sensing element can consist of a single line or grid of metal or conductive ceramic or cermet. A pattern such as that shown schematically in figure 28 provides a small sensor and lead films extending to a point convenient for the attachment of lead wires by resistance welding. The sensing system is, in principal, the same as that described for the conventional wire-form strain gages (Section 5.1.1):

- Component surface
- Insulating layer
- Strain sensing element and temperature compensating element
- Connection to leads
- Lead installation on component surface
- Overcoats and bonding coats
- Data acquisition system.

At temperatures to 700K, thin-film strain gages have been used successfully in gas turbine engines and component rig dynamic strain testing (refs. 94 and 95). Active development is being pursued to extend use in both dynamic and static strain testing on superalloy components of engines and aircraft structures to 1250K (ref. 96).

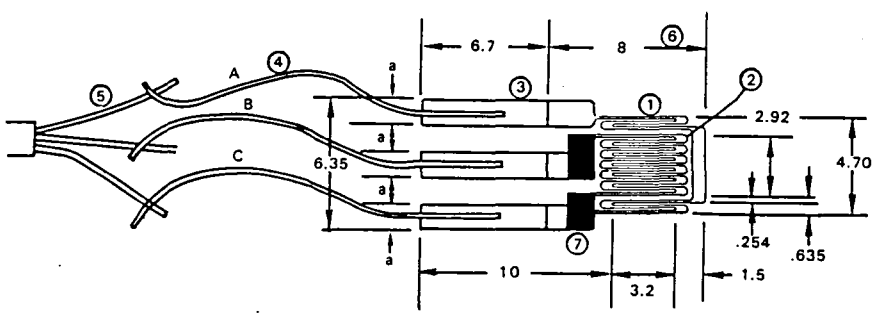

LEGEND

1 COMPENSATION ELEMENT
2 STRAIN ELEMENT
3 LEAD FILM
4 .076 WIRE
5 .25 WIRE
6 OVERCOAT
7 OVERLAP (DARK AREA)

NOTES

DIMENSIONS ARE IN MM
DIMENSION a IS 1.27
LINE WIDTH AND LINE SPACING IS .127 IN GRID PATTERN OF STRAIN ELEMENT AND COMPENSATING ELEMENT
AT GAGE THICKNESS OF 6 um EXPECTED GAGE RESISTANCE IS 50 OHMS.
LENGTH OF LEADS A,B,C < 25 MM
LENGTH OF LEADS A AND B SHALL BE SAME ± 1 MM

Figure 28 Schematic of Thin-Film Strain Gage

The thin-film approach permits applying whole new classes of materials. The sensor material need not be workable in wire form. For example, thin films of cermets or conductive ceramics, such as those under development in the NASA program at Northwestern University (ref. 91), can be produced in desired strain-gage patterns by sputtering directly on components to be tested.

A drawback in the use of thin films is the increased susceptibility to oxidation and contamination by materials in contact. This is due to the large surface-to-volume ratio.

The material properties required for dynamic and static resistance strain gage sensors and insulation layers at high temperatures were discussed in Section 5.1.1. For the fundamental reasons given there, it is not reasonable to expect that thin-film resistance gages can be developed which will meet all goals on all materials at all temperatures of the present program. There is reason to expect that resistance gages can be developed for application on the surface of each of the ceramic material types of Table I, at temperatures up to a maximum between 1600K and 1900K.

5.1.3 Capacitance Strain Gage

Displacements due to mechanical strain can be sensed and measured using the change in electrical capacitance of a suitably constructed system. If the value of the capacitance itself is measured, then a system which acts to change the effective plate area of the capacitor will provide a relation linear in displacement. If the capacitive reactance is measured, then a system which acts to change the distance between plates will provide a relation linear in displacement. Figure 29 shows four concepts analyzed at UTRC under a previous program (ref. 97); concepts A, B, and C are of the second kind and concept D is of the first kind.

Another system of the first kind (figure 30) was developed at the Boeing Aerospace Company with NASA contract support (ref. 98). This system is commercially available from HITEC Corporation. Thermal strain compensation is provided by a compensating link which supports two excitation plates, ideally made of the same material as the part being tested. The system is described in detail by Harting (ref. 99).

The system as configured uses one sensing plate and two excitation plates which form the two arms of an AC Wheatstone bridge excited at high frequency. Using the two elements in a half-bridge connection cancels many small effects which would otherwise be difficult to account for in the strain output.

According to the manufacturer, this system requires recalibration after each use and may be questionably reusable. Since it is an expensive unit, this requirement detracts from its otherwise attractive features.

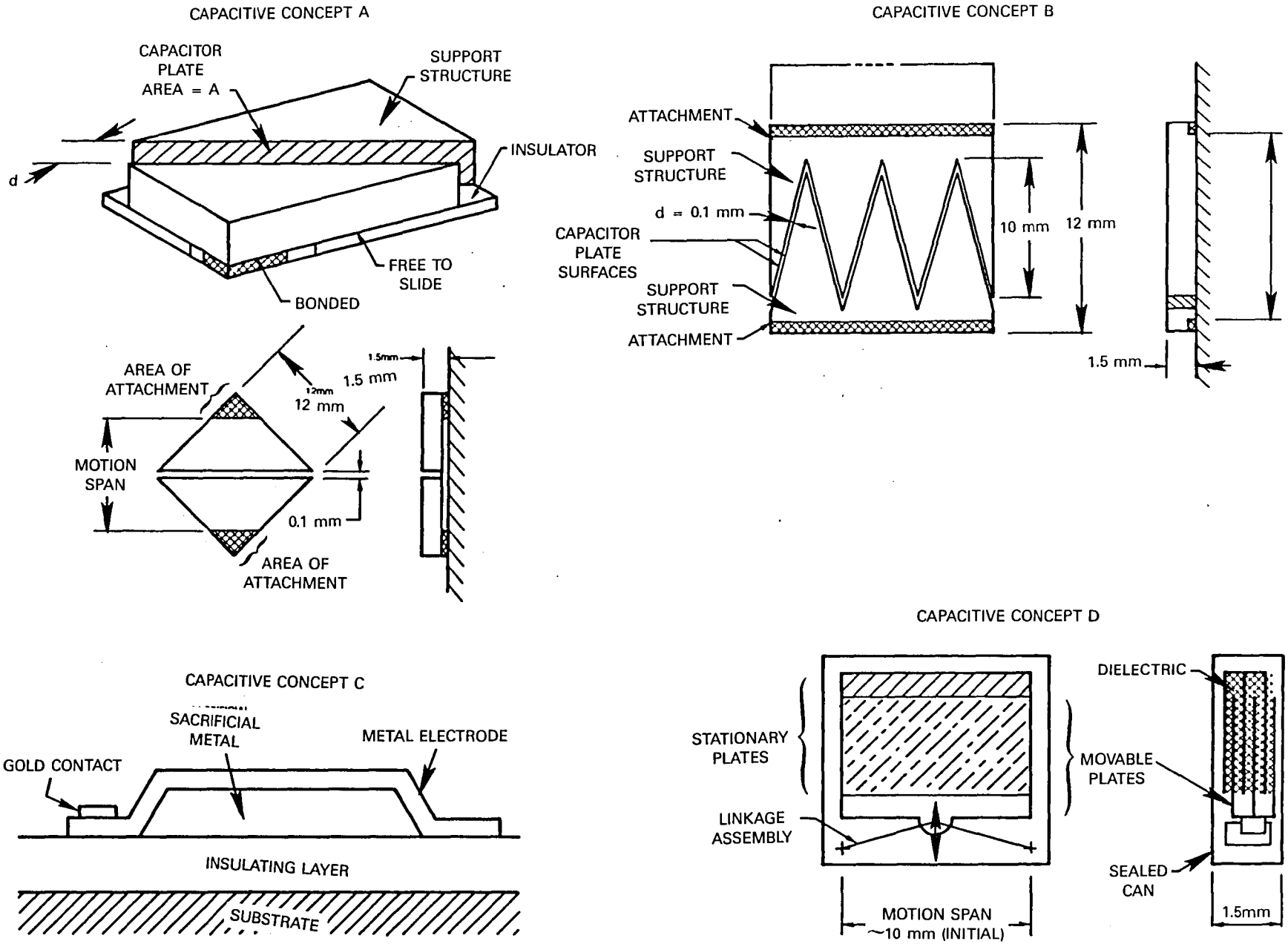

Figure 29 Four Concepts for Capacitance Strain Sensors

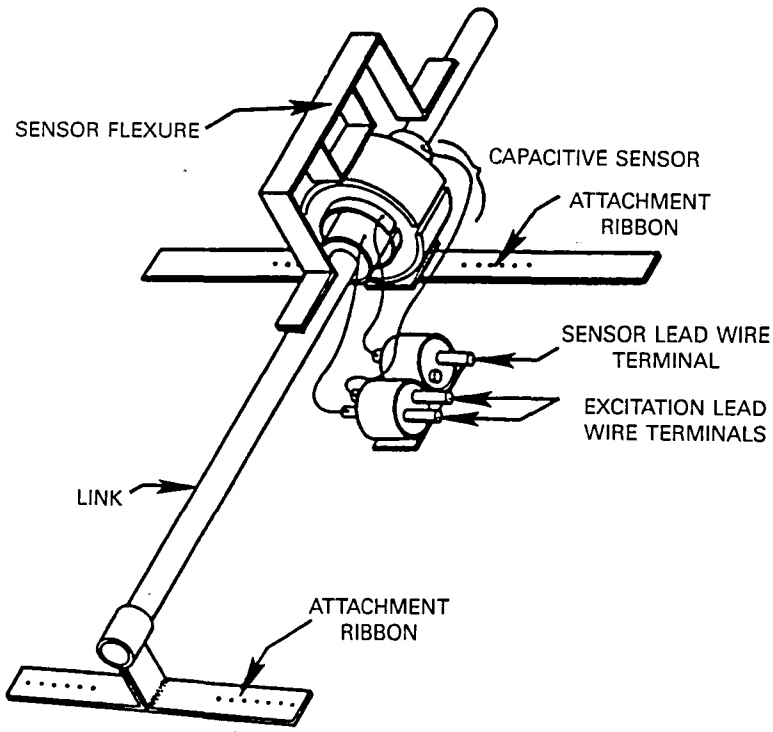

BOEING CAPACITIVE GAGE. THE GAGE LENGTH IS THE DISTANCE BETWEEN ATTACHMENT RIBBONS, ABOUT 2.5 cm

Figure 30 Boeing Capacitance Gage

A system of the second kind (reactance) is also manufactured by HITEC Corporation (ref. 100). The system (figure 31) uses refined electronics to sense extremely small changes in reactance. Although the reactance is inversely proportional to the dielectric constant of the gas medium between the plates, at elevated temperatures, up to the maximum temperature of this program (2200K), this will be a minor nonlinearity. At room temperature, however, the problem can be more severe, since humidity in the atmosphere can have a significant effect on the value of displacement readout using capacitive reactance sensors. The devices, as manufactured, are provided with guard-ring circuitry which eliminates the changing effects of fringing electric fields as the displacement changes, and extends the measurable linear displacement.

The strain measurement systems described above are presently limited to 1100K, but could be considered for measurements up to about 2000K, near the melting point of precious metals. Applying these gages at the higher temperatures would require modifications in construction materials, the method for attachment to the surface, and the method for attachment of the sensing plates to suitably shielded lead wires, and provision of thermal shielding to minimize the effects of temperature gradients. The attachment methods for ceramic surfaces, discussed in the section on resistance strain sensors, are generally applicable to the capacitance sensors and could provide a starting point for further development of capacitance gages. The use of air as the

dielectric in the capacitive gage is feasible up to the maximum temperature, 2200K, of this program, since spontaneous ionization of common gasses does not occur until temperatures well above 2200K. Also, the dielectric breakdown voltage in air at 2200K, while much lower than at room temperature, is still reasonable. The presence of gas ions at the combustor exit due to the combustion process could have a negative effect on the applicability of these sensors to the turbine engine environment.

For these reasons, the capacitive gages are not recommended for development. The units that have been developed are quite large and have a relatively long gage length. Since the gages stand well off the surface, they will perturb the aerodynamic boundary layer. This could introduce unacceptable thermal and strain perturbations in the component being measured in advanced propulsion systems. Development of suitable attachment techniques to bond these capacitive gages to the ceramic components could also prove difficult.

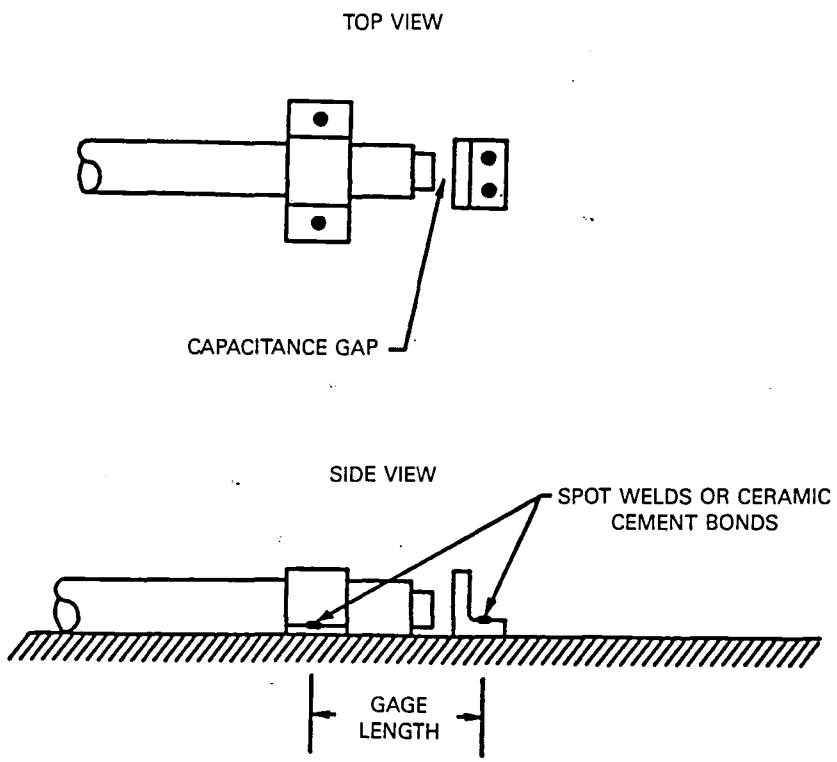

Figure 31 Capacitance Reactive Gage

5.1.4 Acoustic Guided Wave Strain Sensor

The sensing of physical variables, such as pressure and temperature using acoustic wave phenomena, has been successfully demonstrated in prior work at the United Technologies Research Center (ref. 101). The Surface Acoustic Wave (SAW) pressure sensor, for example, relies on the SAW velocity change produced when a pressure differential is applied across a thin diaphragm. Since a SAW delay line is fabricated directly on the diaphragm, the resulting change in SAW phase delay provides a precise indication of the applied pressure.

The approach considered for strain sensing is similar to that of the SAW pressure sensor. A strain-induced change in acoustic propagation velocity, or time delay, would be utilized as a measure of component strain. However, the harsh surface environment for the present application prohibits the use of an acoustic wave which propagates at an exposed surface. Surface contaminants would not only produce a time varying change in SAW time delay greater than the strain-induced effect, but would also tend to attenuate the SAW. In order to avoid effects caused by surface contaminants, another form of acoustic wave would be utilized; one which would propagate within the interior of the film coating.

One such wave is the Stonely Wave which propagates at the interface between two semi-infinite media (refs. 102-105), as shown in figure 32(a). These waves have been found to exist, however, for only a few combinations of materials which satisfy certain density and stiffness requirements. Another form of acoustic guided wave, which has been termed a Modified Stonely Wave, may also exist for a wider range of materials if a three-layer media is considered, as shown in figure 32(b). The existence of this wave would require that the central layer have an acoustic velocity lower than that of the adjoining layers. While the existence of either of the above acoustic guided wave types may be satisfied by materials appropriate to the present application, proof of existence has yet to be achieved.

In addition to the above restrictions, related to acoustic guided wave propagation, the constituent materials forming a composite coating would have to satisfy the following additional requirements:

1. Temperature stability to highest temperature of interest
2. Correct piezoelectric polycrystalline film orientation to medium one
3. Resistance to surface attack by airstream contaminants
4. Smooth surface quality allowing the photolithographic fabrication of interdigital transducer electrodes at the interface.

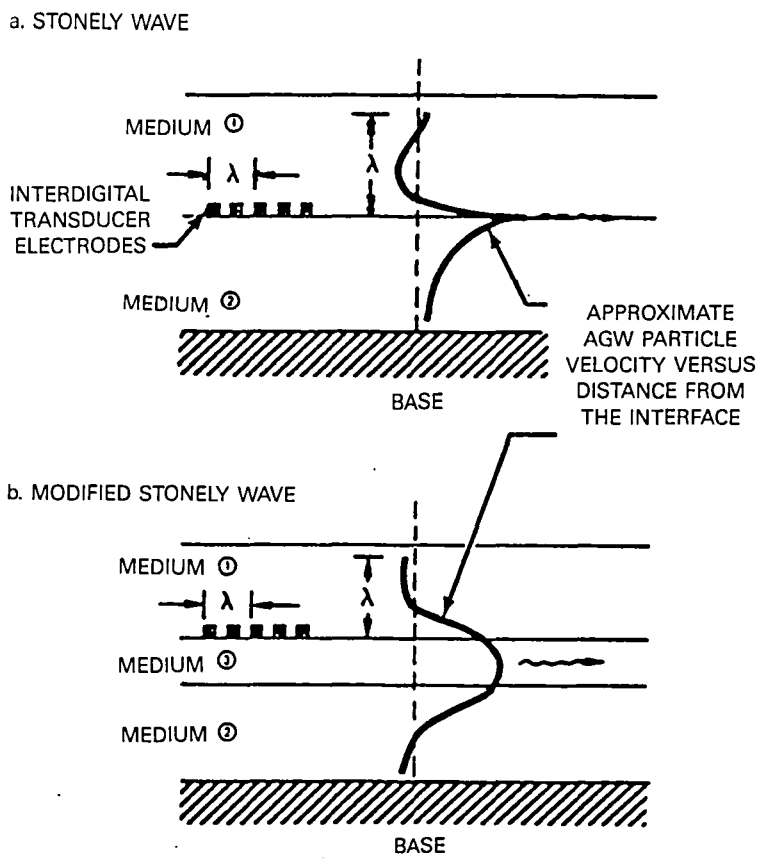

Figure 32 Acoustic Guided Wave Concept

The thickness of mediums one and two of figure 32(a) must exceed the acoustic wavelength in order to avoid surface contaminant effects for medium one and shorting out of the transducers by the underlying metal base for medium two. Medium film thicknesses are determined by the resolution achievable in fabricating the interdigital transducer electrodes.

The material combination which would have the highest probability for satisfying the above requirements over a portion of the desired temperature range is the aluminum nitride (medium one)/aluminum oxide (medium two) system. The melting temperature of aluminum nitride (AlN) is about 2470K. Piezoelectric AlN films, 2 microns thick, have been previously sputter deposited at UTRC in single-crystal form on single-crystal Al_2O_3 substrates for SAW device applications (ref. 106).

The intermediate layer, medium three, in the Modified Stonely Wave system (fig. 32(b)) would be either SiO_2 or a metal with a slower wave velocity. These systems might be formed using the same techniques as described above; however, the technology for such a system has not yet been developed. This acoustic guided wave system, as well as a stress sensor based upon this Modified Stonely Wave (fig. 33), remain unproven concepts.

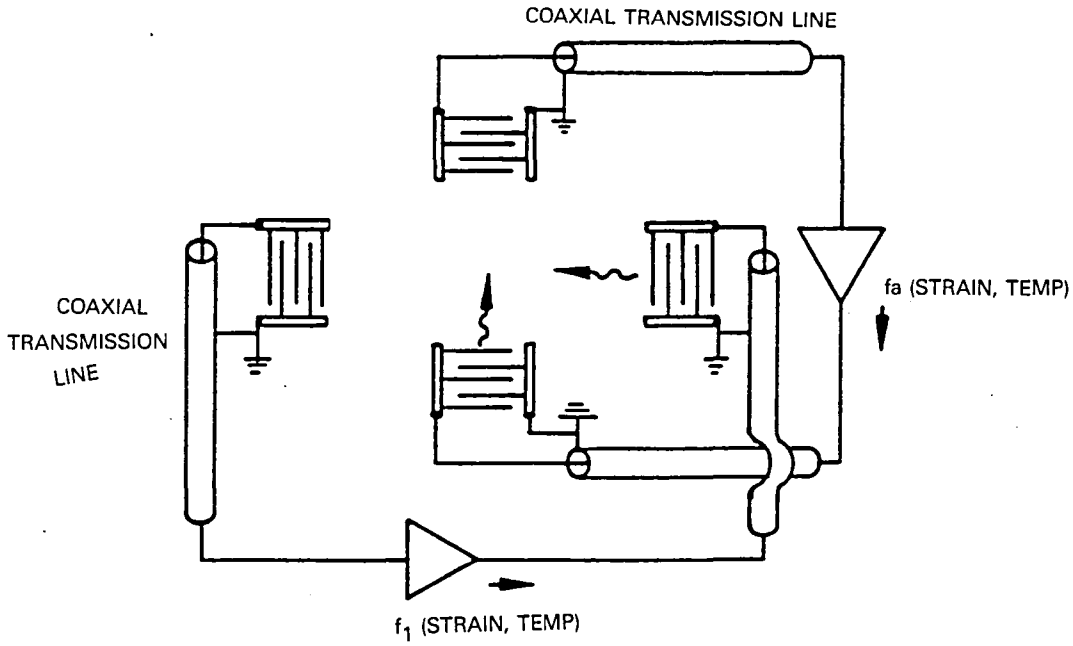

Figure 33 Modified Stonely Wave System

This technique is not recommended for further development. The techniques are immature and often unproven and much additional basic technology needs to be developed. Until the basic technology has been demonstrated in the laboratory, the risks of trying to develop sensors for the engine environment would be very high.

5.2 SUPERLATTICE STRAIN GAGE

Superlattices are layered crystal-structure "sandwiches" (heterostructure) that are made of two or more materials. Superlattice strain gages would be superlattice devices of the form A-B-A-B-A..., where A and B are the two crystalline materials (ref. 107). The layer thicknesses are of atomic dimensions. Those of interest here are in the range 20-200Å thick, with a total heterostructure-device thickness on the order of 1-10 μm. In the usual heterostructure device, which is grown with relatively thick layers, the different lattice constants (atomic spacings) of the different materials cause various atomic dislocations (including vacancies and interstitials) at the interfaces between layers (fig. 34(a)). The dislocations arrange themselves during crystal growth so as to minimize the total internal energy of the crystal. The principal difference in superlattices is that, with the extremely thin layers, the devices do not exhibit dislocations at the layer interfaces. Instead, the lattice constants in the two materials adjust themselves so that they are nearly the same (fig. 34(b)), because this minimizes the total internal energy for the thin-layer case. The stretching and compression of the lattice in the alternating layers causes electric fields to exist in the layers by virtue of the piezoelectric effect. These fields have opposite polarities. Growing a crystal in the (111) direction results in perpendicularly polarized electric fields within the layers (Figure 34(b)). Because the fields in the alternating layers point in opposite directions, they tend to cancel so that the net external field is of the order of 10^3V/cm. On the other hand, the internal electric fields are quite strong (of the order 10^5V/cm).

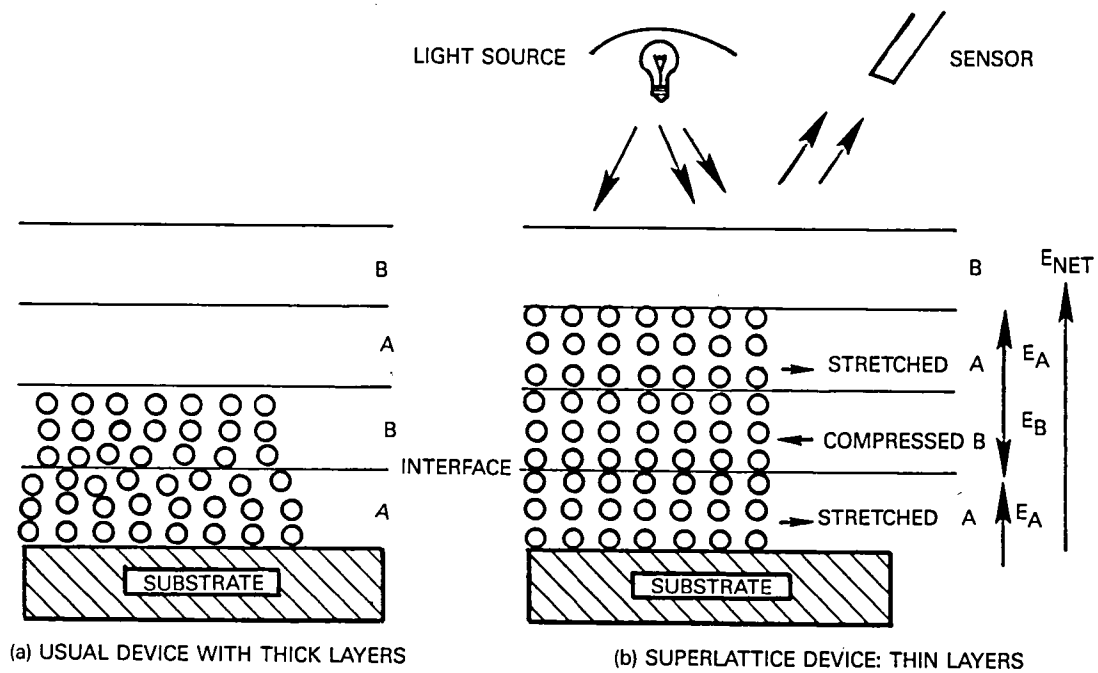

Figure 34 Superlattice Strain Gage

The optical properties of materials are nonlinear. The first term in the power-series expansion describing the nonlinearity goes as the square of the electric field. The built-in fields, therefore, have a profound effect on the optical properties. Any externally applied strain will add vectorially to the built-in strain. Because of this, it will add to the built-in electric field and will also affect the optical properties. Therefore, one can measure strain by attaching an appropriately designed and fabricated superlattice device to the surface to be measured, interrogating it with a modulated light beam, and observing the change in optical properties. Among the many optical properties that can be used are the reflectivity, birefringence, and photoluminescence. These gages, in principle, offer accuracy of approximately 1% at 5000 microstrain, sensitivity to about 50 microstrain and dynamic range on the order of 10^4 microstrain.

While these devices have not been demonstrated, the superlattice strain sensor concept offers the possibility of being a technique that would provide measurement capabilities beyond those currently existing. The sensor would be fabricated using epitaxial deposition techniques and this would require a large development program. Once the first sensor has been developed, the installation of the sensors would be comparable with the installation of a sputtered sensor. Data acquisition, although not a trivial problem, appears to be feasible under realistic test conditions.

A great deal of technology development will be required. Since these gages have not yet been built, a long (and costly) development program in the laboratory will be required for their development. This must occur before the problem of a transition to the propulsion system environment needs to be considered. This technique was considered to be too high risk to be recommended for further development.

5.3 TWIN CORE FIBER OPTIC SENSOR

The twin core fiber sensor, discussed briefly in Section 4.8, is a technique developed by the United Technologies Research Center (refs. 57-59). This technique, as recommended for strain measurement, is shown schematically in figure 35. In this sensor, light of two different wavelengths is conducted in a single fiber with coupled, single-mode twin cores. The optical characteristics of the fiber are configured to limit propagation to two fundamental modes at each wavelength: a symmetric twin-core mode and an asymmetric counterpart. The propagation constants for the two modes are slightly different leading to periodic interference along the device length. This results in complete switching of optical power, alternately, from one core to the other and back again: crosstalk. The length of the crosstalk period is the beat length. External disturbances can result in changes in both the sensor length and the crosstalk beat length. This will yield a net phase

shift between the two modes at the output of the sensor. The phase shift of the modes at the sensor output is a function of wavelength (λ), strain (ϵ), and temperature T.

$$\delta\phi = A(T,\lambda)T + B(T,\lambda)\epsilon \qquad (11)$$

where the coefficients A and B contain the device sensitivity to temperature and wavelength. A combines the effect of thermo-optic and stress-optic changes induced by temperature change. B contains the photoelastic changes induced by mechanical strain. A and B coefficients for a typical device are shown in figure 36 (ref. 59). It can be seen that, to a good approximation, the two coefficients are uncoupled. That is, they vary differently with wavelength. Therefore, if the device is operated simultaneously at two wavelengths, the two resulting phase shifts correspond to two equations with strain and temperature as the two unknowns.

Sensors of this type have been built and tested at the United Technologies Research Center (UTRC). They have been demonstrated both in the laboratory and on actual engine hardware (disk) in a static test rig. This technique has been demonstrated to 925K and the fibers currently in use have been shown to survive to 1150K. UTRC also has a program in place to develop fibers that can be used to much higher temperatures.

The transition of any such technique from the laboratory to the real engine environment requires that several practical issues be addressed. Those include preservation of sensor strength and durability in the harsh environment, connection of input and output coupling fibers, attachment of the sensor to the ceramic, and development of the supporting instrumentation. These issues are currently being addressed under various programs at UTRC. Special coatings are being investigated to preserve fiber strength by protection of the silica surface. A process that has already been demonstrated is one in which an aluminum coating is applied directly in the sensor fabrication line. With this process, the surface is hermetically sealed by the metal buffer prior to any other interaction with the surface. This process will be extended in the near future to metals with higher melting points.

Input and output coupling fibers are attached to the twin core fiber in order to isolate the gauge length. For the input side, a single-mode single-core fiber transmits power from remotely located lasers to the sensor. At the output end, additional fibers are used to collect light from the two cores and deliver the signal to detector circuitry. Since the function of these output fibers is simply to collect light, multimode fiber may be used. Finally, composite multi-wavelength transmitter/receiving systems suitable for use in realistic rotating systems have been demonstrated at UTRC.

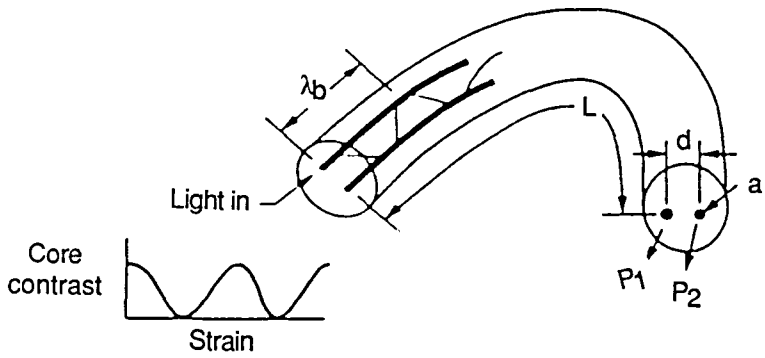

External disturbance changes L and beat length λ_b

Core contrast $(P_1 - P_2) / (P_1 + P_2)$ a function of $\phi = \pi (L/\lambda_b)$

Figure 35 Twin Core Fiber Optic Sensor

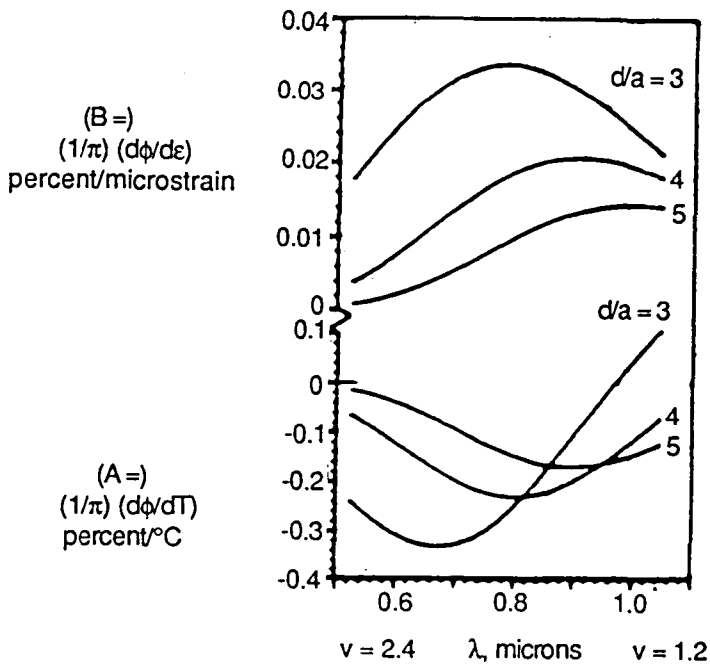

d = Spacing between fibers
a = Fiber radius
NA = Numerical aperture
L = Gage length
n_1 = Core refractive index
$\alpha + \zeta$ = Sum of expansion coefficient and thermal optic coefficient
V = $(2\pi a NA)/\lambda$ = Mode scaling parameter

L = 10 cm a = 1μm
n_1 = 1.5 NA = 0.2
$\alpha + \zeta = 100 \times 10^{-7}/°C$

Figure 36 Temperature and Strain Sensitivity Versus Wavelength

A major advantage of the twin core fiber technique is that the sensor can be embedded directly in composites. Since the load in these composites is carried mostly by the fibers, the strain in those fibers could be measured directly. This technique has been demonstrated at UTRC for low-temperature polymeric matrix materials.

While these sensors may not cover the complete temperature range of interest, they have many very desirable features and offer the possibility of significantly extending the temperature range of strain measurements on and in ceramics.

5.4 NONINTERFERENCE STRESS MEASUREMENT SYSTEM

The noninterference stress measurement system (NSMS) is a noncontact method for measuring blade tip vibratory displacement in rotating turbomachines (refs. 108-110). The measured tip displacement can be used to infer blade stresses using pretest computer modeling (NASTRAN), laboratory calibration of blade stresses versus tip deflection using forced-shaker excitation, or calibration on the rig/engine versus strain gages early in the test program.

The measurement method involves detecting the passage of individual blades using a focused light beam, synchronizing each blade signal with an external reference, and determining the angular differential between actual and expected blade position. No slip ring or telemetry systems are necessary using this technique. A once-per-revolution signal is required to provide angular reference and synchronization. Since tip sensing is used, the sensors are installed from the outside of the propulsion system, and sensor maintenance can be performed throughout a test program.

The noninterference stress measurement system was not considered a viable candidate for this application for three reasons. First, the method is restricted to rotating blades in its current applications, and is not easily transformed to other applications. Second, the first application of ceramics to rotors will be in small, high speed, hot section components. Because of the small rotor size and rigid ceramic airfoils, the tip deflection could be quite small making the accuracy of this technique questionable. Third, the conversion of blade deflection to strain requires a detailed knowledge of both the stress characteristics of the material and the geometry of the blade. The stress characteristics of the new ceramic and composite materials are not known, and a substantial amount of materials testing at high temperatures is required to produce these data. Hence, at this time the noninterference stress measurement system is not appropriate for additional development for materials testing. The technique may be applicable to the testing of ceramic rotors when there is more knowledge of the stress characteristics of the materials.

5.5 X-RAY SENSITIVE PHOSPHORS

The same ceramic materials that produce fluorescence when excited with ultraviolet radiation will also fluoresce when excited with X-rays. This property has been proposed by Dr. Eric Jordan of the University of Connecticut as the basis for strain measurements. Two small spots of the material are bonded to the specimen some distance apart as shown in figure 37. The distance between the spots is precisely determined by exciting the phosphors with an extremely narrow beam from an X-ray source. The amount of movement of the X-ray source beam required to move the excitation between the two spots on the specimen is then measured. The tension or compression of the part is measured by the change in the distance between the spots as measured by the X-ray source positioning. This technique offers advantages over other optical extension techniques in that the X-rays are not affected by thermal distortion or interference from the hot gases.

This approach has technical merit but has not as yet had any feasibility demonstration tests. The major concerns are the need for a highly collimated X-ray source to excite the phosphors and what level of fluorescence is produced. This also appears to be a technique that is better suited to laboratory testing and strength of materials work than engine test work because of the need for X-ray beam steering as well as the shielding required for X-ray sources.

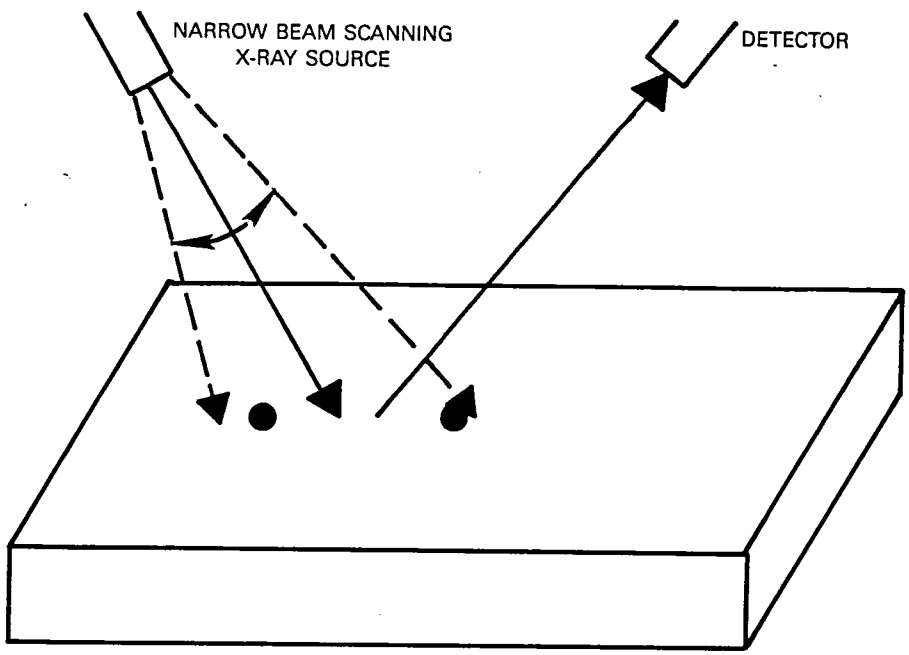

Figure 37 X-Ray Sensitive Phosphors

5.6 X-RAY ABSORPTION STRAIN MEASUREMENT

If the X-ray absorption characteristics of the ceramic materials (or applied coatings) are favorable, the X-ray absorption can be used during either steady-state or transient engine operation. X-rays, much like conventional medical X-rays, are taken of an operating engine. Image analysis techniques are then used to obtain the distortion of engine components due to engine operating loads.

This technique has been used at Pratt & Whitney to investigate internal clearance, rotor motion, etc., in running engines with metallic components. It is not felt that this technique should be pursued. For the relatively small ceramic components that are often of interest, the strain measurement accuracy of this technique is questionable. In addition, the requirement for a large powerful X-ray source and the associated facility required would make this technique extremely costly for widespread use.

5.7 NEUTRON RADIOGRAPHY

As mentioned in Section 4.5, diffraction of a monochromatic beam of neutrons could be used to measure crystalline plane spacing. When an incident neutron beam strikes a specimen, it is diffracted at an angle that depends on the distance between the planes of atoms in the crystal lattice, as shown schematically in figure 38. The plane spacing can be calculated from the diffraction angle. Since this spacing will vary as the ceramic changes dimensions as it is strained, this measurement could be used for strain determination. Using a calibrated neutron source and precise targeting of the beam, the volume of the specimen could be probed. Plane spacing resolution of a fraction of an Angstrom is, in principle, possible.

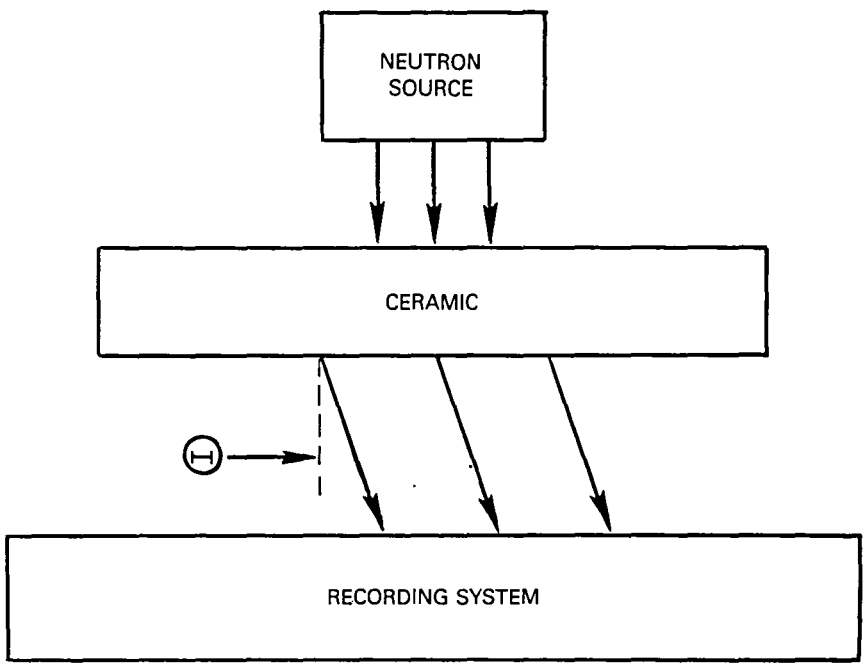

Figure 38 Neutron Radiography

A disadvantage to this technique is the variation in plane spacing due to factors other than strain, such as temperature. The main factor that eliminates this technique from serious consideration is the need for an intense monochromatic neutron source, such as a nuclear reactor, in very close proximity to the test.

5.8 MOIRE' INTERFEROMETRY

This technique, shown schematically in figure 39, involves marking the surface of the sample under study with a fine grid of crossed lines, typically from 10 lines/mm to 40 lines/mm. The grid pattern is photographed with a camera and separate recordings are made for each applied load. The resulting photographs are superimposed for readout in an optical system which generates moire' fringes from the recorded patterns. The basic equation for the relationship between the moire' fringes and strain is:

$$\epsilon = g/m \qquad (12)$$

where ϵ is strain, g is the grid spacing, and m is the spacing of the moire' fringe spacing.

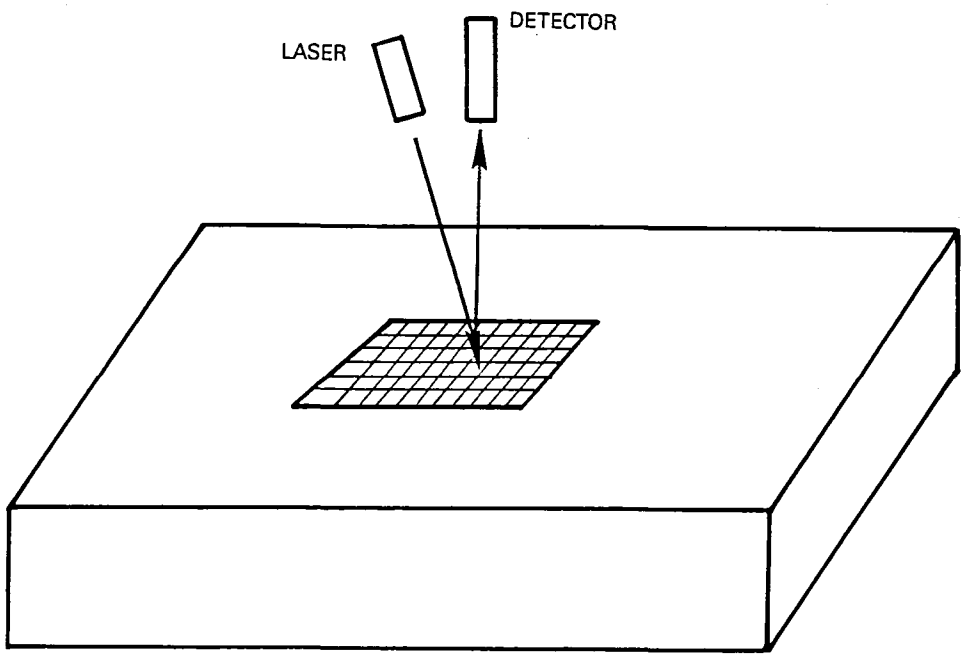

Figure 39 Moire' Interferometry

Moire' interferometry has been applied to strain measurements at temperatures up to 1650K (refs. 111-114). For this reason, it may be considered as a potential technique for strain sensing for ceramic components at high temperatures.

Temperature limitations depend upon the durability of the grid that is bonded to the surface of the object under study, and rejection of the incandescence of the hot object. The most recently reported experiments have used a nickel mesh that is cemented to the surface under study with refractory cement. Nickel melts at 1740K. However, it can be removed and the remaining dots of refractory cement can be used as targets themselves. Refractory cements exist that can withstand very high temperatures. Object incandescence can be eliminated by illumination with a sufficiently bright light source. Flash exposure could be used to achieve intense illumination of the object for a short time interval. This allows suppression of incandescence by reducing the open time of the camera shutter as well as the required lens opening. Shutters can reduce exposure times to the order of one millisecond in cameras suitable for photographing moire' patterns and would require careful synchronization to the flash illumination. Focal-plane shutters are not generally applicable with short flash exposures. The use of shorter flash illumination, such as that obtainable from a pulsed laser, would not reduce incandescent irradiation unless the shutter open time was equally reduced. The use of laser illumination, however, would permit the use of narrow-band interference filters which could greatly reduce the effects of incandescence.

The strain resolution of moire' interferometry is generally low, is obtained at the expense of large gage lengths, and depends upon the fineness of the moire' grid. For example, with a grid of 40 lines/mm, a 25 mm gage length is required to obtain a strain resolution of 1000 microstrain. Work has been done on multiplying the sensitivity of moire' by observing high-order diffraction from high-quality photographic gratings (ref. 115), but it has not been established whether this could be done with gratings photographed on objects at high temperatures. On the other hand, moire' interferometry is well suited to measurement of very large strains, as high as 10% or greater. Although heterodyne readout techniques have been applied to moire' interferometry for measurement of inhomogeneities in transparent media, and have measured phase changes as small as 1 degree (ref. 116), this technology has not been applied to strain measurement.

Moire' interferometry faces a number of problems with respect to applications in the environment of a propulsion system. The first is optical access both for illumination and observation of the part under study. The second problem is that the surface of the part under study must be in focus. For example, the depth over which a pattern of 40 lines/mm may be imaged with acceptable contrast is in the order of 1 mm. This means that the surface under study must not depart by more than 1 mm from a flat surface in order for all points to be in focus. Also, moire' grids photographed with conventional camera lenses will exhibit enlargement if the object moves toward the camera which can generate unacceptable apparent strains. Such effects can be removed only through the use of bulky telecentric lens systems. Finally, the high resolution photography required for moire' interferometry is subject to degradation by vibration and turbulent high-pressure gas flow.

The work reported with moire' interferometry at high temperatures does not indicate any incompatibility between inert cements and the ceramic surfaces.

The life expectancy of a moire' grid will be determined primarily by contamination due to dirt and loss of the grid due to abrasion. In the absence of such problems, the life expectancy of a moire' is essentially infinite.

A moire' grid is required at every point on the object where strain is to be measured. Small sections of grid can be attached at a number of locations if a continuous strain map is not required. If a telecentric lens system is required to eliminate apparent strains, the lens diameter must exceed the diameter of the area to be measured, often by more than a factor of two. A typical telecentric lens to evaluate an area 65 mm in diameter is 1 meter long and 150 mm in diameter.

The cost of implementing moire' interferometry is difficult to estimate. The cost for grid attachment is on the order of strain gage attachment. Telecentric lenses, if required, can cost in the order of $10,000. High resolution photographic plates cost approximately $5 each. A transport mechanism for photographic plates can cost in excess of $5,000. Flash lamps cost in excess of $3,000, and a pulsed laser suitable for moire' interferometry can cost from $13,000 to $20,000.

For moire' interferometry, data are acquired photographically. Facilities for handling and processing photographic plates are required. Data reduction is accomplished by overlay of the recorded photographs and measurement of fringe patterns. If large amounts of data are to be processed from such photographs, methods for automatic fringe processing are required. In this respect, the use of a heterodyne readout would be efficient.

The major special problem for moire' interferometry, in common with other optical techniques, is the need for optical access for illumination and observation of the object under study. No work has been reported with the use of fiber optic bundles for moire' interferometry. It is possible, however, that applications could be developed. Inexpensive nonimaging bundles could be used for illumination. However, for the observation link, relatively expensive imaging fiber optic bundles would be required. This approach would reduce the size and cost of the individual telecentric lens required for each bundle.

Moire' interferometry is not recommended for further development. The need to attach fine grids to the components wherever strain is to be measured, the large gage length, and the sensitivity of the technique to small surface motion make this technique questionable for use in the propulsion system environment.

5.9 HOLOGRAM INTERFEROMETRY

The primary technique involves recording double-exposure holograms between successive loads on an object (ref. 117). Fringes will be observed in the hologram reconstructions that are a measure of the change of deformation of the object for each incremental load increase. Strains and rotations of the object both generate fringes on the object surface that appear as though the object surface were intersected by three-dimensional fringe laminae. These laminae may be defined by a fringe vector, K_f, normal to the laminae with a magnitude inversely proportional to the interlamina spacing. These are related by a strain and rotation matrix, [f], to the vector, K, defined at any object point as the difference between the observation and illumination propagation vectors. The basic equation is:

$$K_f = K\,[f] \tag{13}$$

If data from three or more observations or illuminations are available, a matrix of equations may be formed which may be solved for [f].

$$[f] = [K^T K]^{-1}\,[K^T K_f] \tag{14}$$

where a superscript T indicates the matrix transpose and a superscript -1 indicates the matrix inverse.

Holography is not considered a viable technology for high-temperature strain measurement. The sensitivity of holographic interferograms to object displacements is very high, and relatively small bulk displacements are sufficient to eliminate fringes altogether. Pulsed laser holography is commonly used in hostile environments; however, this generates one interferogram that displays the differential motion of the object over a short time interval. It is not possible to obtain the multiple holographic recordings with differing illuminations, as required for strain analysis, because these would require long time intervals.

5.10 LASER SPECKLE TECHNIQUES

5.10.1 Speckle Correlation Methods

These methods make use of interference effects between speckled fields that occur when diffuse object surfaces reflect laser light (ref. 118). The speckle patterns formed by such interference will show a cyclic correlation each time the relative phase of the two beams changes by one cycle. In the simplest form of this method, shown schematically in figure 40, an object is observed along its surface normal and illuminated by two mutually coherent laser beams that make equal and opposite angles to the observation direction. Data are recorded either as double-exposure photographs, taken between incremental loadings, or concomitantly by observing interference between the field coming from the object and a photograph recorded at some initial loading condition. Surface strain generates a cyclic phase change between the two image fields. When

these two fields interfere to create a single resultant image field, the phase changes cause a corresponding cyclic correlation and decorrelation of the image field when compared to a previous field. These correlation cycles can be converted to fringes whose spatial frequency is proportional to strain. The basic equation relating fringe spacing to strain is:

$$\epsilon = \lambda / 2 x_f \sin\Theta \qquad (15)$$

where ϵ is strain, λ is the wavelength of light, x_f is the fringe spacing, and Θ is the angle between the surface normal and either of the two illumination beams.

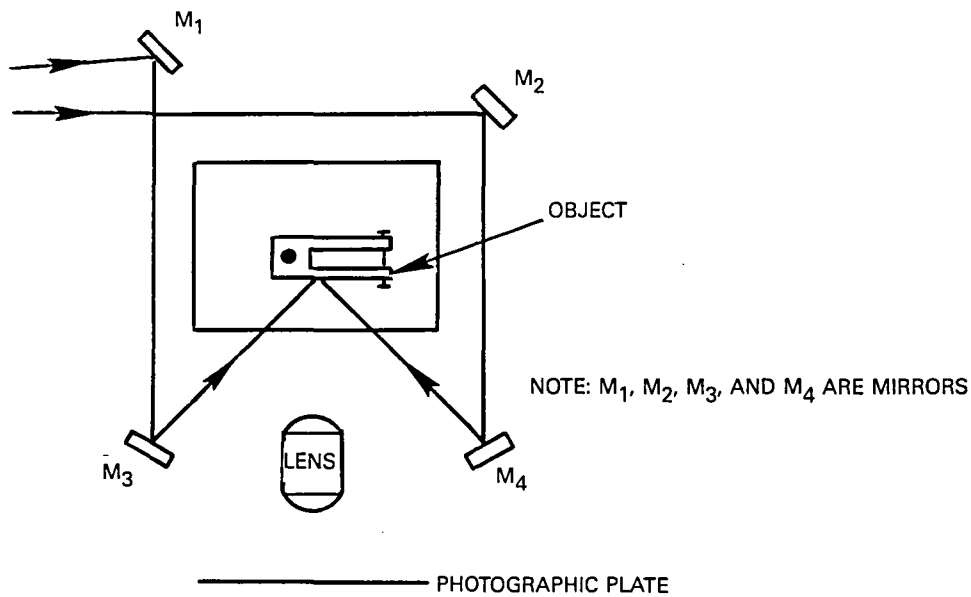

Figure 40 Speckle Correlation

5.10.2 Speckle Photography Methods

These methods make use of the fact that the laser speckles that appear in the image of a diffusely reflecting object move as if attached to the object, provided that the object is in focus. In the simplest form of the technique (fig. 41), double-exposure photographs are recorded between increments of object load. The subsequent speckle displacements are measured by means of fringes that appear in a halo of light diffracted away from the zero-diffraction order when a small region of the photograph is illuminated by a narrow converging beam of light. These fringes are analogous to those that

would be obtained from two point sources separated by the speckle displacement. The equation that relates speckle displacement, h, to fringe spacing, d_f, is:

$$h = \lambda R / d_f \tag{16}$$

where λ is the wavelength of light, and R is the distance from the speckle photograph (specklegram) to the plane at which the halo of light is observed. Strain is measured by subtracting the displacements corresponding to nearby locations on the photograph, and may be expressed as:

$$\epsilon = (h_1 - h_2)/L = \lambda R/L(1/d_{f1} - 1/d_f) \tag{17}$$

where L is the separation between the two locations where displacements are measured.

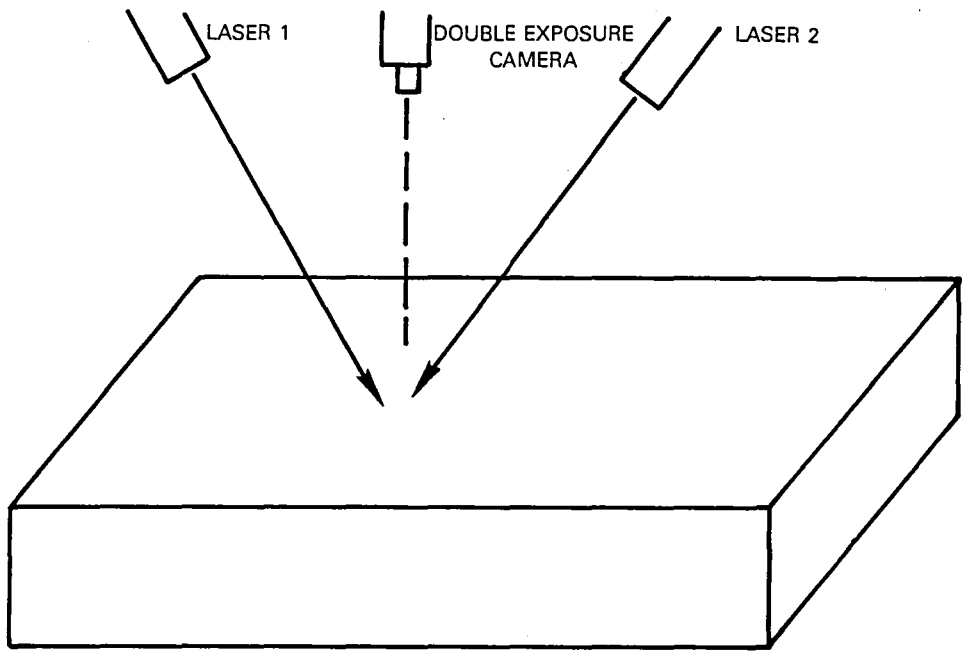

Figure 41 Speckle Photography

At present, only one laser speckle technique has been used for high-temperature strain measurement and that is heterodyne speckle photogrammetry (refs. 119-121), figure 42. In this technique, single-exposure photographs are recorded of the object under study using pulsed laser illumination.

The speckle patterns that result from imaging the object with laser light act as a random moire' pattern which can be compared from one photograph to another. A heterodyne photocomparator is used to make high precision

measurements of the differential speckle displacement between photographs of the object. Provided that the surface is in focus and observed at normal incidence, the changes in speckle displacement can be directly related to strain on the object surface. Defocus of the object surface and oblique observation can cause certain rotations of the object to appear as apparent strains; however, these can generally be controlled. Other laser speckle methods, such as speckle correlation and double-exposure speckle photography, are not suited to the hostile environment of a propulsion system because they are not tolerant of object displacements.

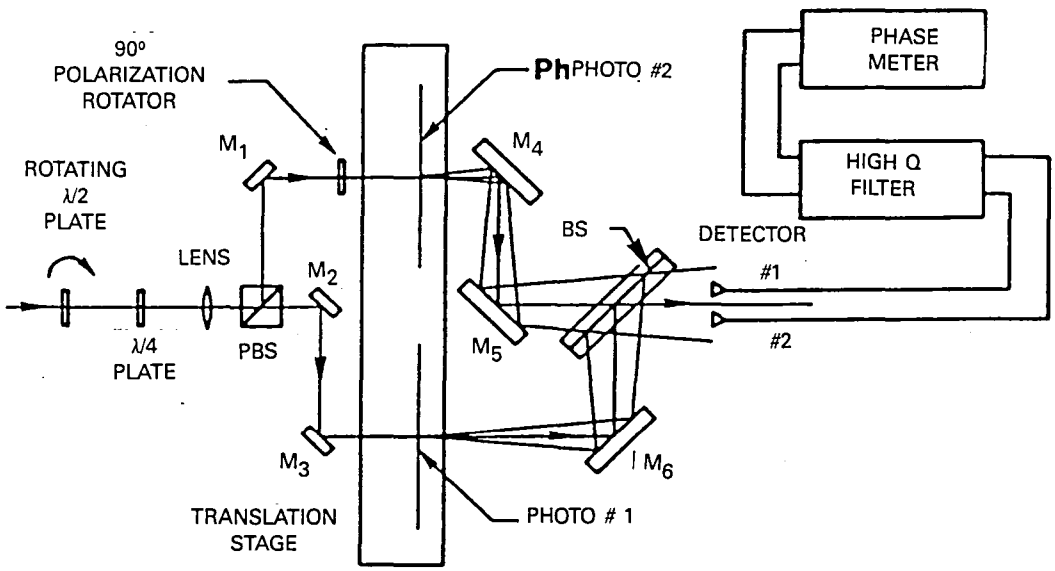

Figure 42 Interferometric Comparator for Heterodyne Readout of Specklegram Halos

The only temperature restriction required by speckle photogrammetry is that the object surface remain sufficiently unchanged so that photographs recorded at different times will possess the same laser speckle patterns. This requires that the object surface must form a stable oxide layer that is sufficiently durable to resist further oxidation. Also, the object surface must not change its microstructure by melting, diffusion, or plastic deformation. These requirements are consistent, however, with requirements on the engineering durability for high-temperature ceramics, except for the formation of compounds like SiO_2 on the surface of some ceramics.

Heterodyne speckle photogrammetry has a theoretical resolution of 10 microstrain and virtually an unlimited strain range. In practice, scintillation noise limits resolution to the order of 100 microstrain, and the range has been demonstrated for greater than 1.5% strain.

Heterodyne speckle photogrammetry has been attempted on an operating combustor (ref. 119) and on a thermal cyclic fatigue rig (ref. 120). In both cases, difficulties were found that made it impossible to apply the technique. On the operating combustor, the turbulence of high-pressure gas blurred the speckles and created random patterns of apparent strain. In the cyclic fatigue rig, buckling of the thin sample under study caused decorrelation of the speckles. Practical results are being obtained using this technique in a spin rig on a rotating turbine disk (ref. 121). A complete strain history of a section of the disk has been obtained for temperatures up to 950K and at rotation speeds up to 13,200 rpm. Laboratory demonstrations have been conducted up to 1144K. Problems of object incandescence can be eliminated by the use of color filters and short exposures to the object irradiation.

The compatibility of materials in contact with the ceramic is inapplicable since the method is noncontacting. There is no limitation on the life of this method.

This method, like moire' interferometry, is sensitive to axial displacements of the object unless telecentric lenses are used. Telecentric lenses exceed the diameter of the area investigated by a factor of two or more. A typical telecentric lens to evaluate an area 65 mm in diameter is 1 meter long and 150 mm in diameter.

Photographic plates for recording laser specklegrams cost about $5 each. Surface preparation for the sample consists of, at most, roughening the surface by grit blasting. Photographic plate transports cost over $5,000; and a pulsed laser suitable for speckle photography of stationary objects costs between $13,000 and $20,000, whereas a Q-switched ruby laser for rotating objects can cost up to $80,000. A heterodyne photocomparator for data analysis will cost in excess of $100,000.

Data are acquired photographically, and facilities for handling and processing photographic plates are required. Data reduction is accomplished by a heterodyne interferometric photocomparator which is under computer control. Data are available through the computer output ports. Accurate temperature information and data on thermal expansion are required in order to extract mechanical strain from the part under study. This is because photogrammetry measured total expansion of the object including thermal expansion in addition to mechanical strain.

Optical access is required for both illumination and observation of the part under study. Techniques utilizing fiber optic bundles have been conceived but have not been tested. As with moire' interferometry, relatively costly imaging bundles are required for transmission of observed data to a photographic plate.

While additional development will be required to transition this technique to full-scale propulsion systems, development of heterodyne speckle photogrammetry is recommended. It can be used on both rotating and stationary parts, is noncontact, and has no theoretical upper temperature limit.

5.11 MECHANICAL EXTENSOMETERS

Extensometers can provide several important advantages as a technique to accomplish many of the strain measuring goals of this program. Commercial models are already used routinely at the United Technologies Research Center (UTRC) to make strain measurements in air up to 1500K. The preferred types (MTS Corporation, Minneapolis, Minnesota; ref. 122) consist of water-cooled strain gaged flexures located in a relatively cool area. These flexures are rigidly connected to pointed ceramic rods which are spring-loaded against the sample of interest (fig. 43).

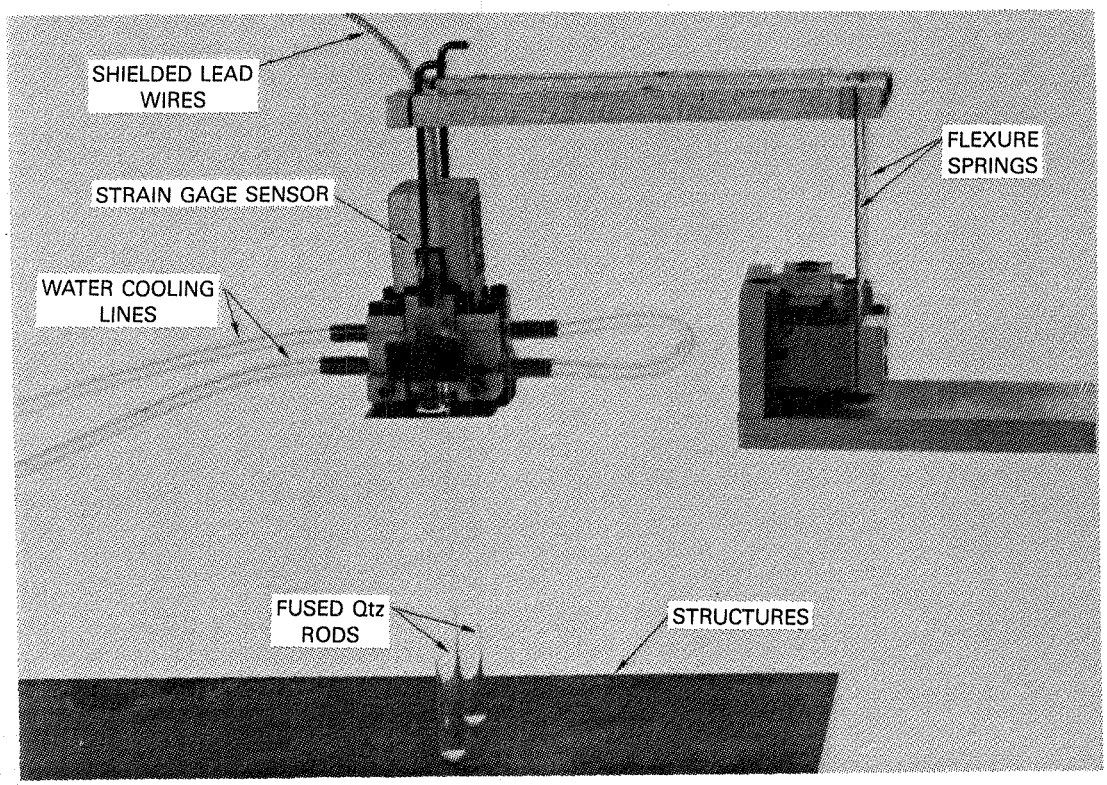

Figure 43 MTS Extensometer

The advantages of extensometer systems are high accuracy (within a few microstrain) and high-temperature capability (limited only by the rod material). Measurements up to 1800K are planned in one program described below.

The disadvantages center on the large size of the device, ruling out measurements on rotating components. Typically, a gage length of at least 6 mm is required in strain measurement, and room is needed for the two rods extending normal to the measurement surface (not permissible in small flow passages).

One important use of an extensometer in this work would be as a standard of accuracy. In any strain measurement development program, a reliable measure of the correct strain is needed in order to evaluate other strain-measuring systems. The commercial extensometer system mentioned above has a typical measurement accuracy in the range of ± 5 microstrain. The extensometers are often used in closed-loop hydraulic testing machine programs for machine control during both static and dynamic (fatigue) testing at high temperatures.

The use of these commercial extensometers is usually limited to 1500K, only because of the temperature limit of the special furnaces made for use with these extensometers. There is no fundamental reason why the single crystal sapphire rods cannot be used to much higher temperatures. The use of a small piece of a precious metal foil (Ir or Pt-Rh) between the sapphire points and a ceramic sample could be used to reduce or eliminate the possibility of chemical reactions at extremely high temperatures.

In development work at UTRC, systems of this type have been modified to involve four ceramic rods in a clamping type extensometer and used to measure axial tensile strains of ceramic composites up to approximately 1700K. When used in this manner, no side forces are involved which might cause misalignment in a loading system, which includes pivots. In another UTRC development program, this type of extensometer is being modified to measure the fatigue properties of ZrO_2 gas turbine seal materials up to 1800K in air. In this application, single-crystal sapphire measurement rods are spring loaded inside SiC end loading blocks in the axial direction. In another effort at UTRC (ref. 123), a variation of this type of commercial extensometer is being developed to measure the structural response of hypersonic aircraft components up to 1150K in air.

Due to the size and physical contact required, this technique is not recommended for development for use on ceramics in advanced propulsion systems. It should definitely be considered for the Materials Lab testing that will be required for the development of these advanced ceramic materials.

5.12 LASER EXTENSOMETRY

5.12.1 Light Beam Scanning (Zygo Corporation)

A system of extensometry has been developed by Zygo Corporation that utilizes a scanning light beam from a laser source (ref. 124). The beam is swept through an angle by a rotating mirror, and special optics have been designed to bring the beam to focus and convert the angular scan to a linear scan with no angular deviation to the beam. If a tensile specimen is designed to have shoulders that occlude the light beam, the time during which the beam is not occluded is a measure of the length of the beam. The change in length of the beam divided by the beam length is the average strain for the section measured.

5.12.2 Reflections from Indentations (W. N. Sharpe)

This technique measures the displacements of fringes formed in the reflections obtained by illuminating small pyramidal indentations made in the sample under test (refs. 125-127), figure 44. The sample is illuminated normally and the fringes are observed from equal and opposite angles. Strain generates equal and opposite motion of the fringes, whereas surface tilt generates motions in the same direction. The equation relating fringe motions to strain is:

$$\epsilon = (c_1 - c_2)\,\lambda \,/\, 2d_0 \sin\Theta \qquad (18)$$

where: ϵ is strain

c_1 and c_2 are the displacements (in cycles) of the two fringe patterns

λ is the wavelength of light

d_0 is the separation of the two indentations, and

Θ is the angle between the surface normal and the reflections.

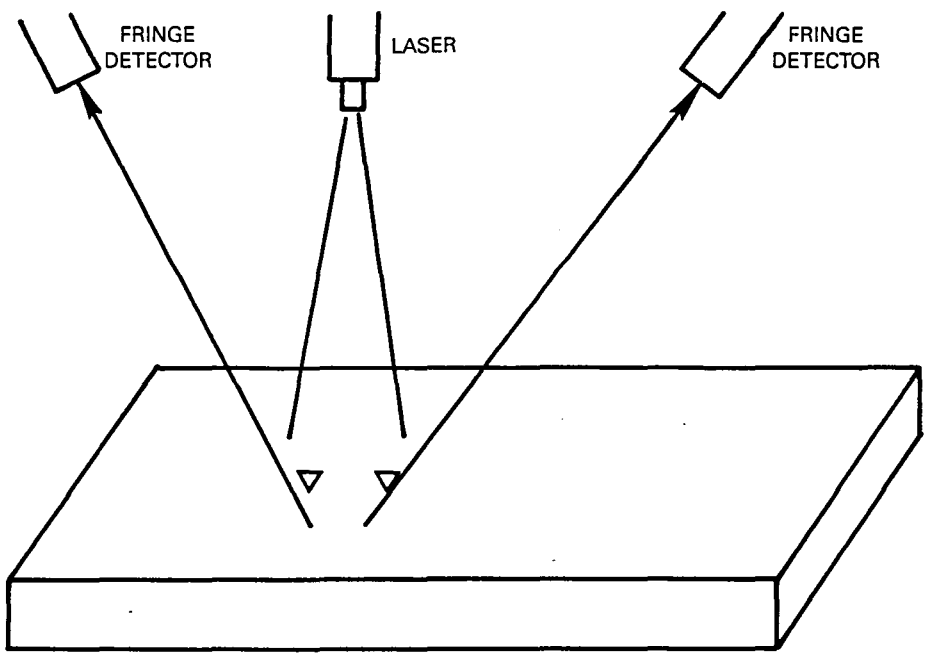

Figure 44 Reflections from Indentations (W. N. Sharpe)

5.12.3 Heterodyne Optical Strain Sensor (UTRC)

This technique is similar to the previous one except that two neighboring spots on the object are illuminated from along the surface normal (fig. 45). The combined speckle patterns from these spots are observed from equal and opposite angles to the surface normal through Fourier transform lenses (refs. 130 and 131). The patterns observed for an initial condition of the object are recorded as transparencies and relocated for use as pseudo moire' masks. A doppler shift is introduced between the illuminations for the two spots which results in a sinusoidal modulation of the light transmitted through the transparencies. Strain is measured by measuring the differential phase shift between these two signals. The equation relating strain to the measured phase shift is:

$$\epsilon = (ph_1 - ph_2)\,\lambda \,/\, 4\pi\, d \sin\Theta \qquad (19)$$

where: ϵ is strain

ph_1 and ph_2 are the changes in phase of the two signals

λ is the wavelength, and

Θ is the angle between the illumination and the observation directions.

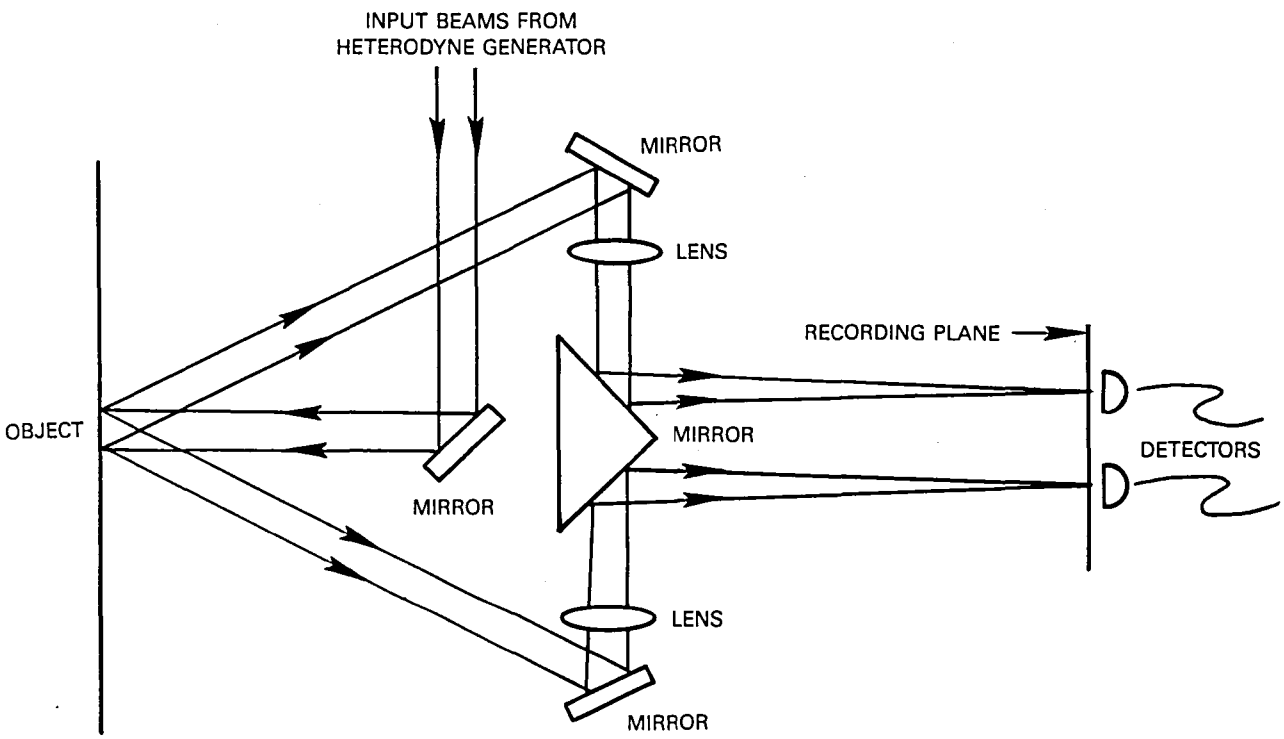

Figure 45 Heterodyne Optical Strain Sensor

5.12.4 Far-Field Speckle Displacements (I. Yamaguchi)

This technique is similar to that of W. N. Sharpe except that no marks are made on the surface and the measurements are made of motion of the speckle patterns created in the light scattered by the sample (refs. 128 and 129), figure 46. Illumination may be either along the surface normal with observation along equal and opposite angles to the illumination, or observation may be along the surface normal with illumination coming alternately from either of the equal and opposite angles. A similar equation relates strain to speckle displacements as for the previous method:

$$\epsilon = (A_1 - A_2) \; / \; 2L_o \sin\Theta \qquad (20)$$

where: ϵ is strain

A_1 and A_2 are speckle displacements

L_o is the distance from the object to the plane of measurement, and

Θ is the angle between the surface normal and the directions of the illuminations.

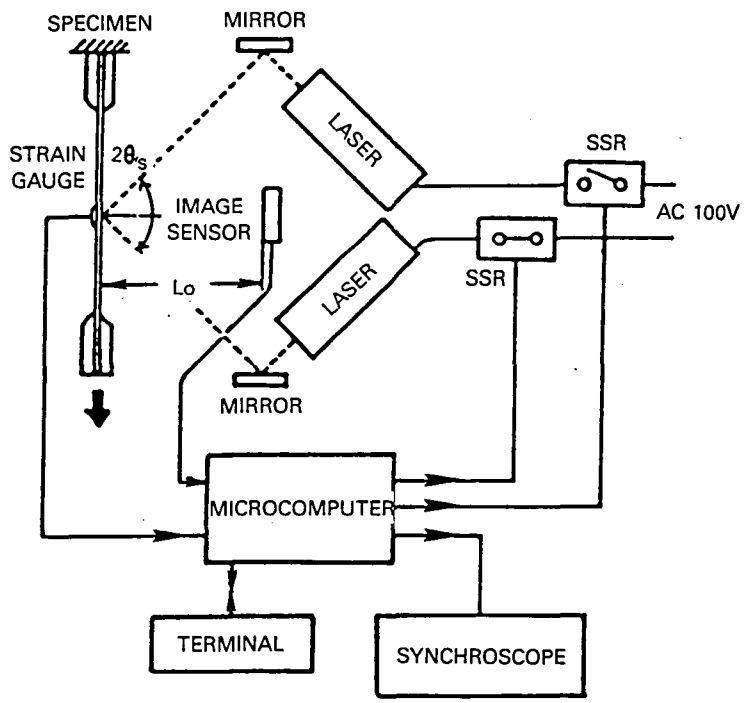

Figure 46 Far-Field Speckle Displacement

5.12.5 Heterodyne Laser Extensometry (Optra, Inc.)

Optra, Inc. (ref. 132) has developed a displacement sensing system which illuminates the object with doppler shifted light beams from two directions that make equal and opposite angles to the surface normal and observe the scattered light from along the surface normal. The observed light field is a set of speckles, all of which are modulated at the frequency of the doppler shift, but with random phases and amplitudes. No recording is used to establish an initial reference as in the UTRC system. Rather, the residual modulation of the sum of the speckles illuminating the detector is measured. The phase change of this signal is related to position change of the object surface to within an error tolerance which is determined by the statistics of the speckles. A pair of such displacement sensors may be used to measure strain by measuring the difference between displacements at nearby locations.

Although most of the techniques of laser extensometry have been utilized for high-temperature strain measurement (refs. 124-133), none are suitable for use on ceramic components in propulsion system environments. Laser extensometry systems are all subject to errors due to noise from vibration, and from large bulk displacements of the part under study. Introducing these systems into the propulsion system would also be very difficult. These systems are generally applicable to laboratory test measurements.

5.13 RECOMMENDATIONS FOR STRAIN SENSORS

The two techniques recommended for further development for strain gage work on ceramic materials are variations of the optical speckle technique and the twin-core fiber optic strain sensor. These techniques appear capable of being developed to the point where they can produce valid strain measurements and also are amenable to the harsh environmental conditions associated with the advanced propulsion systems.

The speckle techniques are noncontact and are well suited to the high-temperature applications of the ceramics. The technique has been shown to be capable of the required accuracy. One area requiring further development is an investigation of the ceramic surface properties at high temperatures. If the surface becomes glassy and flows, the speckle pattern may be associated with movement unrelated to strain. If the glassy layer becomes transparent, it then indicates that the movement measured by the speckle is internal to the component and it complicates the interpretation of the measurement. Another development area is the minimization of the optical distortion caused by the hot gases.

The twin-core fiber optic strain sensor offers the opportunity to directly measure the strain in the fibers of a composite material. In advanced composites, the load is carried by the fibers which are only weakly bonded to the low strength matrix materials. This allows microcracks to propagate through the low strength matrix without damaging the load carrying fibers. The twin-core fiber optic sensor could be embedded into the composite during fabrication. The strain on the sensor would then directly measure the strain seen by the load bearing fibers. The fiber optic sensors have been demonstrated in surface applications as well as in low-temperature composite materials. They have been shown to have sufficient resolution and accuracy. Development is required to increase the temperature capabilities of the fiber optic sensors.

6.0 SENSORS FOR HEAT FLUX MEASUREMENT

Ceramic components for advanced propulsion systems are required because the high temperatures in those systems provide an environment in which superalloy components cannot be adequately cooled without unacceptable system performance penalties. It is anticipated that the ceramic components will require much less cooling and in many cases will be uncooled. The heat flux into the components becomes smaller as the cooling is decreased, and the measurement of the heat flux becomes more difficult. For uncooled hardware, the heat flux into the component is only that required to balance the losses, and the measurement yields little useful information for improving hardware design, except for transient data.

For heat flux measurements on uncooled ceramic components, transient techniques would, in general, be more appropriate than steady-state techniques because of very low heat flux at steady state. To get sufficient output at very low heat flux (which implies very small temperature gradients across a thermal barrier) the steady-state sensors would have to be made either very large in area or very thick. Both these alternatives are opposite to the directions required to obtain the data needed to design advanced propulsion systems.

6.1 TRANSIENT TECHNIQUES FOR HEAT FLUX MEASUREMENTS

6.1.1 Slug Calorimeter Measurements

A slug calorimeter, shown schematically in figure 47, is a mass of known size and physical properties that is embedded in the surface of the ceramic component. The slugs are, generally, thermally isolated from the component, but in the case of the monolithic ceramic components, the thermal conductivity of the ceramic is low enough to produce inherent thermal isolation. The sensor is fabricated by installing a slug of material with known mass, dimensions and specific heat into a hole or well in the component. For lower temperature applications, it is common to use a metal, such as copper, for the slug. In this instance, it would be more appropriate to use a higher temperature material such as platinum or another ceramic for the slug that has a significantly higher thermal conductivity than the ceramic component of interest. The temperature of the slug would be measured during engine transient operation either optically with pyrometry or thermographic phosphors or directly with a thermocouple or resistance thermometer. The heat flux is then calculated according to the equation:

$$\frac{Q}{A} = m\ Cp\ \frac{dT}{dt} \qquad (21)$$

where: m = mass of the slug
Cp = specific heat of the slug
dT = temperature rise
dt = change of time.

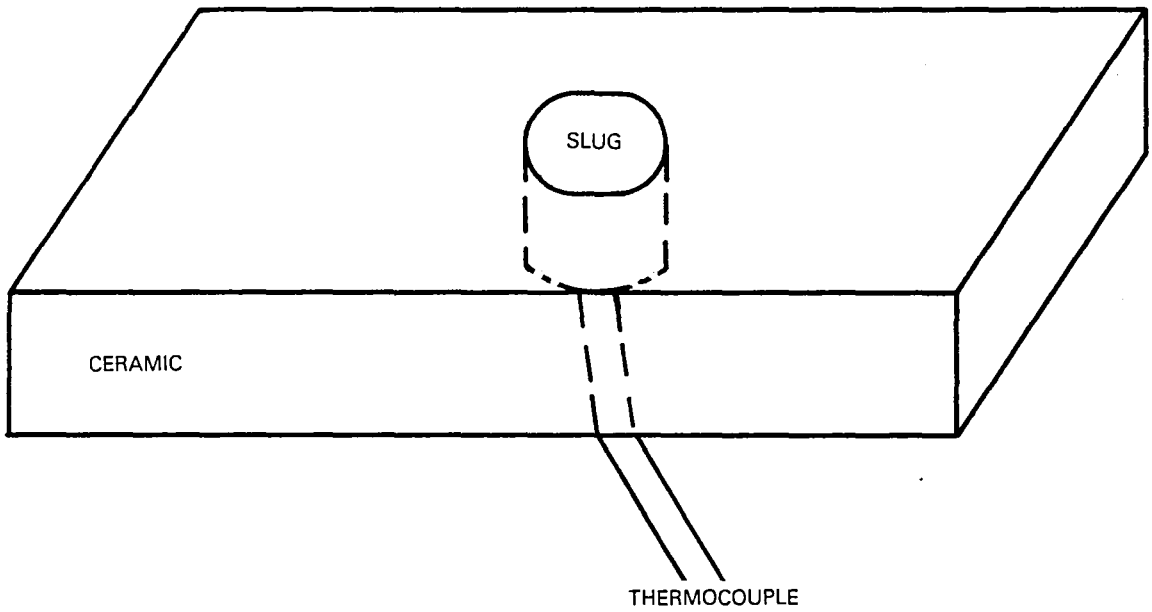

Figure 47 Schematic of Slug Calorimeter

6.1.2 One-Dimensional Transient Sensor

Another type of transient sensor is the one-dimensional transient heat flux sensor. This is a sensor that can be embedded in the wall of a component. The sensor is thermally isolated from the component.

A thermocouple or resistance thermometer is applied to the front face of the sensor surface and tracks the time-temperature history. Considering this sensor as an insulated rod, the heat flux can then be calculated using the one-dimensional conduction equation as the heat flux to the sensor is changed.

Figure 48 shows a typical one-dimensional transient heat flux sensor design that could be used on a metal component. For a ceramic component that is an electrical insulator, this design can be greatly simplified. The ceramic itself can be used as the sensor body and all that is required is a thin-film thermocouple or resistance thermometer on the ceramic surface. Figure 49 shows such a simplified sensor. For applications in areas where the temperature will exceed the useful range of available thermocouple or resistance thermometer materials, the time/temperature history of the hot side of a ceramic one-dimensional transient heat flux sensor could be recorded by optical pyrometry or other optical noncontact means.

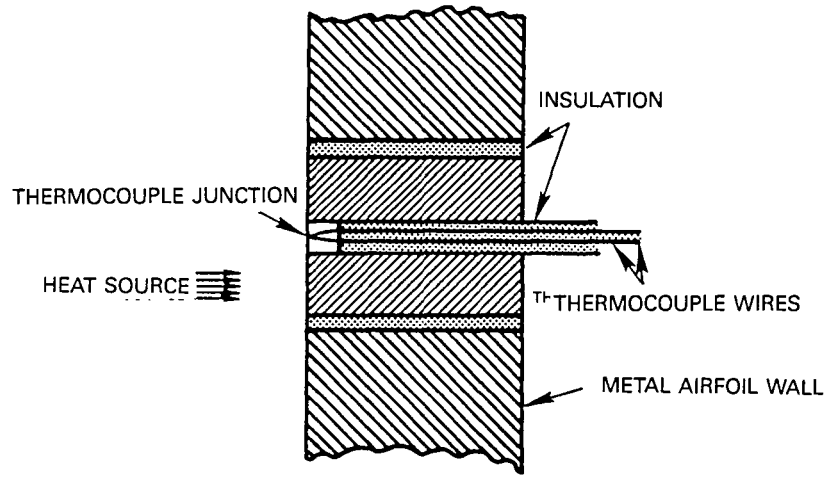

Figure 48 Schematic of One-Dimensional Transient Sensor

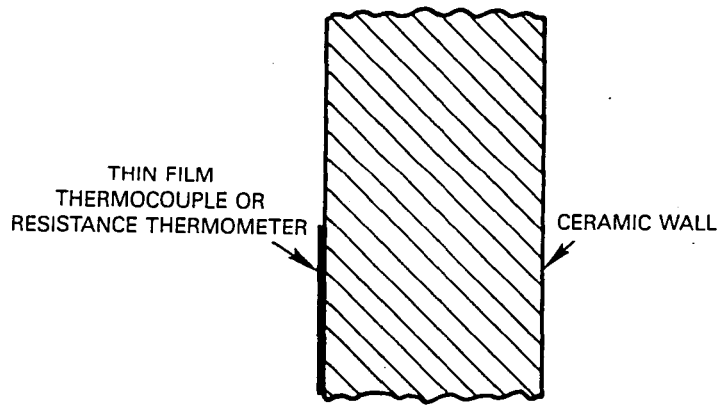

Figure 49 Schematic of One-Dimensional Transient Sensor for Ceramic Component

A variation of this one-dimensional technique, shown schematically in figure 50, has been used extensively (refs. 198 and 199) for testing of turbines in a shock tube facility. The gages consist of a thin film (approximately 1000A) of platinum painted on a pyrex substrate. A coating of magnesium fluoride is deposited over the gage to protect the platinum element against abrasion. These sensors are then mounted in the component of interest. The thin film of platinum, with a resistance of approximately 100 ohms, is used as a resistance thermometer. The response time of this sensor is extremely fast (about 10^{-8} seconds). These are, therefore, effectively surface temperature sensors with no time lag. For test times on the order of a few tens of milliseconds in a shock tube, the pyrex may be considered a semi-infinite heat sink. The heat flux may be determined from the one-dimensional transient conduction equation. High-temperature versions of these sensors have been produced using silica rather than pyrex for the substrate (ref. 150).

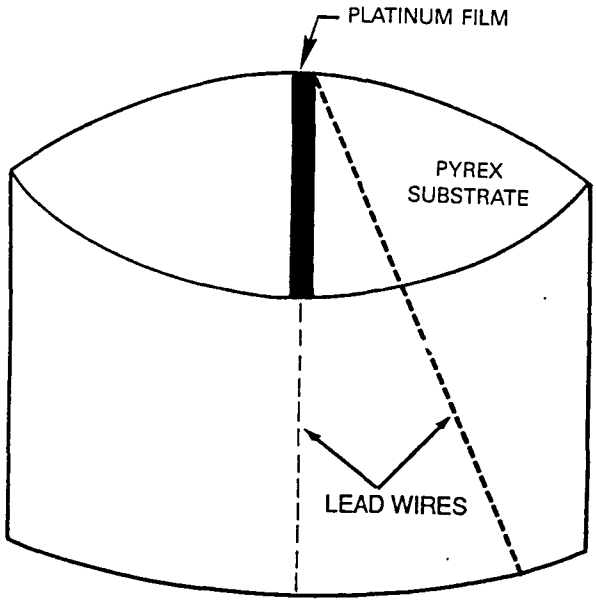

Figure 50 Variation of One-Dimensional Technique

The major problem with the use of transient sensors for turbine engine testing is to create a transient condition within the engine that is sufficiently fast to produce valid heat flux data while at the same time sufficiently slow for the engine to be at steady-state conditions. This, coupled with the fact that heat flux measurements from uncooled hardware are of limited engineering value, has led us to eliminate transient techniques from the list of measurement techniques to be considered further.

6.2 DYNAMIC STEADY-STATE SENSOR

An interesting extension of the one-dimensional transient sensor involves measurement of the dynamic temperature variation under "steady-state" operating conditions (refs. 40 and 151). In this application, the periodic temperature variation of the hot side free stream gas is determined using fine-wire thermocouples or, for higher temperature gas streams, advanced techniques such as the optical fiber thermometer developed by the National Bureau of Standards (NBS). The hot side temperature of the component, such as a turbine vane, is also measured by either a thin-film thermocouple, resistance thermometer, or by noncontact optical means.

The heat transfer coefficient can be determined by a comparison of the relative amplitude of the periodic temperature variation in the free stream gas temperature and the surface temperature fluctuation. It can be shown that the relative amplitude of the two temperature oscillations is given by:

$$|\widetilde{Ts}/\widetilde{Tg}| = 1 \; / \; \sqrt{1 + 2\beta + 2\beta^2} \tag{22}$$

where: $\beta = (1/h)\sqrt{(F)(Cp)(\rho)(K)}$

$\widetilde{Ts}$ = amplitude of component surface temperature oscillation

$\widetilde{Tg}$ = amplitude of free stream gas temperature fluctuation

h = surface heat transfer coefficient

F = frequency of the periodic wave

Cp, ρ, K = material properties.

For all conditions of interest for advanced propulsion systems: $\beta \gg 1$.

Therefore:

$$|\widetilde{Ts}/\widetilde{Tg}| \approx 1 \; / \; \sqrt{2\beta} \tag{23}$$

$$|\widetilde{Ts}/\widetilde{Tg}| \approx h \; / \; \sqrt{2\pi(F)(Cp)(\rho)(K)}$$

Therefore, for a solid with known material properties in any frequency band, the ratio of the magnitude of the surface thermal wave to the gas stream thermal wave is linearly related to the heat transfer coefficient. The heat transfer coefficient can, thus, be directly calculated from the relative wave amplitudes.

The useful part of the gas temperature wave is that containing components which:

1. Contain sufficient power to induce measurable surface temperature fluctuations

2. Are of wavelengths sufficiently long that the heat transfer coefficient at each temperature can be considered steady and equal to the time averaged heat transfer coefficient

3. Have thermal wavelengths $\lambda T = 2\sqrt{\pi(K)(F)/(\rho)(Cp)}$ in the solid small enough for the solid to be considered semi-infinite and to give adequate spatial resolution but large enough for the thermal wave to be unaffected by minute irregularities in the solid.

These considerations will limit the frequency band of interest to a range of roughly 10 Hz to a few hundred Hz. Since most ceramics have relatively low density and thermal conductivity, it can be seen from the equation for the relative temperature amplitudes that the magnitude of the surface wave for ceramics will be larger than for most metals which would increase the accuracy of the heat flux measurement.

This technique was not recommended for additional development primarily due to the problems involved in measuring the fluctuating gas temperature in the advanced propulsion system environment.

6.3 STEADY-STATE SENSORS

Steady-state sensors are generally those sensors whose operation is based on steady-state heat conduction through a thermal barrier. One-dimensional steady-state sensors determine the heat flux by measuring the temperature differential across a material of known thermal conductivity. There have been a wide variety of configurations that have been used in the construction of these sensors (refs. 152-155) providing flexibility in design with regard to size, geometry, and materials. The thermal barrier may be placed on one surface of the test section, or the wall of the test section may be used as the thermal barrier. In the case of ceramic thermal barrier on metallic substrates, the substrate may be used as the thermal barrier. There are several possible configurations of one-dimensional steady-state heat flux sensors for use in ceramics that are discussed below.

If the distance between the two temperature measurements is ΔX, the heat flux through the sensor per unit area, (Q/A), can be related to the measured temperature difference ΔT using the relationship:

$$Q/A = (K / \Delta X)\, \Delta T \qquad (24)$$

where K is the thermal conductivity of the thermal barrier material.

6.3.1 Surface Mounted Sensors

6.3.1.1 Thin-Film Surface Heat Flux Sensor

A steady-state heat flux sensor, such as that shown in figure 51, could be fabricated by sputtering a thin-film temperature sensor on the surface of the ceramic component, sputtering a thermal barrier of electrically and thermally insulating material over the temperature sensor, and then sputtering a second temperature sensor on top of the insulating material. The temperature sensors could be either thin-film thermocouples or resistance thermometers, and could be fabricated from either metallic or semiconductor thermoelectric elements. The thermal barrier layer would be a ceramic material with the thickness being determined by the thermal conductivity of the material and the design heat flux range of the sensor. The operation of the sensor is based on the heat conduction equation. As heat flows across the thermal barrier, a temperature difference is created across the barrier. The temperature drop across the barrier can be related to the heat flow across the barrier by appropriate calibration techniques. The design of the sensor provides for an adequate electrical output by either increasing the thickness of the thermal barrier, using a barrier material with a lower thermal conductivity or connecting multiple thermocouple junctions in series to form a thermopile. Sensors of this type, often with a kapton barrier, have found wide use in low-temperature applications (refs. 156 and 157) and have been very successful. The fabrication of high-temperature sensors on ceramic materials is dependent on advances in the state-of-the-art in sputtering on the new materials. If the fabrication techniques can be developed, the major problem area may turn out to be adherence of the relatively thick thermal barrier to the surface. At the extreme temperatures, the differences in the coefficients of thermal expansion may create shear problems at the interface.

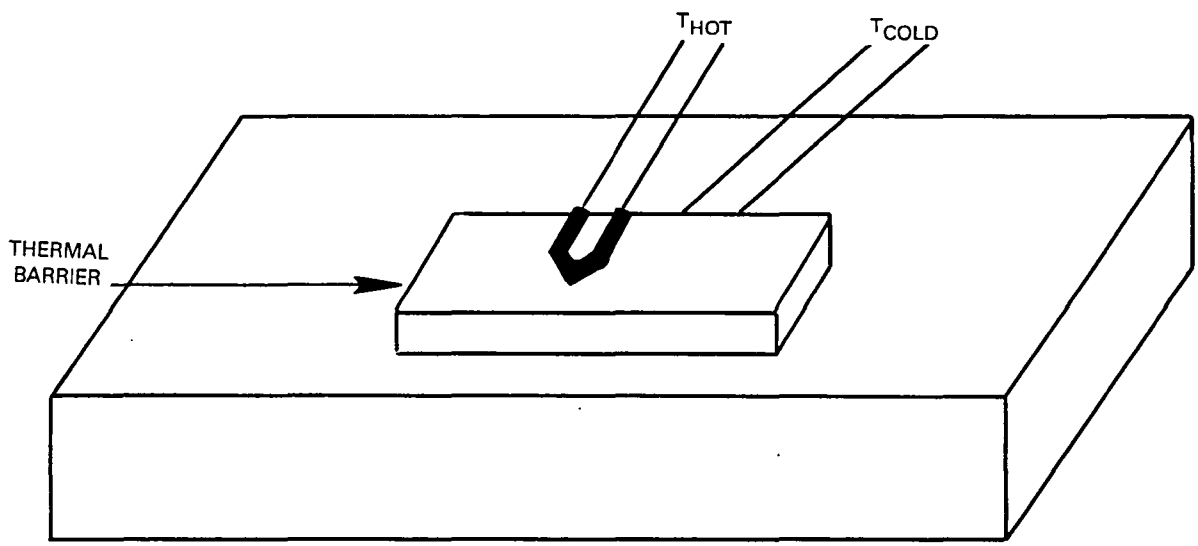

Figure 51 Thin-Film Surface Heat Flux Sensor

The usable temperature range of these sensors is material dependent and with metallic thermoelectric elements should be capable of 1900K. Higher temperatures may be possible if semiconductor thermal elements, such as silicon carbide or boron nitride, are used.

Similar sensors, using wire thermocouples on metallic components, have demonstrated that an accuracy of ±5% of full-scale heat flux is obtainable with appropriate high-temperature calibration techniques under laboratory test conditions. When installed into a propulsion system component, both the installation and the environment will have a profound effect on the accuracy of the sensor. Non-one-directional heat flow through the thermal barrier, arising either from steep lateral temperature gradients or from severe curvature of the component surface, can degrade the accuracy.

The thermal expansion of the thermal barrier will cause the distance between the temperature sensors to increase with temperature. At the extreme temperatures anticipated for the ceramic components, the distance changes may be large enough to require analytical correction of the calibration procedures. Likewise, the thermoelectric output and thermal conductivities of the materials change with temperature and this effect must be accounted for.

The surface mounted sensors are compatible with the propulsion system environment and produce a minimum perturbation of the airstream due to possible design of very thin sensors.

The life expectancy of these sensors is dependent on the durability of the temperature sensors. Bond failure between the thermal barrier and the substrate may be a limiting factor if proper care is not exercised in selecting the thermal barrier material.

The sensor can be made small in the size of the sensing area, but the barrier must extend far enough away from the sensing area to prevent shunting the heat flow around the sensing area.

The data acquisition and reduction requirements are the same as those for thermocouples or resistance temperature sensors. The output of the two temperature sensors can be measured differentially for thermocouples or in a bridge circuit for resistance thermometers to produce millivolt output directly proportional to heat flux. A measurement of the bulk temperature of the sensor is required to account for changes in thermal conductivity and thermoelectric output with temperature.

The fabricability of the sensors is identical to the installation of thin-film sensors. There are no special application techniques required.

6.3.1.2 Thermographic Phosphor Surface Sensor

A second variation of the thin-film surface heat flux sensor is to measure temperature on either side of the thermal barrier with thermographic phosophors or laser induced fluorescence as shown in figure 52. This would require the use of two different thermographic phosphors, one on the hot side or top of the thermal barrier and a second underneath or on the cold side of the barrier. The barrier material would have to be transparent to both the ultraviolet energy used to excite the phosphors and to the fluorescent radiation from the phosphors under the barrier. A single ultraviolet source could be used to excite both phosphors. The two phosphors would fluoresce at different wavelengths and, hence, the signals could easily be discriminated. The temperature difference across the barrier can be related to the heat flow through the barrier by appropriate calibration techniques. The feasibility of this technique is dependent on the identification of a thermal barrier material that has the required optical properties. If a suitable thermal barrier material is found, it is anticipated that the major problem area will be bonding the thermal barrier to the ceramic component surface. At the extreme temperatures anticipated for the ceramic components, small differences in the coefficient of thermal expansion may cause bond failures.

The ultimate feasibility of a thermal phosphor surface heat flux sensor is dependent on the results of further development work on thermographic phosphors aimed at high temperature applications as well as the identification of thermal barriers with suitable optical properties.

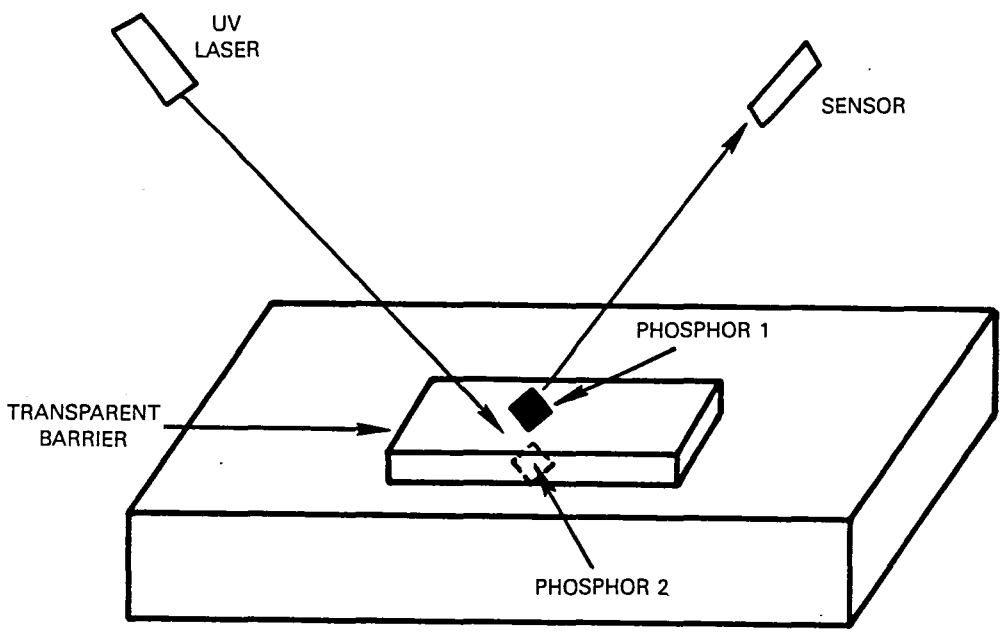

Figure 52 Thermographic Phosphor Surface Sensor

6.3.1.3 Pyrometry Surface Sensor

A variation of the above surface sensor would be to mount a thermal barrier on the surface and then read the top and bottom temperatures of the thermal barrier with pyrometers. This is possible if we select two pyrometers that operate at different spectral ranges and have a thermal barrier material that is transparent to one pyrometer and opaque to the other. This is shown schematically in figure 53. The pyrometer to which the barrier is opaque will provide the hot side temperature, and the other pyrometer looking through the transparent barrier will read the cold side or component surface temperature. The temperature difference across the barrier can be related to heat flow through the barrier through an appropriate calibration. The feasibility of this approach depends first, and foremost, on the identification of a thermal barrier material that has the desired optical properties. If a material can be identified, there are still three potential problem areas for this technique. If there is reflected energy present, the pyrometer readings will be biased high. Suitable techniques may be developed to correct for this radiation but that greatly increases the complexity of this technique. A second concern would be contamination (dirt) that accumulated on the sensor. This would tend to decrease the transparency of the barrier and decrease the accuracy of the pyrometer reading the cold side of the barrier. The third area of concern is the bonding of the thermal barrier material to the ceramic component. At the extreme temperatures of the ceramic components, the differences in the coefficients of thermal expansion may cause bond failures.

The feasibility of using pyrometry in this heat flux measurement technique is highly dependent on the outcome of any pyrometry development efforts that might occur under the development of temperature measurement techniques under the current contract.

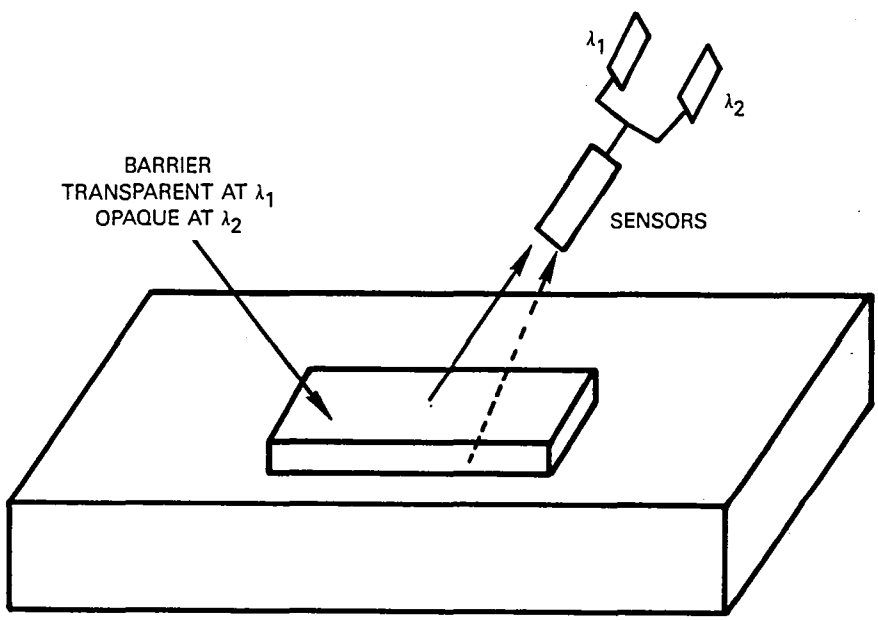

Figure 53 Pyrometry Surface Sensor

6.3.2 Component Used as a Thermal Barrier

6.3.2.1 One-Dimensional Steady-State Sensor

The heat flux through a cooled ceramic component can be determined by using the component material as a thermal barrier and measuring the temperature difference across the component created by the heat flow (fig. 54). It often is not possible to provide optical access to both sides of the component, so optical temperature measurement techniques have limited application. Therefore, surface sensors, such as thermocouples or resistance temperature sensors, must be applied to the surface. Sputtering techniques appear promising for the installation of those temperature sensors. In the case of composite materials, it may be possible to embed thin film or thin foil temperature sensors into the material during fabrication. The temperature difference across the component can be related to the heat flow through the component by suitable calibration techniques.

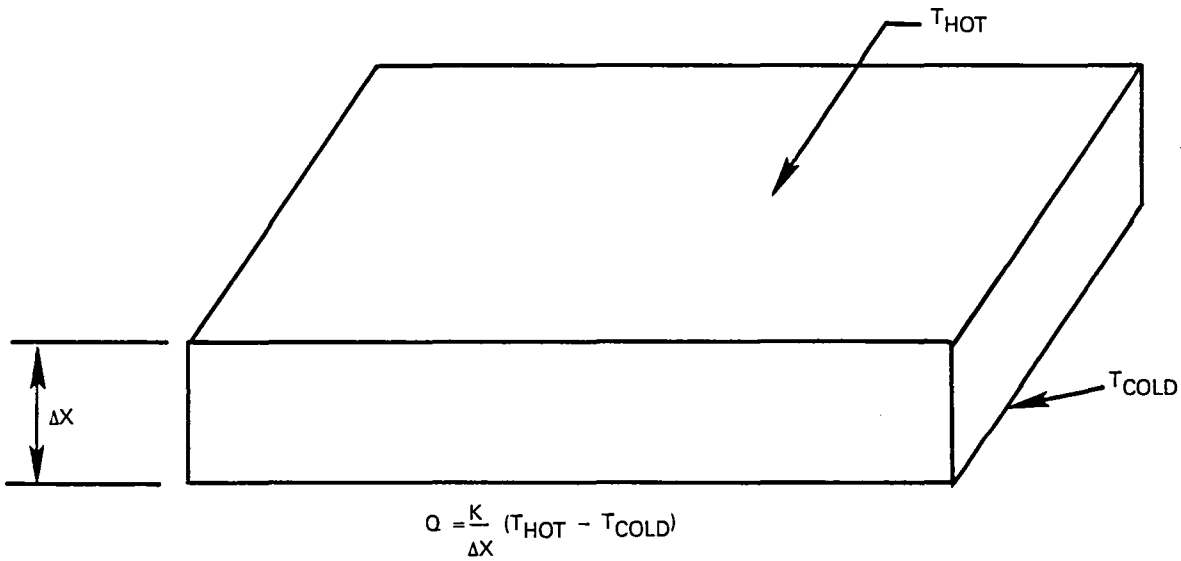

Figure 54 Component Used as a Thermal Barrier

The usable temperature range of this technique is restricted by the temperature limit of the temperature sensors. The technique may utilize ceramic thermoelements to increase the temperature capability above noble metal thermoelement limits.

The sensor can be calibrated under laboratory conditions to ±5% of full-scale heat flux. Under realistic test conditions, the accuracy will be dependent on the component geometry and the lateral thermal gradients in the component. Since the ceramic components have lower thermal conductivities than metallic components, we can expect the amount of non-one-directional heat flow to increase accordingly.

This technique provides good compatibility both with the propulsion system environment and the ceramic materials.

The life expectancy is determined by the durability of the thermoelements. The maximum test temperature has a significant effect on sensor lifetime. The hotter the test environment, the shorter the lifetime of the sensor.

The sputtered temperature sensors can be made small and the thermal conductivity is low so that the surface temperatures are very localized.

The data acquisition and reduction requirements are equivalent to those for a thermocouple or resistance temperature sensor. The sensor can be connected to read differentially to produce a millivolt signal that can be calibrated in terms of heat flux. The bulk temperature of the sensor is required to account for changes in thermal and thermoelectric properties.

Fabricability of these sensors is complicated by the requirement to attach a temperature sensor on the inside surface of the component. This can cause difficulties related to the routing of lead wires. In addition, special fabrication procedures may be required for components such as blades and vanes where the components may have to be made in two halves and joined after instrumentation.

There are no special application techniques required beyond the application of thin-film sensors on the ceramic materials and the routing of leads.

6.3.2.2 Gardon Gauge Sensor

The Gardon gauge sensor (ref. 158), shown schematically in figure 55, uses the radial temperature differential generated in a circular thin section of the material as a result of the heat flux through the surface to determine heat flux.

For the ideal case, the heat flux to the gauge may be calculated using the relationship:

$$Q/A = (4K\Delta X/R^2)\Delta T \qquad (25)$$

where: Q/A = heat flux per unit area

K = thermal conductivity of foil

ΔX = foil thickness

R = foil radius

ΔT = differential temperature from center to edge of foil.

GARDON GAUGE

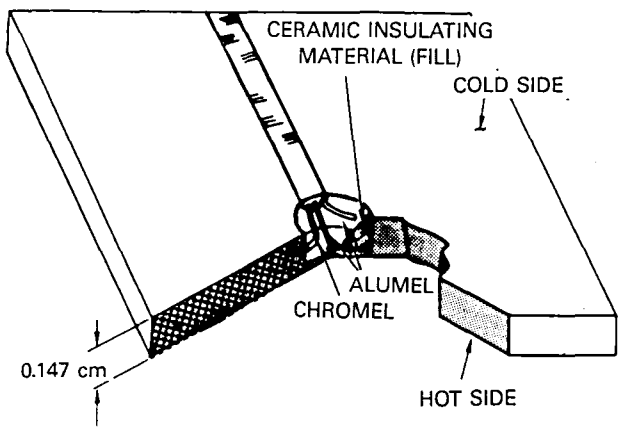

*NOT TO SCALE

ELECTRICAL SCHEMATIC GARDON GAUGE SENSOR

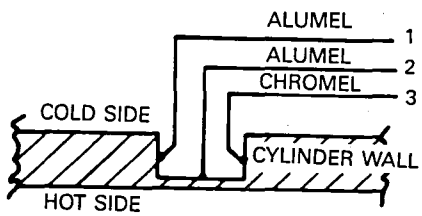

1-2 = SENSOR OUTPUT

1-3 = REFERENCE TEMPERATURE

Figure 55 Gardon Gauge Sensor

In real components, this idealized case is never realized and individual sensor calibrations are required. Adapting this type of sensor to ceramic components will present several problems. The Gardon gauge cavity must be formed without initiating cracks. In addition, installation of the differential temperature thermocouple is more difficult for ceramic components than for superalloy components. For metallic components, a section of the component wall can be used as the foil in the Gardon gauge, and the temperature difference is obtained from thermocouple leads which are resistance welded directly to the wall.

The analysis of this sensor type revealed that on nonmetallics the temperature sensors required internal to the gauge could not be easily fabricated and the sensor could not be miniaturized sufficiently for use on engine components. Considerable development work has been done on these sensors for engine applications (refs. 152-155) (combustor liners, turbine blades, and vanes) but the change of materials renders those efforts inapplicable to the ceramic materials of interest in this program.

6.3.3 Temperature Drop Across Metallic Substrate

For ceramic thermal barrier materials installed on metallic substrates, it may be possible to use existing heat flux sensor designs (refs. 150-154) to obtain the desired data. Figure 56 shows the cross section of one such sensor installation. During steady-state operation with one-dimensional heat flow, all of the heat flux through the ceramic thermal barrier must also pass through the metallic substrate. Therefore, the heat flux through the ceramic may be determined by measuring the heat flux through the metal. If the sensors were installed in the metal prior to application of the thermal barrier coating, it would be possible to use standard embedded wire thermocouples for this type of sensor. In many cases, it would even be advisable to complete the calibration of this type of sensor prior to application of the ceramic.

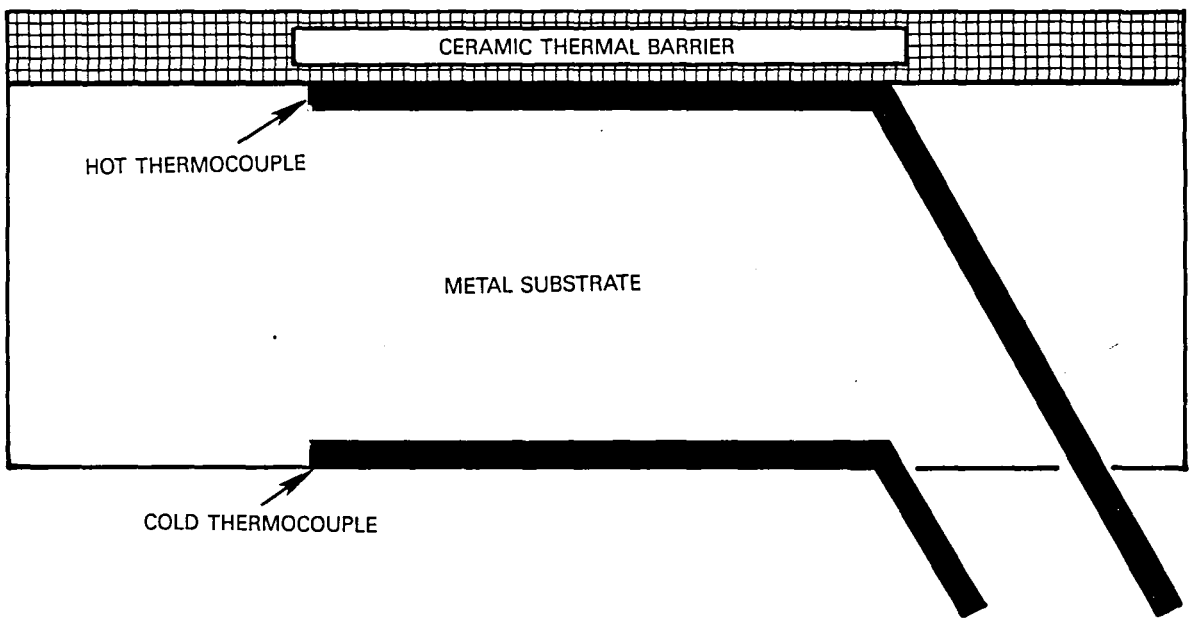

Figure 56 Temperature Drop Across Metal Substrate

Since sensors of this type are based on existing technology, they should have very low risk. Accuracy of $\pm$5% of full-scale heat flux has been demonstrated for this type of sensor.

The temperature limit of this type of sensor is that of the thermocouples. This is not really a problem since the metallic substrate will be limited to about 1450K, and thermocouples are available with higher temperature limits.

While this type of sensor is not applicable to all ceramic installations, it should work well for such components as thermal barrier coated combustor liners and outer air seals.

6.4 MISCELLANEOUS SENSOR TYPES

In addition to the above broad sensor classes, several other techniques have been used to determine heat flux or heat transfer coefficients. For example, I^2R heaters consist of a number of resistively heated strips, each of which is monitored by two thermocouples at known distances along the strip. The strips are heated until a uniform temperature is reached. The environmental conditions are then changed and the strips are adjusted until the same uniform temperature is regained. The power needed to regain uniformity represents the difference in heat transfer from the strips between the two conditions and is calculated from the voltage drop across the thermocouple leads and current through the strips. While this technique has worked well in relatively low temperature applications, it is doubtful that it can readily be extended to high temperature applications.

Mach-Zender or differential interferometers may be used to determine temperature distributions in thermal boundary layers. This information, combined with the known gas properties and measured surface temperature, allows calculation of the convective heat transfer coefficient.

Radiometers may be used to determine radiant heat loads in applications where it is desired to identify the relative radiant and convective heat load contribution. Radiometers developed for use on metallic components should be suitable for use on ceramics. Consideration must be given, however, to the higher heat loads, ambient temperatures, and gas velocities that will be encountered in the current application.

6.5 RECOMMENDATIONS FOR HEAT FLUX SENSORS

The measurement of heat flux on uncooled hardware is of little interest in engineering terms and consequently the transient techniques are not recommended for further development.

The two techniques recommended for further development are a surface mounted sensor and measurement of the temperature drop across the component or substrate. The specific form of the surface mounted sensor, i.e., whether it utilizes thin films, pyrometry, or thermographic phosphors for temperature measurement, should be governed by the progress made in developing these techniques in Phase II of this contract. The major development task will be to identify suitable thermal barrier materials and to develop techniques to bond them to the surface.

Using the ceramic component as a thermal barrier provides a technique that would be readily applicable to components where there is access to both the hot and cold sides. In the case of composite materials, it may be possible to install the temperature sensors during fabrication of the component. For ceramic airfoils the major development requirement will be two-piece fabrication methods to permit installation of the temperature sensors on the inside or cold surface.

For thermal barrier coatings on metallic substrates, the technique of measuring the heat flux through the substrate should be pursued.

7.0 SUMMARY

The purpose of this contract effort is to overcome the deficiencies in the current generation of instrumentation in meeting the requirements of future applications. Ceramic and other nonmetallic materials are being introduced into propulsion systems much more rapidly than had been predicted a few years ago, and the instrumentation development required to work with the new materials has not been able to keep pace. The new requirements call for radically different measurement techniques rather than extensions or improvements of the existing techniques. This is a result of three different factors.

A major advantage of the ceramic materials is that they can operate at temperatures substantially above metallic components. This requires that any sensor applied to the hardware must be able to withstand the extreme temperatures. This causes severe restrictions and tends to favor noncontact techniques over contact techniques. Optical techniques are hampered by thermal distortions caused by the hot gases surrounding the hardware. The temperature levels anticipated pose a formidable challenge to the instrumentation designers. This survey also has indicated that there is a need for high temperature strength of materials data.

The second factor is the environment anticipated in advanced propulsion systems. Along with the high temperatures and high pressures, high levels of radiant heating and correspondingly high levels of reflected energy can be expected. The radiant heat load increases with both temperature and pressure. New combustor designs have shorter lengths, moving the flame closer to the turbine components, and wide chord vanes are more open than the smaller narrow chord vanes.

The physical and optical properties of the ceramic materials themselves are the third major factor. The emittance of the surface governs the extent to which radiation pyrometry is applicable. Materials that become transparent at high temperature are particularly troublesome. The composite materials are often covered with an oxidation prevention layer on the surface. At high temperatures, these layers become glassy and tend to flow. This makes the measurement of strain by dimensional changes on the surface very questionable. In some components, the strength is in the fibers and the fibers have a lubricant on their surface so that they move freely within the matrix. In this instance, it is difficult to define exactly what is the parameter to be measured to determine the strain in the material.

Methods for the measurement of temperature, strain, and heat flux have been identified that appear to have the potential of providing information on the new materials in the environment of the advanced propulsion systems. Further development is required on all the recommended techniques to exploit their potential.

For temperature measurement, both pyrometry and thermographic phosphors have the potential to make measurements up to and beyond the melting point of the ceramic materials. The thin-film techniques are limited in temperature capability, but offer advantages in the installation of temperature sensors for lower temperature test programs.

Optical strain measurement techniques are recommended in that they offer the possibility of being useful at very high temperature levels, but the effects of gradients must be surmounted. For composite materials, the twin-core fiber optic strain sensor offers the prospect of being built into the composite material.

Techniques for the measurement of heat flux are recommended for development based on both a surface mounted sensor and the measurement of the temperature differential across a portion of a ceramic component or metallic substrate. The details of these techniques will be dependent on the results of the investigation into temperature measurement methods.

8.0 REFERENCES

8.1 MATERIALS

1. Stearns, C. A., "Thermal Barrier Coatings," Aerospace America, May 1987. New TBC's.

2. Levine, S. R., "Ceramics for Engines," Aerospace America, May 1987. Development of ceramic materials for engine applications.

3. Charles Rivers Associates, Advanced Ceramic Materials, Noyes Publications, 1985.

4. Johnson, R. A., "AGT 100 Experimental Ceramic Component Test Bed," ASME 86-GT-93, Automotive Gas Turbine Development.

5. "Development of High Temperature Oxidation Protection for Carbon-Carbon Composites," Air Force Program N62269-84C-0217, DARPA/UTRC Contract in progress.

6. Pond, J. B., "Hot and Getting Hotter," Metalworking News, May 25, 1987.

7. Linger, K. R., et al, "Carbon Fiber Composite Materials for Intermediate Temperatures," 1977 Composites, July.
Carbon fiber composite, oxidation.

8. Evans, A. G., et al, "Some Aspects of the High Temperature Performance of Ceramics and Ceramic Composites," 1986.
Failure in ceramics.

9. Burke, J. J., Proc Ed, "Ceramics for High Performance Applications-II," Army Matls Conf., 1977.
Cassidy: 6 NDE techniques; Arnon: Gas turb, pyrometry, tc's.
Heckel: Calc stress from temp.
Larsen: 4-pt bend equip and results.
Booher: Vanes in cascade rig.
Becker: Brazing of Si_3N_4.

10. Strife, J., et al, Proc Ed, "Fifth International Conference on Composite Materials, ICCM-V," 1985 The Met Soc.
See notes on anisotropy, fiber bundle failure, 3D matrix, strain gages on a lamina.

11. Singhal, S. C., "Oxidation of Silicon-Based Structural Ceramics," 1977.
Basic oxidation Si_3N_4, SiC, SiAlON.

12. Keyes, L. H., "The Oxidation of Silicon Carbide," 1977.
Oxidation of SiC: "Passive": parabolic, not pres dep; "Active": volatile, pres dependent.

13. Yoshimura, M., et al, "Electrical Breakdown Strength of Alumina at High Temperatures," JAmCeramicSoc 404, 1981.
Electrical breakdown Al_2O_3.

14. McMillan, D.P.W., "Review: Ceramic-Matrix Composites," JMatlsSci II 949, 1976.
Survey ceramic matrix composites.

15. Katz, R. N., "US National Programs in Ceramics for Energy Conversion," 1983 ProgInNitrogenCeram.
Survey of U.S. applications (Army, etc.).

16. Volynets, F. K., "Optical Properties and Areas of Application of Optical Ceramics," Soviet Journal of Optical Technology, Volume 40, October 1978.
Optical properties of polycrystalline materials with possible applications as detectors for sensors.

8.2 TEMPERATURE

8.2.1 Thermal Properties of Ceramics

17. Turner, W. D. and T. J. Love, "Directional Emittance of a Two-Dimensional Ceramic Coating," AIAA Journal, Volume 9, Number 9, September 1971.
Numerical study using Monte Carlo technique to illustrate optical parameters on directional emittance of ceramic coatings.

18. Wood, W. D., H. W. Deem and C. F. Lucks, "Emittance of Ceramics and Graphites," Battelle Memorial Institute, Contract AF-33616-7747, Report Number DMIC-MEMO-148, March 28, 1962.
Normal spectral and normal total emittance for SiC, zirconia, MoS_2, AlO_2, etc.

19. Liebert, C. H., "Emittance and Absorptance of the National Aeronautics and Space Administration Ceramic Thermal Barrier Coating," Thin Solid Films, Volume 53, 1978.
Emittance of yttria stabilized zirconia.

20. Richmond, J. C., G. J. Kneissl, D. L. Kelley and F. J. Kelly, "Procedures for Precise Determination of Thermal Radiation Properties," NBS Technical Note Number 292, February 10, 1967.
Method for making emittance measurements and result for alumina, magnesia, zirconia.

21. Boganov, A. G., Y. A. Pirogov and L. P. Makarov, "Investigation of the Effective Thermal Conductivity and Total Emissivity of Heat-Resistant Ceramic Coatings of Refractory Oxides Produced by Gas-Flame Spraying," High Temperature, Volume 3, January/February 1965.
Thermal properties of TBC materials.

22. Men, I. V., F. K. Volynets and Ye.P. Smirnaya, "Emissivity of KO-1 Optical Ceramic," Soviet Journal of Optical Technology, Volume 41(2), February 1974.
Possible applications in sensor development. Emittance determined analytically.

23. Seban, R. A. and R. E. Rolling, "Thermal Radiation Properties of Materials," WADD Technical Report Number 60-370, Air Force Contract Number AF-33-616-6630.
Methods of making emittance measurements in air up to 2500F.

24. Seibeck, J. H. and D. P. H. Hasselman, "Thermal Conductivity and Diffusivity of Engineering Ceramics," Ceramics Research Laboratory for Department of the Navy Agreement Number N00014-75-C-0760.
Section on the effect of conductivity on radiation heat transfer across spherical pores and thermal diffusivities of ceramics.

25. Abramov, A. S., B. M. Barykin, A. I. Romanov and E. G. Spiridonov, "Study of Emissivity of Oxides and Concretes in Infrared Region of the Spectrum," Materialy dlya Kanala MGD-Generatora, USSR, 1969.
Silica and alumina emissivities at 5u.

26. Taylor, R. E., D. P. DeWitt and P. E. Johnson, "Spectral Emissivity at High Temperature," Thermophysical Properties Research Laboratory, Annual Report for Grant 77-3280, April 1980, Number AFOSR-TR-80-0417.
SiC, Si_3N_4, pyroceram to 1900K.

27. Cox, R. L., "Fundamentals of Thermal Radiation in Ceramic Materials," Symposium on Thermal Radiation of Solids, S. Katzoff, ed., NASA SP-55, 1965, pp. 259-275.

28. Holmes, J. T., R. M. Edgar and P. F. Gerrish, "Screening Ceramic Materials for Intense Radiant Heat Applications," Ceramic Engineering Science Proceedings, Volume 6-7, July-August 1985.
Submitting board and blanket type insulations to solar furnace and measuring heat flux at failure.

29. Hayes, R. J. and W. H. Atkinson, "Thermal Emittance of Materials for Spacecraft Radiator Coatings," Ceramic Bulletin, Volume 43, Number 9, 1964.
Emittances of SiC, etc., and endurance testing at high temperatures.

30. Haury, G. L., "A Calorimeter for Measuring the Low Temperature Hemispherical Emissivity of Metallic and Ceramic Surfaces," Air Force Materials Laboratory Technical Documentary Report ML-TDR-64-223, August 1964.
Apparatus to measure emissivities at temperatures to 60K.

31. DeWitt, D. P., R. E. Taylor and P. E. Johnson, "Spectral Emissivity of Ceramics at High Temperatures: Silicon Carbide and Silicon Nitride," American Society of Mechanical Engineers, Paper Number 79-HT-24.
Using emissometer to measure emittance of ceramics to 1900K.

32. Adisson, A., M. Billy, P. Fauchais, P. Goursat, C. Martin and B. Peteyron, "Emissivity of Silicon Oxynitride Ceramics by Infrared Thermography," British Ceramic Society Transactions and Journal, Volume 76(1), January-February 1977.
Using AGA system and spectrophotometer.

33. Crosbie, A. L., "Emittance of a Finite Scattering Medium with a Refractive Index Greater than Unity," AIAA Journal, Volume 18, June 1980.
Numerical investigation for finite medium.

34. Reitter, T. A., "Calorimetric Measurements of Emittance of Pipe Surfaces: Influence of Enclosure Diameter, Test Pipe Length, and an Argon Atmosphere," Lawrence Livermore Laboratory, Paper Number UCRL-53213, 1981.
Measuring emittance of pyrex pipe surface.

35. Turner, W. D. and T. J. Love, "Directional Emittance of Two-Dimensional Ceramic Coating," AIAA 8th Aerospace Sciences Meeting, Paper Number 70-67, January 19-21, 1970.
Monte-Carlo technique illustrating effects of optical pyrometers on direction emittance.

36. Reitter, T. A., "Design and Operation of an Apparatus for Calorimetric Emittance Measurements of Pipe Surfaces," Lawrence Livermore Laboratory, Paper Number UCRL-53214, 1981.
Measuring emittance of pyrex pipe surface.

37. Lee, M. C. and J. L. Allen, "Non-Contact True Temperature Measurements II," Jet Propulsion Laboratory and Cal. Tech., June 1987.

38. Yeaple, F, "Laser-Set Hot Pyrometer Corrects for Emissivity," Design News, December 1985.

8.2.2 Temperature Measurement

39. Gladden, H. J. and M. P. Proctor, "Transient Technique for Measuring Heat Transfer Coefficients on Stator Airfoils in a Jet Engine Environment," NASA TM 87005, July 1985.

40. Searcy, A., et al, "Electronic Ceramics in High-Temperature Environments," 1980 JAmCeramicSoc 216.
Electrical properties semi-cond.

41. Grant, H. P., J. S. Przybyszewski and R. G. Claing, "Turbine Blade Temperature Measurements Using Thin Film Temperature Sensor," NASA CR-165201, March 1981.

42. Grant, H. P., J. S. Przybyszewski, R. G. Claing and W. L. Anderson, "Thin Film Temperature Sensors, Phase III," NASA CR-165476, January 1982.

43. Prakash, S., R. C. Budhani and R. F. Bunshah, "Development of Thin Film Temperature Sensors for High Performance Turbo-Jet Engines," Mat. Res. Bull., Vol. 23, No. 2, February 1988, pp. 187-196.
Pt-Pt/Rh tc's for use on monolithic ceramics state of the industry in ceramic usage.

44. "Noncontacting Thermometer," NASA Tech. Briefs, June 1987.

45. Wisnieff, S. F. and H. Bardach, "A Radioactive Krypton Diffusion Technique for Temperature Mapping of Turbine Blade Surfaces," SAE Paper 650704.
Kr-85.

46. Planck, M., "Distribution of Energy in the Spectrum," Ann. Physics, Vol 4, No. 3, 1901.

47. Atkinson, W. H. and R. N. Guenard, "Turbine Pyrometry in Aircraft Engines," Electro-78 Conference Rec., Boston, Massachusetts, May 23-25, 1978.

48. Atkinson, W. H. and R. R. Strange, "Pyrometer Temperature Measurements in the Presence of Reflected Radiation," ASME Paper 76-HT-74, August 1976.

49. Atkinson, W. H., M. A. Cyr, J. R. Gebhart and R. R. Strange, "Design of a Scanning Pyrometer System for Hot Section Static Structures," AFWAL-TR-86-2116.

50. Goss, L. P. and A. A. Smith, "Application of Laser Induced Fluorescence to Measurement of Surface Temperatures in Solid Fuel Propellants," Work done under contract F49620-83-C-1038 with Air Force Office of Scientific Research.
$Dy^{+3}:LaF_3$ - phosphors
$Cr^{+3}:Al_2O_3$ and $Er^{+3}:CaF_2$.

51. Smith, A. A. and L. P. Goss, "Application of Fluorescence to Measurement of Surface Temperature in Solid Propellants," AFOSR Contractors Meeting, Stanford, California, June 16-17, 1986.

52. Noel, B. W., et al, "Thermographic Phosphor Temperature Measurements in Turbine Engines: Program Review," Los Alamos Labs Paper Number LA-UR-87-979, 1986.
Used both lifetime and spectral measurement.

53. Cates, M. R., S. W. Allison, L. A. Franks, M. A. Nelson, T. J. Davies and B. W. Noel, "Remote Thermometry of Moving Surfaces by Laser Induced Fluorescence of Surface Bonded Phosphor," November 1983.

54. Noel, B. W., et al, "Proposed Method for Remote Thermometry in Turbine Engines," AIAA/SAE/ASME 21st Joint Propulsion Conference, Monterey, California, July 8-10, 1985, AIAA-85-1468.

55. Noel, B. W., "Application of Pulsed Laser Techniques and Thermographic Phosphors to Dynamic Thermometry of Rotating Surfaces," et al, LIA Volume 45 ICALEO, 1984.

56. Borella, H. M., L. A. Franks and B. W. Noel, "Development of Bonding Techniques for High Temperature Applications of Thermographic Phosphors," EGG-10282-2085.

57. Meltz, G. and J. R. Dunphy, "Fiber Optic Sensors for the Nondestructive Evaluation of Composite Materials," SPIE Volume 566, Fiber Optics and Laser Sensors III, 1985.

58. Mack, R., "Fiber Sensors Provide Key for Monitoring Stress in Composite Materials," Laser Focus/Electro-Optics, May 1987.

59. Dunphy, J. R. and G. Meltz, "Development of a Fiber Optic Sensor for Turbine Disk Diagnostics," AIAA-85-1469, AIAA/SAE/ASME/ASEE 21st Joint Propulsion Conference, Monterey, California, July 8-10, 1985.

60. Budhani, R. C., S. Prakash and R. F. Bunshah, "Thin Film Temperature Sensors for Gas Turbine Engines: Problems and Prospects," Journal of Vacuum Science Technology, Nov/Dec 1986.
Pt/Rh Tc's - sputtering onto blades.

61. Budhani, R. C., S. Prakash, N. J. Doerr and R. F. Bunshah, "Summary Abstract: Oxygen Enhanced Adhesion of Platinum Films Deposited on Thermally Grown Alumina Surfaces," Journal of Vacuum Science Technology, Nov/Dec. 1987.
Bonding metal tc's to ceramic substrate.

62. Dils, R. and P. Follansbee, "High Temperature Sputtered Surface Sensors," Proc. 21st Int'l Inst. Symp., ISA, Philadelphia, Pennsylvania, May 1978, pp. 127-132.

63. Grant, H. P. and J. S. Przybyszewski, "Thin Film Temperature Sensor," NASA CR-159782, February 1980.

64. Eckbreth, A. C., "CARS Thermometry in Practical Combustors," Combust. Flame. 39, 1980, pp. 133-147.

65. Eckbreth, A. C., G. M. Dobbs, J. H. Stufflebeam and P. A. Tellex, "CARS Temperature and Species Measurements in Augmented Jet Engine Exhausts," Appl. Opt. 23, 1984, pp. 1328-1339.

66. Kreider, K. G., S. Semancik and C. Olson, "Advanced Thin Film Thermocouple," National Bureau of Standards NBSIR 84-2949, October 1984.

67. Wickersheim, K. A. and R. A. Lefever, "Luminescent Behavior of the Rare Earths in Yttrium Oxide and Related Hosts," J. Electrochem. Soc. 3, 1964, pp. 47-51.

68. Dobbs, G. M. and J. J. Sangiovanni, "Optical Diagnostics for Diesel-Engine Applications," UTRC Report R85-957012, 1985.

8.3 STRAIN

8.3.1 Mechanical Properties of Ceramics

69. Sciammarella, C. A. and M. P. K. Rao, "Failure Analysis of Stainless Steel at Elevated Temperatures," Experimental Mechanics, 19, 1979, pp. 389-398.

70. Prewo, K. M., "Tension and Flexural Strength of Silicon," 1986 JMatlSci 21 3590.
Compglas® (SiC/LAS technology).

71. Bold, S. E., et al, "Tensile Creep and High-Temperature Fracture in a LiO2-Al2O3-4SiO2 Glass-Ceramic," 1978 JMatlSci 13 611.
LiO_2-Al_2O_3-4SiO_2 creep.

72. Lankford, J., "Temperature-Strain Rate Dependence of Compressive Strength and Damage Mech in Al203," 1981 JMatlSci 16 1567.
Al_2O_3 failure.

73. Krishnamachari, V., "Interpretation of High-Temperature Creep of SiC by Deformation Mapping Techniques, 1977 MatlsSci&Eng 27 83.
SiC creep.

74. Dagleish, B. J., et al, "High Temperature Failure of Ceramics," 1986 JMatlsForEnSys 8 2.
Failure in ceramics.

75. Davies, C. K. L., et al, "A Simple Apparatus for Carrying Out Tensile Creep Tests on Brittle Materials Up to 1750F," 1971 JPhysE.
Apparatus for tensile creep.

76. Wiederhorn, S. M., et al, "Mechanical Properties of Ceramics for High Temperature Applications," 1976 AGARD-R-651.
Design criteria, diagnostics for ceramics.

77. Davidge, R. W., et al, "Mechanical Property Testing of High Temperature Materials," 1975 AGARD-R-634.
Design criteria, diagnostics for ceramics.

78. Budiansky, B., "Matrix Fracture in Fiber-Reinforced Ceramics," 1985 Report MECH-64.
SiC/LAS cracking theory and exper.

79. Fu, L. S., et al, "Fundamentals of Microcrack Nucleation Mechanics," 1985 NASA CR-3851.
Theory, ultrasonics and brittle fracture.

80. Langdon, G., "Factors Influencing the Stress-Strain Behavior of Ceramic Materials," 1971 Plenum.
Stress-strain behavior (ref. Hulse).

81. Lackey, W. J., "Effect of Temperature on Electrical Conductivity and Transport Mechanisms in Sapphire," 1971 Plenum.
Elec cond mech in Al_2O_3 (sapphire).

82. Bortz, S. A., "Properties of Structural Ceramics," 1981 Sampe Journal.
Properties (mechanical, oxidation, erosion, thermal).

83. Langdon, T. G., "Deformation of Polycrystalline Materials at High Temperatures," 1981 Proc 2nd Riso Denmark.
Defor of polycrys and superplasticity.

84. Burke, J. J., Proc Ed., "High Voltage Electron Micrscope (HVEM)," 1983 HVEM Conf Berkeley.
Valle: Strain, temp, test apparatus.
Mitchell: grain boun., swelling, void.
Fujita: HVEM hot stretched Al_2O_3, etc.
Vanhellemont: disloc SiO at mask edge.
Ruhle: 60 um Al_2O_3-ZrO_2 ion thinned.
Several papers: disordering under HVEM; cracks, fiber E and alpha mismatch, shear, rf heating of nonuniform thickness samples as a method for therm. induced strain.

85. Nakayama, J., "Thermal Shock Resistance of Ceramic Materials," 1973 Plenum.
3-pt bending firebrick, equations.

86. Polyakov, Y. A., et al, "Analysis of Thermal Stresses in Thin-Film Resistance Thermometers," 1973 Plenum UDC 536.531.
3-D stress in glass substrate of Pt film (no discussion of film fab or stress).

87. Stonely, R., Proc. Roy. Soc., Vol. 245A, January 1970, p. 372.

88. Maerfeld, C. and P. Tournois, "Pure Shear Elastic Wave Guided by the Interface of Two Semi-Infinite Media," App. Phys. Lett., Vol. 19, 1971, p. 117.

89. Owen, T. E., Prog. Appl. Mat. Res. (GB), Vol. 6, 1964, p. 64.

8.3.2 Strain Measurement Techniques

90. Dolleris, G. W., H. J. Mazur and E. Kokoska, "Strain Gage System Evaluation Program, Final Report," NASA CR-159486, March 1979.

91. Brittain, J., D. Geslin and J. Lei, "Elevated Temperature Strain Gages," NASA Conference Publication 2444, Turbine Engine Hot Section Technology 1986, pp. 69-84.

92. Perry, C. C. and H. R. Lissner, The Strain Gage Primer, McGraw-Hill, 1965.

93. Englund, D. R., "The Dual Element Method of Strain Gage Temperature Compensation," 4th Annual Hostile Environments and High-Temperature Measurements Conference Proceedings, SEM, March 1987, pp. 40-43.

94. Grant, H. P., J. S. Przybyzewski, W. L. Anderson and R. G. Claing, "Thin Film Strain Gage Development Program," NASA CR-174707, December 1983.

95. Stowell, W. R. and R. Weise, "Application of Thin Film Strain Gages and Thermocouples for Measurement on Aircraft Engine Parts," AIAA-83-1292, AIAA/SAE/ASME 19th Joint Propulsion Conference, Seattle, Washington, June 27-29, 1983.

96. Hulse, C. O., R. S. Bailey, H. P. Grant and J. S. Przybyszewski, "Development of a High Temperature Thin Film Static Strain Gage," NASA Conference Publication 2493, Turbine Engine Hot Section Technology 1987.

97. Hulse, C.O., et al, "High Temperature Static Strain Sensor Development, Final Report," NASA CR-179520.

98. High Temperature Capacitive Strain Measurement System, NASA Tech. Brief B75-10069, May 1975.

99. Harting, D. L., "Evaluation of a Capacitive Strain Measuring System for Use to 1500F," Advances in Test Measurement, Vol. 12, ISA Proceedings of 21st International Symposium, Philidelphia, Pennsylvania, 1975.

100. Hitec Products Corp., Proximic Materials Testing Measurement Systems, Transducers and Sensors.

101. Cullen, D. E. and T. M. Reeder, 1975 IEEE Ultrasonics Symposium Proceedings, 1976, p. 519.

102. Lim, T. C. and M. J. P. Musgrove, "Stonely Waves in Anisotropic Media," Nature, Vol. 2, January 1970, p. 372.

103. Stonely, R., Proc. Roy. Soc., Vol. 245A, January 1970, p. 372.

104. Maerfeld, C. and P. Tournois, "Pure Shear Elastic Wave Guided by the Interface of Two Semi-Infinite Media," Applied Physics Letter, Vol. 19, 1971, p. 117.

105. Owen, T. E., Prog. Appl. Mat. Res. (GB), Vol. 6., 1964, p. 64.

106. Shuskus, A. J., T. M. Reeder and E. L. Paradis, "RF Sputtered Aluminum Nitride Films on Sapphire," Appl. Phys. Lett., Vol. 24, February 1974, p. 155.

107. Noel, B. W., et al, "A Superlattice Strain Gage," 1987 AIAA-87-1759. Superlattice strain gage.

108. Chi, R. M., D. C. Haas, McClurg and P. E. Zwicke, "Conceptual Development of Strain Gage Signal Interpretation System for Jet Engine Applications," AFWAL-TR-85-2052, UTRC R83-956394-R1, October 1985.

109. Camarata, D. L., R. M. Chi, M. D. Page and L. G. Puffer, "Conceptual Design of a Noninterference Stress Measurement System for Gas Turbine Engines," AEDC-TR-84-12, UTRC R83-956204-R1, May 1984.

110. Chi, R. M. and J. H. Shu, "Analysis of Point Focus Optical Probe Data from JTDE First Fan," UTRC R85-257029, December 1985.

111. Cloud, G., R. Radke and J. Peiffer, "Moire' Gratings for High Temperatures and Long Times," Experimental Mechanics, 19, 19N-21N (1979).

112. Bayer, M. and G. Cloud, "Moire' to 1370°C," Proc. SEM Spring Conf. on Exp. Mech., New Orleans, Louisiana, June 1986.

113. Cloud, G. and M. Bayer, "High Temperature Moire'," Proc. SEM 4th Annual Hostile Environments and High Temperature Measurements Conf., Windsor Locks, Connecticut, March 1987.

114. Post, D., "Analysis of Moire Fringe Phenomena," Appl. Opt., 6, 1938-1942 (1967).

115. Stetson, K. A., "The Use of Heterodyne Speckle Photogrammetery to Measure High-Temperature Strain Distributions," Proc. SPIE, Vol. 370, 46-55 (1983).

116. Stricker, J., "Electronic Heterodyne Readout of Fringes in Moire' Deflectrometry," Opt. Let., 10, 247-249 (1985).

117. Vest, C. M., Holographic Interferometry, Wiley & Sons, New York, 1979.

118. Erf, R. K., Speckle Metrology, Academic Press, New York, 1978.

119. Stetson, K. A., "Demonstration Test of Burner Liner Strain Measuring Systems," NASA CR-174743, 1984.

120. Stetson, K. A., "Demonstration of Laser Speckle System on Burner Liner Cyclic Fatigue Rig," NASA CR-179509, 1986.

121. These are interim results obtained on Air Force Contract F33615-83-C-2330, Advanced Structural Instrumentation.

122. Meyer, R, "Axial-Torsional Extensometer for Use to 1200C," MTS Systems Corp., Box 24012, Minneapolis, Minnesota, 55424, SEM 4th Annual Hostile Environments and High Temperature Measurements Conference Proceedings, Windsor Locks, Connecticut, March 24-25, 1987.

123. Hulse, C. O., R. S. Bailey and H. P. Grant, "Development of -325 to +1600F Strain Measuring System," work conducted under Air Force Contract F33615-85-C-3208, ISA 33rd International Instrumentation Symposium, Las Vegas, Nevada, May 3-8, 1987.

124. ZYGO Industries Inc., Dept. G, P.O. Box 1008, Portland, Oregon, 97207.

125. Sharpe, W. N., "Interferometric Surface Strain Measurement," International Journal of Nondestructive Testing 3, 56-76 (1971).

126. Sharpe, W. N., "Application of the Interferometric Strain/Displacement Gage," Opt. Eng., 21, 483-488 (1982).

127. Sharpe, W. N., "Preliminary Development of an Interferometric Strain Gage for Use on Nosetip Materials," 1976 AFML/TR 76-63.
Interferometric SG on graphite.

128. Yamaguchi, I., "A Laser Speckle Strain Gauge," J. Phys. E: Sci. Inst., 14, 1270-1273 (1981).

129. Yamaguchi, I., T. Furukawa, T. Ueda and E. Ogita, "Accelerated Laser Speckle Strain Gauge," Opt. Eng. 25, 671-676 (1986).

130. Stetson, K. A. and R. K. Erf, "An Optical Heterodyne Strain Sensor," Report No. F33615-80-C-2067, AFAPL, Wright-Patterson AFB, Ohio, September 1981.

131. Stetson, K. A., "A Heterodyne Optical Strain Sensor," Proc. of Inst. Soc. of Amer., Albuquerque, New Mexico, 1983, pp. 65-70.

132. Herscher, M., G. Wyntjes and H. DeWeerd, "Non-Contact Laser Extensometer," Optra, Inc.

133. Herscher, M., G. Wyntjes and H. DeWeerd, "A Non-Contact Laser Extensometer," Proc. SPIE, Vol. 746, 1987, pp. 185-191.

134. Nemanich, R. J., Proc Ed, "Thin Films - Interfaces and Phenomena," 1985 MatResSoc Sym, Boston.
Epitaxy, film fracture, decohesion.

135. Stewart, P. A. E., "Neutron and Positron Techniques for Fluid...and Remote Temp and Stress Measurement," 1987 ASME 87-GT-219.
Stress by neutron diffraction and review of nonintrusive methods.

136. Shetty, D. K., et al, "Stress-Relaxation Technique for Deformation Studies in Four-Point Bend Tests," 1979 JMatlsSci 2163.
Errors in 4-point bend tests.

137. Russell, J. D., "Carbon Strain Gage," 1982 US Patent 4,309,686.
Weldable carbon strain gage in Al_2O_3.

138. Peiter, A., et al, "X-Ray Integral Method" (RIM), 1987 JBrSocStrMeas.
Strain by 3D "X-Ray Integral Method" (RIM).

139. Hulse, C. O., et al, "High Temperature Static Strain Sensor Development Program NAS3-23169," 1982 NASA HOST Conf.
Strain gage alloy ratings.

140. Moreno, V., "Creep-Fatigue Life Prediction for Engine Hot Section Materials (Isotropic)," 1982 NASA HOST Conf.
Objectives of creep-fatigue progress.

141. Kaufman, A., "Constitutive Model Development for Isotropic Materials," 1982 NASA HOST Conf.
Crack initiation, constitutive modeling.

142. Thompson, R. L., "Validation of Structural Analysis Methods Using the In-House Liner Cyclic Rigs," 1982 NASA HOST Conf.
Testing in Liner Cyclic Rig.

143. Schultz, D., "HOST Liner Cyclic Facilities Facility Description," 1982 NASA HOST Conf.
Description of Liner Cyclic Rig.

144. Shirley, J. A. and L. R. Boedeker, Monthly Reports, NASA Contract NAS3-36861, in progress, 1986.

145. Hulse, C. O., R. S. Bailey and F. D. Lemkey, "High Temperature Static Strain Gage Alloy Development Program," NASA CR-174833, March 1985.

146. Jameikis, S. M., et al, "Steady State Strain Gage Development Program, Interim Report for Period August 1980-July 1981," Section 3.2, Resistive Sensors, USAF Contract F33615-80-C-2044, Report No. AFWAL-TR-82-2002, May 1982.

147. Dandliker, R., Progress in Optics XVII, North-Holland, Amsterdam, 1980, pp. 1-84.

8.4 HEAT FLUX MEASUREMENT

148. Dunn, M. G., W. J. Rae and J. L. Holt, "Measurement and Analysis of Heat Flux Data in a Turbine Stage: Part I-Description of Experimental Apparatus and Data Analysis," Transactions of the ASME Journal of Engineering for Power, May 31, 1983; Paper Number 83-GT-121.
Platinum on pyrex sensor.

149. Dunn, M. G. and A. Hause, "Measurement of Heat Flux and Pressure in a Turbine Stage," Transactions of the ASME Journal of Engineering for Power, Vol. 104, January 1982.

150. Guernigou, J., C. Indrigo, Y. Maisonneuve and P. G. Mentre, "Development of Surface Temperature Fluxmeters," La Researche Aerospatiale, May/June 1980.
Slug calorimeter using silica.

151. Dils, R. R. and P. S. Follansbee, "Heat Transfer Coefficients Around Cylinders in Crossflow in Combustor Exhaust Gases," ASME 77-GT-9, Gas Turbine Conference, Philidelphia, Pennsylvania, March 27-31, 1977.

152. Atkinson, W. H. and R. R. Strange, "Development of Advanced High Temperature Heat Flux Sensors," NASA Contract NAS3-22133, CR-165618, September 1982.

153. Atkinson, W. H., M. A. Cyr and R. R. Strange, "Turbine Blade and Vane Heat Flux Sensor Development - Phase I Final Report," NASA Contract NAS3-23529, CR-168297, August 1984.

154. Atkinson, W. H., M. A. Cyr and R. R. Strange, "Development of Advanced High Temperature Heat Flux Sensors - Phase II Verification Testing," NASA Contract NAS3-22133, CR-174973, August 1985.

155. Atkinson, W. H., M. A. Cyr and R. R. Strange, "Turbine Blade and Vane Heat Flux Sensor Development - Phase II Final Report," NASA Contract NAS3-23529, CR-174995, October 1985.

156. RdF Corporation, 23 Elm Avenue, Hudson, New Hampshire, 03051, 603-882-5195.

157. Epstein, A. H., G. R. Guenette, R. J. G. Norton and C. Yuzhang, "High Frequency Response Heat Flux Gage for Metal Blading."

158. Gardon, R., "A Transducer for the Measurement of Heat Flow Rate," Transactions of ASME, J Heat Transfer 82, Ser. C.4, 1960.

159. Semco Inc., "Metal Sheathed Mineral Oxide Insulated Materials," North Hollywood, California, 1972, p. 17.

9.0 DISTRIBUTION LIST

NASA-Lewis Research Center
Attn: Library, MS 60/3
21000 Brookpark Road
Cleveland, OH 44135

NASA-Lewis Research Center
Attn: Report Control Office, MS 60/1
21000 Brookpark Road
Cleveland, OH 44135

NASA-Lewis Research Center
Attn: Wayne R. Girard, MS 500/305
21000 Brookpark Road
Cleveland, OH 44135

NASA-Lewis Research Center
Attn: Ray Holanda, MS 77/1
21000 Brookpark Road
Cleveland, OH 44135 (50 copies)

NASA Headquarters
Attn: RP/John R. Facey
Washington, DC 20546

NASA Headquarters
Attn: MPS/Paul N. Herr
Washington, DC 20546

NASA Langley Research Center
Attn: R. E. Wright, Jr., MS 234
Hampton, VA 23665

NASA Langley Research Center
Attn: S. L. Ocheltree, MS 235A
Hampton, VA 23665

NASA Marshall Space Flight Center
Attn: William T. Powers, Code EB-22
Marshall Space Flt. Center, AL 35812

NASA Marshall Space Flight Center
Attn: Joseph Zimmerman, Code EB-22
Marshall Space Flt. Center, AL 35812

NASA Sci. and Tech. Info. Facility
Attn: Acquisition Department
P. O. Box 8757
BWI Airport, MD 21240 (25 copies)

Air Force Wright Aeronautical Lab.
Attn: William Stange, AFWAL/POTA
Wright-Patterson AFB, OH 45433

Air Force Wright Aeronautical Lab.
Attn: Less Small, AFWAL/POTC
Wright-Patterson AFB, OH 45433

Air Force Wright Aeronautical Lab.
Attn: John Reed, AFWAL/POTA
Wright-Patterson AFB, OH 45433

Air Force Wright Aeronautical Lab.
Attn: Roger R. Craig, AFWAL/POPT
Wright-Patterson AFB, OH 45433

Applied Sensors International
Attn: Richard Stillmaker
7834 Palace Drive
Cincinnati, OH 45242

Arnold Engineering Dev. Center
Attn: Carlos Tirres, AEDC/DOT
Arnold Air Force Station, TN 37389

Arnold Engineering Dev. Center
Attn: Marshall Kingery, AEDC/DOT
Arnold Air Force Station, TN 37389

AVCO Lycoming Textron
Lycoming Division
Attn: Mr. K. Collinge
Diagnostic Technology Manager
550 South Main Street
Stratford, CT 06497

AVCO Lycoming Textron
Lycoming Division
Attn: E. Twarog, Manager
Electronics and Instr.
550 South Main Street
Stratford, CT 06497

Aviation Applied Technology Dir.
USAARTA (AVSCOM)
Attn: Joel Terry/SAVRT-TY-ATA
Ft. Eustis, VA 23604-5577

Babcock & Wilcox
R&D Division
Attn: John Berthold
P. O. Box 835
Alliance, OH 44601

Battelle Columbus Laboratories
Attn: Ross G. Luce, Manager
Aerospace Programs Office
Columbus, OH 43201

Boeing Commercial Airplane Co.
Attn: R. D. (Ric) Tatman
P. O. Box 3707, MS 25-09
Seattle, WA 98124-2207

Boeing Commercial Airplane Co.
Attn: Ted Nykreim
P. O. Box 3707, MS 79-22
Seattle, WA 98124-2207

Boeing Aerospace Company
Attn: Darrell R. Harting
P. O. Box 3999, MS 87-09
Seattle, WA 98124-2499

Boeing Aerospace Company
Attn: L. C. (Larry) Shrout
P. O. Box 3999, MS 86-11
Seattle, WA 98124-2499

Boeing Aerospace Company
Attn: J. L. Howard
P. O. Box 3999, MS 86-12
Seattle, WA 98124-2499

Calspan Field Services, Inc.
AEDC Div.
Attn: C. T. Kidd
Arnold Air Force Station, TN 37389

Carnegie-Mellon University
Attn: Dr. Norman Chigier
Dept. of Mechanical Engineering
Pittsburgh, PA 15213

Case Western Reserve University
Attn: Dr. Alexander Dybbs
Mechanical & Aerospace
Engineering Dept.
Cleveland, OH 44106

Case Western Reserve University
Attn: Dr. Robert V. Edwards
Chemical Engineering Dept.
Cleveland, OH 44106

Caterpillar Tractor Company
Attn: Mr. Donald W. Heston
Research Department
Technical Center, Building F
100 Northeast Adams Street
Peoria, IL 61629

Combustion Engineering
Attn: John Fishburn
Dept. 9001-2226
Windsor, CT 06095

Combustion Engineering
Attn: J. Niziolek
Dept. 9005-0301
Windsor, CT 06095

Cranfield Institute of Technology
Attn: Dr. Robin L. Elder
School of Mechanical Engineering
Cranfield, Bedford MK43 OAL
UNITED KINGDOM

Dantec Electronik
Attn: Dr. Lars Lading
Medicinsk og Videnskabeligt
Maleudstyr A/S
Mile Parken 22, DK-2740 Skovlunde
DENMARK

DFVLR
Attn: Dr. Ing R. Schodl
Inst. Fur Antriebstechnik
Postfach 90 60 58
5000 Koln 90
FEDERAL REPUBLIC OF GERMANY

Douglas Aircraft Company
Attn: J. R. S. Findlay
Intl, Mail Code 36-41
3855 Lakewood Blvd.
Long Beach, CA 90846

Eaton Corporation
Attn: Earl D. Jacobs, President
Electronic Instrumentation Division
5340 Alla Road
Los Angeles, CA 90066

Eaton Corporation
Attn: Dr. Lamont Eltinge
P. O. Box 766
Southfield, MI 48037

FluiDyne Engr. Corporation
Attn: Mat Matsuura, Group Leader
Controls and Instrumentation
5900 Olson Memorial Highway
Minneapolis, MN 55422

Garrett Turbine Engine Company
Attn: N. Fred Pratt, MS 47-40/302-2 C
P. O. Box 5217
Phoenix, AZ 85010

Garrett Turbine Engine Company
Attn: Mr. Joe Allan, MS 47-451/320-2
P. O. Box 5217
Phoenix, AZ 85010

General Electric Company
Attn: Patrick J. Poinsot, Engineer
Stress & Vibration Instrumentation
1000 Western Avenue, M.Z. 129 KD
Lynn, MA 01910

General Electric Company
Attn: Ronald J. Casagrande, MS 43A
Aircraft Equipment Division
50 Fordham Road
Wilmington, MA 01887

General Electric Company
Aircraft Engine Business Group
Attn: Gary Poppel, MS H-45
Cincinnati, OH 45215

General Electric Company
Aircraft Engine Business Group
Attn: Paul W. Mossey, MS H-78
Cincinnati, OH 45215

General Electric Company
Aircraft Engine Business Group
Attn: E. L. Pauly, MS H-78
Cincinnati, OH 45215

General Motors Corporation
Allison Gas Turbine Division
Attn: Mr. Ed Nitka
Speed Code T-12
P. O. Box 420
Indianapolis, IN 46206-0420

General Motors Corporation
Allison Gas Turbine Division
Attn: David Willis
P. O. Box 420
Indianapolis, IN 46206-0420

General Motors Corporation
Allison Gas Turbine Division
Attn: Ralph Fox, MS W16
P. O. Box 420
Indianapolis, IN 46206-0420

General Motors Corporation
Allison Gas Turbine Division
Attn: Dr. Donald R. Zimmerman
P. O. Box 420
Indianapolis, IN 46206-0420

General Motors Corporation
Allison Gas Turbine Division
Attn: Ken Cross
P. O. Box 420
Indianapolis, IN 46206-0420

HITEC Corporation
Attn: Steve Wnuk
P. O. Box 790
87 Fitchburg Road
Ayer, MA 01432

Kulite Semiconductor Products, Inc.
Attn: John R. Hayer
1039 Hoyt Avenue
Ridgefield, NJ 07657

Lewis Engineering Company
Attn: C. B. Stegner
238 Water Street
Naugatuck, CT 06770

Massachusetts Inst. of Technology
Attn: Dr. Alan Epstein, Rm. 31-266
Cambridge, MA 02139

Medtherm Corporation
Attn: Larry Jones
P. O. Box 412
Huntsville, AL 35804

National Bureau of Standards
Attn: George Burns
Inst. for Basic Research
Washington, DC 20234

National Bureau of Standards
Attn: Ken Kreider, 221-B310
Gaithersburg, MD 20899

Naval Air Propulsion Test Center
Attn: Gaelan J. Mangano
P. O. Box 7176
Trenton, NJ 08628

Naval Air Propulsion Test Center
Attn: Russ Vizzini, Code PE32
Trenton, NJ 08628-0176

Naval Air Propulsion Test Center
Attn: Joseph De La Cruz
P. O. Box 1776
Trenton, NJ 08628

Naval Air Systems Command
Attn: Andrew Glista/Code 933E
Washington, DC 20361

Naval Post Graduate School
Attn: Prof. R. P. Shreeve
Dept. of Aeronautics (Code 67Sf)
Monterey, CA 93943

O.N.E.R.A.
Attn: Alain Boutier
29 Ave. de la Division Le Clerc
92320 Chatillon Sous Bagneus
FRANCE

Pennsylvania State University
Attn: Prof. B. Lakshminarayana
233 Hammond Building
University Park, PA 16802

Physical Sciences Dept.
Attn: M. G. Dunn
Arvin/Calspan Adv. Tech. Ctr.
Buffalo, NY 14225

PRC Kentron
Attn: Dr. M. M. Lemcoe
P. O. Box 273
Facility Support Complex (FSC)
Edwards, CA 93523-5000

Public Service Elect. & Gas Company
Attn: Dr. Melvin L. Zwillenberg
Research & Development Dept.
80 Park Plaza
Newark, NJ 07101

RdF Corporation
Attn: Frank Hines
23 Elm Avenue
Hudson, NH 03051

Rockwell International
Rocketdyne Division
Attn: Mr. Sarkis Barkhoudarian
6633 Canoga Avenue
Canoga Park, CA 91303

Rockwell International
Rocketdyne Division
Attn: Dr. John C. Lee
6633 Canoga Avenue
Canoga Park, CA 91303

Rosemont, Inc.
Attn: Mr. Larry Miller, MS F-10
P. O. Box 959
Burnsville, MN 55337

Spectron Development Laboratories
Attn: Dr. Chris W. Busch
3535 Hyland Avenue
Suite 102
Costa Mesa, CA 92626

Stanford University
Attn: Dr. R. J. Moffatt
Asst. Prof., Mech. Engr.
Thermosciences Division
Stanford, CA 94305

Stein Engineering Services, Inc.
Attn: Mr. Peter K. Stein
5602 East Monte Rosa
Phoenix, AZ 85018-4646

Sverdrup (AEDC)
Attn: Paul McCarty
M/S 930
Arnold AFB, TN 37389

Teledyne CAE
Attn: Julie J. Senn
1330 Laskey Road
P. O. Box 6971
Toledo, OH 43612-0971

Teledyne CAE
Attn: Joseph Pacholec
1330 Laskey Road
P. O. Box 6971
Toledo, OH 43612-0971

Teledyne CAE
Attn: Jim Shortridge
1330 Laskey Road
P. O. Box 6971
Toledo, OH 43612-0971

The Univ. of Tennessee Space Institute
Attn: James W. L. Lewis
Applied Physics Research Group
Tullahoma, TN 37388

Thermogage, Inc.
Attn: Charles E. Brookley
330 Allegany Street
Frostburg, MD 21534

Thermonetics Corporation
Attn: H. J. Poppendiek
1028 Garnet Avenue
San Diego, CA 92109

TSI Instruments
Attn: Dr. Rajan Menon
P. O. Box 64394
St. Paul, MN 55164

United Technologies Corporation
Pratt & Whitney
Attn: M. Carl Williams, MS 116-01
400 Main Street
East Hartford, CT 06108

United Technologies Corporation
Pratt & Whitney
Attn: W. Gilbert Alwang, MS 162-29
400 Main Street
East Hartford, CT 06108

United Technologies Corporation
Pratt & Whitney
Attn: W. Barry Lunn, MS 731-36
P. O. Box 109600
West Palm Beach, FL 33410-9600

United Technologies Corporation
Pratt & Whitney
Attn: Bill Davies, MS 731-67
P. O. Box 109600
West Palm Beach, FL 33410-9600

United Technologies Optical Systems
Attn: Dr. Jaime Roman
P. O. Box 4181
West Palm Beach, FL 33410

United Technologies Research Center
Attn: Dr. A. Eckbreth, MS 129-90
Silver Lane
East Hartford, CT 06108

United Technologies Research Center
Attn: Dr. G. M. Dobbs, MS 129-90
Silver Lane
East Hartford, CT 06108

Virginia Polytechnic Institute
and State University
Attn: W. F. O'Brien, Jr.
Mechanical Engineering Dept.
Blacksburg, VA 24061

Williams International
Attn: Chloral L. Shew, MS 4-10
P. O. Box 200
Walled Lake, MI 48088

Williams International
Attn: David Easton
P. O. Box 200
Walled Lake, MI 48088

End of Document